National Library of Canada
Canadian Theses Service
Ottawa, Canada
K1A 0N4

Bibliothèque nationale du Canada
Services des thèses canadiennes

CANADIAN THESES

THÈSES CANADIENNES

NOTICE

The quality of this microfiche is heavily dependent upon the quality of the original thesis submitted for microfilming. Every effort has been made to ensure the highest quality of reproduction possible.

If pages are missing, contact the university which granted the degree.

Some pages may have indistinct print especially if the original pages were typed with a poor typewriter ribbon or if the university sent us an inferior photocopy.

Previously copyrighted materials (journal articles, published tests, etc.) are not filmed.

Reproduction in full or in part of this film is governed by the Canadian Copyright Act, R.S.C. 1970, c. C-30.

AVIS

La qualité de cette microfiche dépend grandement de la qualité de la thèse soumise au microfilmage. Nous avons tout fait pour assurer une qualité supérieure de reproduction.

S'il manque des pages, veuillez communiquer avec l'université qui a conféré le grade.

La qualité d'impression de certaines pages peut laisser à désirer, surtout si les pages originales ont été dactylographiées à l'aide d'un ruban usé ou si l'université nous a fait parvenir une photocopie de qualité inférieure.

Les documents qui font déjà l'objet d'un droit d'auteur (articles de revue, examens publiés, etc.) ne sont pas microfilmés.

La reproduction, même partielle, de ce microfilm est soumise à la Loi canadienne sur le droit d'auteur, SRC 1970, c. C-30.

THIS DISSERTATION HAS BEEN MICROFILMED EXACTLY AS RECEIVED

LA THÈSE A ÉTÉ MICROFILMÉE TELLE QUE NOUS L'AVONS REÇUE

NL-339 (r.86/06)

Canada

THE UNIVERSITY OF ALBERTA

RELATIVE PERMEABILITY MEASUREMENTS IN OIL SANDS

(C)

by

MARCEL POLIKAR

A THESIS

SUBMITTED TO THE FACULTY OF GRADUATE STUDIES AND RESEARCH

IN PARTIAL FULFILLMENT OF THE REQUIREMENTS FOR THE DEGREE

OF DOCTOR OF PHILOSOPHY

IN

PETROLEUM ENGINEERING

DEPARTMENT OF MINING, METALLURGICAL AND PETROLEUM ENGINEERING

EDMONTON, ALBERTA

SPRING 1987

Permission has been granted to the National Library of Canada to microfilm this thesis and to lend or sell copies of the film.

The author (copyright owner) has reserved other publication rights, and neither the thesis nor extensive extracts from it may be printed or otherwise reproduced without his/her written permission.

L'autorisation a été accordée à la Bibliothèque nationale du Canada de microfilmer cette thèse et de prêter ou de vendre des exemplaires du film.

L'auteur (titulaire du droit d'auteur) se réserve les autres droits de publication; ni la thèse ni de longs extraits de celle-ci ne doivent être imprimés ou autrement reproduits sans son autorisation écrite.

ISBN 0-315-37661-9

THE UNIVERSITY OF ALBERTA

RELEASE FORM

NAME OF AUTHOR Marcel Polikar

TITLE OF THESIS Relative Permeability Measurements in Oil Sands

DEGREE FOR WHICH THESIS WAS PRESENTED DOCTOR OF PHILOSOPHY

YEAR THIS DEGREE WAS GRANTED 1987

Permission is hereby granted to THE UNIVERSITY OF ALBERTA LIBRARY to reproduce single copies of this thesis and to lend or sell such copies for private, scholarly or scientific research purposes only.

The author reserves other publication rights, and neither the thesis nor extensive extracts from it may be printed or otherwise reproduced without the author's written permission.

Permanent address: 542 Wolf Willow Road
Edmonton, Alberta T5T 1E4

DATED March 13, 1987.

THE UNIVERSITY OF ALBERTA

FACULTY OF GRADUATE STUDIES AND RESEARCH

The undersigned certify that they have read, and recommend to the Faculty of Graduate Studies and Research, for acceptance, a thesis entitled RELATIVE PERMEABILITY MEASUREMENTS IN OIL SANDS submitted by MARCEL POLIKAR in partial fulfillment of the requirements for the degree of Doctor in Philosophy in Petroleum Engineering.

.....

Dr. S.M. Farouq Ali (Supervisor)

.....

Dr. R.G. Bentsen

.....

Prof. P.M. Dranchuk

.....

Dr. J.H. Masliyah

.....

Dr. V.R. Puttagunta

.....

Dr. H.Y. Lo (External Examiner)

DATED .....

à mon fils Sébastien

Patience et longueur de temps
Font plus que force ni que rage.

Jean de La Fontaine
(le lion et le rat)

ABSTRACT

Petroleum reservoir engineers use relative permeability to describe the simultaneous flow of oil, water and gas in the reservoir during oil recovery operations. For thermal recovery processes in oil sand systems, there are very few published experimental data on residual fluid saturations or relative permeability curves. The effect of temperature on these parameters has not been established. This study was initiated to address these deficiencies and is the first extensive report of bitumen-water relative permeability functions measured for temperatures up to 250°C.

An apparatus was developed for the determination of two phase oil-water relative permeabilities. A packing technique was developed for preparing laboratory cores containing clean unconsolidated Ottawa sand, homogenized heavy oils and deionized water. Experiments were conducted over a large temperature range (20°C to 250°C) with both clean sands and reservoir sands for evaluating differences between ideal and real systems, using proven and reliable experimental procedures. The experimental work comprised the measurement of bitumen-water end point relative permeabilities and residual saturations as functions of temperature, followed by the determination of bitumen-water and Kaydol-water relative permeability curves by the steady and unsteady state methods.

No significant temperature effects were found for the Athabasca bitumen-water system in clean or reservoir sands, nor for the Kaydol-water system in clean sands. More reactive fluid-fluid-solid combinations may show temperature effects on relative permeability. End point experiments with clean sand gave reproducible results, whereas the reservoir sand results showed the variation that can be encountered in heterogeneous systems such as those containing clays. The convex shape of the oil curves reflected the recovery mechanism of heavy oil by hot water under adverse mobility ratio conditions.

A comparison of normalized relative permeability curves for heavy oils of Alberta showed that wide variations existed among the reported data. Therefore, a range of relative permeability curves may be necessary to describe the various recovery mechanisms of heavy oils by hot water from heterogeneous unconsolidated sands.

ACKNOWLEDGEMENTS

I wish to express my sincere and grateful thanks to my academic supervisor, Dr. S.M. Farouq Ali, and to my project manager, Dr. V.R. Puttagunta for their valuable guidance, encouragement, support and discussions throughout the course of and in preparation of this thesis. I would also like to acknowledge Dr. R.G. Bentsen for his useful suggestions.

I would like to express my appreciation to the Alberta Oil Sands Technology and Research Authority (AOSTRA) and to the Alberta Research Council (ARC) for funding this study under the AOSTRA/ARC Joint Oil Sands Research Program. The experimental work was carried out in the laboratories of the Oil Sands Research Department of ARC in Edmonton.

I would further like to thank Frank Ferracuti and Victor DeCastro for the technical assistance provided during the experiments, Dave Cuthiell, Cheng Fu, Kevin Kimber, Dean Wallace and Wendy Zwickel for valuable discussions and helpful suggestions. The efforts of all persons who participated directly or indirectly in the completion of this thesis are gratefully appreciated.

And last but not least, I would like to express my gratitude to my family for providing the moral support that greatly contributed to the accomplishment of this thesis.

TABLE OF CONTENTS

CHAPTER		Page
1.	INTRODUCTION AND PROBLEM STATEMENT	1
2.	BACKGROUND AND LITERATURE REVIEW	5
	2.1 Determination of Relative Permeability	5
	2.1.1 Measurement	6
	2.1.2 Theoretical Description	13
	2.2 Factors Affecting Relative Permeability	17
	2.2.1 Wettability	19
	2.2.2 Viscous and Capillary Forces	20
	2.2.3 Pressure and Temperature	24
	2.3 Published Heavy Oil Relative Permeability Data	28
	2.3.1 Observations	33
3.	EXPERIMENTAL APPARATUS AND PROCEDURES	35
	3.1 Apparatus	35
	3.1.1 Core Holder	35
	3.1.2 Injection Equipment	38
	3.1.3 Production Equipment	39
	3.1.4 Pressure Measurement	39
	3.2 Materials	40
	3.2.1 Sand	40
	3.2.2 Water and Brine	41
	3.2.3 Bitumen	43
	3.2.4 Kaydol	44

3.3 Core Packing Procedure 44
3.3.1 Preliminary Packing Experiments 47
3.3.2 Packing Density 49
3.3.3 Packing Procedure 51
3.3.4 Cleaning Procedure for Reuse of Cores . . . 52
3.3.5 Packing of Reservoir Oil Sand 52
3.4 Flooding Sequence 53
3.4.1 Absolute Permeability Measurements 53
3.4.2 Preparation of Synthetic Oil Sand Cores . . 53
3.4.3 Displacement Experiments 54
3.4.3.1 End Point Calculations 56
3.4.3.2 Water-Bitumen Mixture Injection . 57
3.4.3.3 Dynamic Displacements 59
3.4.3.4 Sampling and Analysis 61
3.4.4 Kaydol Experiments 62
4. SAND PACK AND HEAVY OIL PROPERTIES 65
4.1 Ottawa Sand Pack Properties 65
4.1.1 Porosity 65
4.1.2 Absolute Permeability 66
4.1.3 Effect of Temperature on Absolute Permeability 67
4.2 Reservoir Sand Pack Properties 72
4.3 Heavy Oil Properties 74
4.3.1 Bitumen Viscosity 74
4.3.2 Bitumen Density 77
4.3.3 Property Correlations 77

4.3.4 Kaydol Properties 79

5. EXPERIMENTAL RESULTS 80

5.1 End Points 80

5.1.1 End Point Criterion 80

5.1.2 Bitumen Floods 82

5.1.3 Hot Water and Brine Floods 83

5.1.4 Effect of Sand Grain Size and Overburden . 84

5.1.5 Effect of Temperature 85

5.1.6 Fluid Properties and Capillary Number . . . 89

5.1.7 Stabilization Criterion 92

5.1.8 Reservoir Sand Experiments 92

5.2 Relative Permeability Curves 95

5.2.1 Initial Oil Sand Core Parameters 95

5.2.2 Steady State Experiments 98

5.2.3 Dynamic Displacement Experiments 105

5.2.3.1 Bitumen-Water Curves 105

5.2.3.2 Kaydol Experiments 111

6. DISCUSSION 122

6.1 Effect of Temperature on Relative Permeability . 122

6.1.1 Review of Theoretical Models 122

6.1.2 Experimental Studies 127

6.2 Comparison of Steady and Unsteady State Results. 131

6.2.1 Shape of the Relative Permeability Curves 131

6.2.2 Stability Analysis 135

6.3 Relative Permeability Curves for Alberta Heavy Oils 144

7. CONCLUSIONS 150

8. RECOMMENDATIONS 153

BIBLIOGRAPHY 154

APPENDICES 178

A. Packing Experiments 178

B. Data Measurement and Calculations 181

C. Ottawa Sand Pack Properties 196

D. Fluid Properties 205

E. End Point Results 212

F. Unsteady State Experiments 217

G. Kaydol Experiments 223

H. Statistical Analysis 240

CURRICULUM VITAE 248

LIST OF TABLES

TABLE		Page
2.1	Summary of Temperature Effects on Relative Permeability Studies in Unconsolidated Porous Media	26
2.2	Summary of Temperature Effects on Relative Permeability Studies in Consolidated Porous Media	27
3.1	Experimental Flooding Conditions	55
3.2	Bitumen/Water Mixtures for Steady State Experiments	58
3.3	Experimental Conditions for Bitumen Displacement Experiments	60
3.4	Experimental Conditions for Kaydol Displacement Experiments	64
4.1	Average Core Parameters as a Function of Temperature	68
4.2	Statistical Parameters for Temperature Dependence of Absolute Permeability	71
4.3	Experimental Core Parameters for Reservoir Sand Samples	73
4.4	Viscosity of Bitumen Measured at 7 MPa	75
4.5	Density of Bitumen Measured at 7 MPa	78
5.1	Average Bitumen-Water End Point Results as a Function of Temperature	81
5.2	Statistical Analysis of End Point Results	88
5.3	Average Fluid Properties as a Function of Temperature in End Point Experiments	91
5.4	End Point Results for Reservoir Sand	93
5.5	Comparison of Initial Oil Sand Core Parameters	96
5.6	Intermediate Data for Relative Permeability Curves (steady state)	99
5.7	Best Fit Results for Steady State Relative Permeability	102

5.8 Bitumen Displacement Results 107

5.9 Fitting Parameters for JBN Calculations 112

A.1 Preliminary Packing Experiments 179

C.1 Sieve Analysis of Ottawa Sand 197

C.2 Particle Size Distribution of Outcrop Sand 198

C.3 Core Dimensions and Packing Properties 199

C.4 Absolute Permeability at Low Temperature 201

C.5 Absolute Permeability at High Temperature 203

D.1 Viscosity and Density of Water at 7 MPa 206

D.2 Viscosity and Density of 0.0704 Molal Aqueous Sodium Sulfate Solution 207

D.3 Chemical Analysis of Athabasca Bitumen 208

D.4 Specific Bitumen Properties 209

D.5 Measured Fluid Properties at 7 MPa 210

E.1 Data for End Point Calculations 213

E.2 End Point Relative Permeabilities and Saturations . . 214

E.3 Fluid Properties in End Point Experiments 215

E.4 Initial Oil Sand Core Parameters 216

F.1 Measured Parameters for Unsteady State Experiments - Bitumen , 125°C - 218

F.2 Data for JBN Calculations - Bitumen , 125°C - 219

F.3 Relative Permeability and Fractional Flow Curves - Bitumen , 125°C - (from JBN calculations) 220

G.1 Refractive Index Calibration for Kaydol-Mineral Spirit Mixtures 224

G.2 Measured Data for JBN Calculations - Kaydol #1 , 20°C - 225

G.3 Relative Permeability and Fractional Flow Curves - Kaydol #1 , 20°C - (from JBN calculations) 226

G.4 Measured Data for JBN Calculations
- Kaydol #2 , 20°C - 227

G.5 Relative Permeability and Fractional Flow Curves
- Kaydol #2 , 20°C - (from JBN calculations) 228

G.6 Measured Data for JBN Calculations
- Kaydol #3 , 100°C - 229

G.7 Relative Permeability and Fractional Flow Curves
- Kaydol #3 , 100°C - (from JBN calculations) 230

G.8 Measured Data for JBN Calculations
- Kaydol #4 , 20°C - 231

G.9 Relative Permeability and Fractional Flow Curves
- Kaydol #4 , 20°C - (from JBN calculations) 233

G.10 Measured Data for JBN Calculations
- Kaydol #5 , 100°C - 234

G.11 Relative Permeability and Fractional Flow Curves
- Kaydol #5 , 100°C - (from JBN calculations) 236

H.1 Data for Variance Analysis 245

H.2 Variance Analysis Results 247

LIST OF FIGURES

FIGURE		Page
2.1	Graphical Representation of Relative Permeability	7
3.1	Schematic Diagram of the Relative Permeability Apparatus	36
3.2	Core Holder (end cap detail)	37
3.3	Comparison of Particle Size Analysis (clean versus outcrop sand)	42
3.4	Schematic of the Packing Apparatus	46
3.5	Packing Density along the Length of the Core	50
4.1	Temperature Dependence of Absolute Permeability	69
4.2	Fluid Properties in Displacement Experiments	76
5.1	Bitumen-Water End Point Relative Permeabilities as a Function of Temperature	86
5.2	Initial and Residual Bitumen Saturations as a Function of Temperature	87
5.3	Bitumen-Water Relative Permeability Curves (steady state)	100
5.4	Normalized Bitumen-Water Relative Permeability Curves (steady state)	104
5.5	Bitumen Recovery Data at 125°C	108
5.6	Bitumen Recovery Function (semi-logarithmic)	110
5.7	Bitumen-Water Relative Permeability Curves (from dynamic displacement experiments)	113
5.8	Recovery Curves for Kaydol Experiments	115
5.9	Kaydol-Water Relative Permeability Curves (low temperature)	119
5.10	Kaydol-Water Relative Permeability Curves (high temperature)	121

6.1 Bitumen-Water Relative Permeability Curves (steady versus unsteady state) 132

6.2 Bitumen-Water Relative Permeability Ratio Functions . 134

6.3 Fractional Flow Curves for Bitumen-Water 136

6.4 Comparison of Experimental Heavy Oil-Water Relative Permeability Curves (normalized) 146

6.5 Comparison of Normalized Oil-Water Relative Permeability Curves 147

B.1 Pressure Drop Measurement System 194

B.2 Comparison of Relative Permeability Data Obtained from Two Methods (after Jones and Roszelle, 1978) . . 195

F.1 Post-Breakthrough Recovery Function for Bitumen Experiments 221

F.2 Relative Injectivity Function for Bitumen Experiments 222

G.1 Refractive Index Calibration for Kaydol-Mineral Spirit Mixtures 237

G.2 Post-Breakthrough Recovery Functions for Kaydol Experiments 238

G.3 Relative Injectivity Functions for Kaydol Experiments 239

NOMENCLATURE

A	cross sectional area
a,e	parameters (equations 5.4 to 5.7)
a_i, b_i	parameters (equations B.41 to B.44)
C	concentration
C^*	wettability number
D	diameter
E_d	displacement efficiency
E_m	microscopic displacement efficiency
F	statistical F-distribution
f	fractional flow
g	gravitational acceleration
H	height
I_r	relative injectivity
I_{sc}	instability number for cylindrical system
k	permeability
k_a	absolute permeability (all temperatures)
k_e	effective permeability
k_o	absolute permeability (room temperature only)
k_r	relative permeability
k_{rbiw}	bitumen relative permeability at irreducible water
k_{roiw}	oil relative permeability at irreducible water
k_{rwrb}	water relative permeability at residual bitumen
k_{rwro}	water relative permeability at residual oil
k_{wor}	effective water permeability at residual oil

L	length
M_f	multiplying factor
M_r	end point mobility ratio
m	molality
N_c	capillary number
N_p	cumulative pore volumes of oil produced
N_s	stability number
n_D	refractive index
P	pressure
P_c	capillary pressure
q	volumetric flow rate
r	radius
r^2	correlation coefficient
$\bar{r}_m$	average macroscopic mean radius of curvature
S	saturation
S_{bi}	initial bitumen saturation
S_{br}	residual bitumen saturation
S_{or}	residual oil saturation
S_{wi}	irreducible water saturation
T	temperature
V	volume
v	velocity
W_i	cumulative pore volumes of water injected
w	weight
z	height

Greek Letters

Δ	difference
ϵ	saturation exponent (equation 2.4)
f	function
λ	mobility (ratio of permeability to viscosity)
μ	viscosity
$\mu_{b/w}$	bitumen-to-water viscosity ratio
μ_r	oil-to-water viscosity ratio
ρ	density
σ	interfacial tension
θ	contact angle
ϕ	porosity
Φ	potential

Abbreviations

ID	internal diameter
JBN	Johnson-Bossler-Naumann
M	molarity
MW	molecular weight
OOIP	original-oil-in-place
PV	pore volume

Subscripts

$_b$	bitumen
$_{bpr}$	back-pressure regulator

br	brine
b/w	bitumen-to-water
c	capillary
co	core
corr	correction
crit	critical
d	downward
e	effective
exp	experimental conditions
f	fluid
flow	flowing
i	refers to ith phase
K	Kaydol
meas	measured
o	oil
ovb	overburden
pf	production fluids
pump	pump setting
pyc	pycnometer
ref	reference
room	room conditions
s	sand
tc	total core
u	upward
v	viscometer
w	water

2	core outlet

Superscripts

*	normalized

STATISTICAL

CL	confidence level
DF	degrees of freedom
F	F-distribution
m	population mean
MS	mean squares
N	number of populations
n	number of observations
R	denotes a statistical population
s	standard deviation
SS	sum of squared deviations
t	t-distribution
x	variable

Subscripts

error	error (statistical)
factor	factor (statistical)
i	ith observation (statistical)
j	jth population (statistical)
p	pooled (statistical)

Superscript

*	tabulated value in statistical distribution (F or t)
-	average value

1. INTRODUCTION AND PROBLEM STATEMENT

In the last twenty years, computer assisted reservoir simulation has become a major tool for evaluating and predicting reservoir performance. Description of the reservoir and understanding of oil displacement mechanisms due to primary, secondary or tertiary recovery processes are among the most important features of a good reservoir simulator. Since the advent of computers, and the use of enhanced oil recovery methods for light as well as heavy oil deposits, the concept of relative permeability has been revived and is now one of the most important input variables for numerical reservoir simulators. Petroleum reservoir engineers use relative permeability to describe the characteristics of simultaneous flow of oil, water and gas in a formation during oil recovery operations. One needs to know residual fluid saturations and relative permeability curves to determine the ultimate recovery and the rate of oil production, respectively.

As reliable parameters are needed to carry out a satisfactory history match, and must be carefully measured in the laboratory, the objective of this study is to experimentally measure the relative permeability to water and bitumen of unconsolidated sand cores. The difficulties of this task are compounded by innumerable variables, combined with the high temperatures and pressures of the system, and the high viscosity of the bitumen.

Relative permeability has generally been represented as a function of saturation. Experimental measurement techniques were developed in the 1950s and early 1960s for light oil reservoirs, with no major breakthroughs since then, and are performed either by the steady state technique, or by the unsteady state or dynamic method. The latter has received more attention due to faster turnaround time. However, neither method seems to be superior because of limitations inherent in each. Usually, the experimental conditions are idealized and simplified by the use of small core plugs or reconstituted sand cores, and refined oils rather than native reservoir materials.

Relative permeability curves have traditionally been obtained in the laboratory on two phase systems and extended to three phase systems by mathematical correlation. In the absence of laboratory data, history matching techniques have been used, where relative permeability is treated as an adjustable parameter for matching past reservoir performance using empirically developed correlations that replace experimental data. For the Athabasca oil sand system, there are no published experimental data on residual fluid saturations, relative permeability curves, and the effect of temperature on these parameters.

Because of the vastly different results in the literature, the first goal of this study was to use as simple a system as possible to focus on fundamental properties that might cause temperature effects. The second goal was to reproduce the temperature and

pressure conditions encountered in the recovery of heavy oils[1] from deeply buried formations. The system initially selected consisted of pure unconsolidated quartz sand, deionized water and solvent-extracted Athabasca bitumen. These idealized conditions minimized clay migration and high temperature corrosion, and the use of crude oil more closely represented field conditions. Such a system would alleviate some experimental difficulties and ease the interpretation of relative permeability determinations.

The experimental approach consisted of determining the end point relative permeabilities and corresponding residual saturations for bitumen and water as a function of temperature in the range of 100°C to 250°C. The upper limit was chosen as the maximum temperature found ahead of a condensing steam front, whereas the lower limit was determined from the viscosity at which bitumen could be mobilized. Next, bitumen-water relative permeability curves were determined by both steady and unsteady state techniques for providing comparisons. Temperature effects were also considered in view of the end point results.

Temperature was the only external property modified; this in turn affected fluid and flow properties. The flow rate for all experiments was chosen to be approximately one pore volume per hour

---

1. Heavy oils (15°-25° API) are mobile at reservoir conditions, whereas oil sand bitumens (8°-14° API) are not. However, these two terms will be used interchangeably in this document when referring to either of them in general.

(PV/h), which translates into 2 m/d (6.5 ft/d) for field conditions, and was sufficient to minimize capillary end effects present in core-size experiments. However, viscous fingering resulting from the displacement of a more viscous by a less viscous fluid may not be avoided and was considered accordingly.

This study is the most exhaustive experimental work undertaken to date for the determination of temperature effects on relative permeability relationships. Experiments were performed under controlled conditions of pressure, temperature and flow rate. Quality control was achieved by the reproducibility of the results in duplicating several experiments. Following a thorough investigation of the bitumen-water-clean sand system, a few experiments using mineral oil instead of bitumen and others using reservoir sand instead of clean sand were conducted to provide explanations and comparisons with previous studies. An analysis of theoretical models gave further evidence as to the effect of temperature on relative permeabilities.

At present, the literature on relative permeability is exhaustive and encompasses all aspects of experimental and theoretical determinations, as well as factors which affect it. In light of the present study, the published work is reviewed in the next chapter.

2. BACKGROUND AND LITERATURE REVIEW

2.1 Determination of Relative Permeability

The most widely used equation for flow through porous media is due to Henry Darcy (1856), a French engineer, who derived an empirical relationship based on experimental evidence. It shows the dependence of flow velocity on both porous medium and fluid properties assuming homogeneous, linear, steady state, incompressible and laminar flow for a single fluid:

$$v = -\frac{k\rho}{\mu}\frac{d\Phi}{dL} \tag{2.1}$$

where $\Phi = \frac{P}{\rho} + gz$ is called the fluid potential. (2.2)

In petroleum reservoirs, single phase flow rarely occurs and the Darcy equation cannot be used in the form given above. The concept of permeability established for the flow of a single phase through a porous medium can still be applied to two phase flow by modifying its value to take into account the presence of the second phase. In the case of the simultaneous steady flow of two incompressible fluids through a homogeneous and isotropic porous medium, Darcy's equation can be extended to describe the flow of each fluid:

$$v_i = -\frac{k_i\rho_i}{\mu_i}\frac{d\Phi_i}{dL} \tag{2.3}$$

where k_i is the effective permeability to fluid i (oil, water, gas) and is proportional to the area open to flow in the presence of the other phase(s). The total capacity of flow through the porous medium is therefore reduced ($\Sigma k_i \leq k$).

Often the ratio of effective permeability to a specific fluid and of some base permeability (usually the absolute permeability) is used in reservoir engineering calculations. Such a dimensionless ratio is called the relative permeability and is considered to be a single-valued function of fluid saturation only. The concept of relative permeability has meaning only in the interval of saturation of the wetting fluid, $S_{wi} \leq S_w \leq 1-S_{or}$. This is illustrated in Figure 1. In a later section, relative permeability is shown to depend on many other factors.

2.1.1 Measurement

Measurements of relative permeability have been performed since the mid-30s (Wyckoff and Botset, 1936). The simultaneous flow of oil, gas and water through a porous medium was believed to be governed by fluid properties, the relative saturation of each fluid and the characteristics of the medium itself. Most of the concepts in the experimental approach for determining relative permeability were developed in the early-50s (Geffen et al., 1951; Osoba et al., 1951; Richardson et al., 1952). Steady state and unsteady state or dynamic methods were used for direct determination. Both methods have been extensively used to study two and

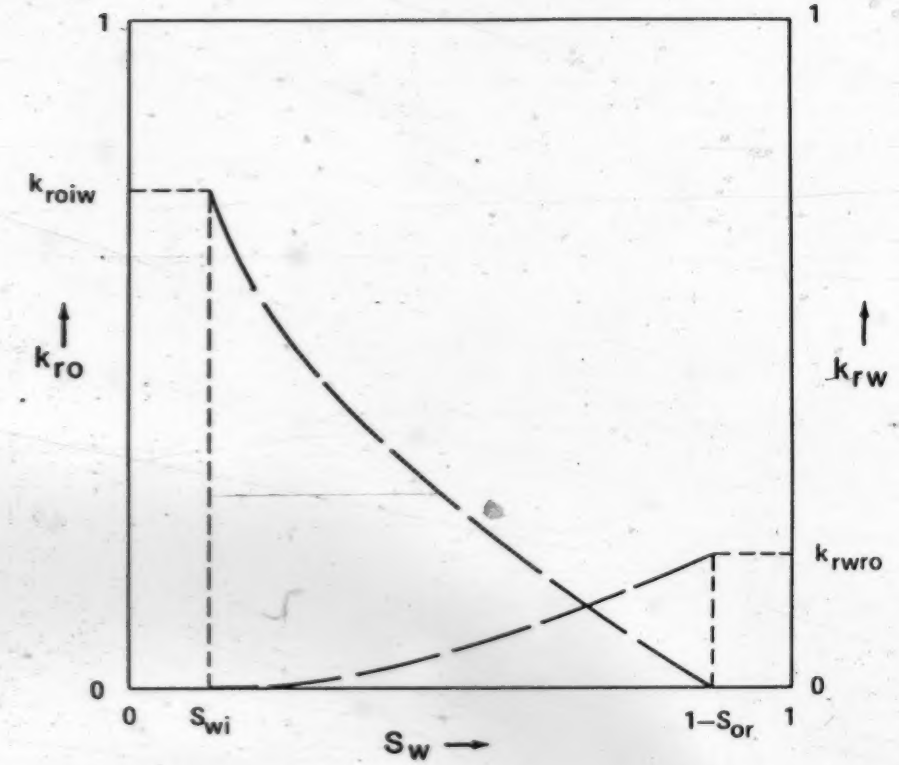

Figure 2.1 : Graphical Representation of Relative Permeability

some three phase flow situations; neither method has proven to be free of limitations.

Reservoir cores, outcrop rock samples and sand packs were all used in relative permeability and oil displacement studies. Reservoir rock is obviously preferred for specific field evaluations, but many situations can arise where preliminary tests with reasonably homogeneous samples are advisable. The wettability of a sample can be the most difficult factor to maintain or re-establish at its reservoir condition for core flooding tests. Preferential wettability of the reservoir rock to oil or water governs to a great extent the oil recovery in a waterflood (Rathmell et al., 1973) and influences the success of any enhanced recovery method.

Anderson (1986) compiled a thorough literature survey covering the effects of wettability on core analysis. An accurate representation of reservoir wettability is important for obtaining realistic relative permeabilities and residual saturations from core tests. The majority of oil reservoirs seem to possess an intermediate wettability (Craig, 1971), with the rock surfaces exhibiting no strong wetting preference for either the water or oil phases. Mungan (1972) showed that at all water saturations, the water/oil relative permeability ratio is higher for a preserved core with reservoir fluids than for a clean core with purified fluids. The water/oil flow characteristics of such reservoir cores cleaned to a strongly water-wet condition could be quite misleading.

The steady state method requires the test specimen to be homogeneous and provides flexibility in controlling saturation changes. Calculation of relative permeability from experimental data is straight-forward and does not involve elaborate assumptions. The Penn State method (Morse et al., 1947) is considered the best steady state method available. A fixed ratio of fluids is allowed to flow simultaneously through a single core made of three segments. The front piece serves to distribute the fluids and the last piece to absorb undesirable capillary end effects that cause saturation gradients in the test sample. Saturations and pressure drops are measured in the middle test section. Several fluid ratios are injected to cover the entire saturation range, each one until saturation and pressure equilibria are established. The experiments are difficult to set up to minimize the presence of end effects, and there are difficulties associated with obtaining accurate saturation profiles from non-intrusive measurements.

Today, the modified Penn State method is being successfully used in single cores by eliminating or at least minimizing inlet and outlet end effects. Pressure drop and saturation distributions are measured in the central portion with non-intrusive devices when the system reached a steady state condition. With this approach, end and intermediate point relative permeabilities and saturations can be measured with confidence for specific experimental conditions. However, it is a time consuming method if one wants to obtain a complete set of relative permeability curves.

Dynamic displacement methods, on the other hand, are considered to be more representative of reservoirs since saturation changes may occur too rapidly to allow equilibrium to be attained. In these experiments, water or gas are injected to displace the oil, and production and pressure drop are monitored continuously during the flooding operation. Measurements are quick and simpler to make but their interpretation may be questionable under certain circumstances because of porous medium inhomogeneities, scaling requirements, and flow instabilities. The unsteady state methods are usually based on the Buckley and Leverett (1942) frontal advance theory that assumes negligible gravitational and capillary forces compared to viscous forces. Capillary pressure effects can be minimized with the use of high flow rates in displacement experiments, resulting in stabilized flow (Bentsen, 1978). Most experiments are performed on short horizontal cores to eliminate or at least minimize the contribution of gravitational forces.

A discontinuity in the capillary forces causes the wetting phase to be held back upon leaving the core so that the wetting phase saturation increases near the outlet (Leverett, 1941). Osoba et al. (1951) found relative permeability to be rate sensitive only when boundary effects were present but the sensitivities disappeared as the boundary effects became negligible with higher flow rates. Richardson et al. (1952) predicted the influence of boundary effects from equations of fluid flow and showed that errors from these effects could be eliminated in laboratory measurements. The boundary effect was described as a laboratory phenomenon and

was found negligible in actual reservoir flow. Today inlet and outlet boundary end effects are minimized by the use of front pieces to ensure proper mixing of the phases before entering the core and by the choice of flow rates so that viscous forces exceed and dominate capillary forces on a macroscopic (core) scale. This means that, in practice, experimental flow rates may be several orders of magnitude higher than field rates.

Flow instabilities occur during the displacement of a more viscous fluid by a less viscous fluid. Viscous fingering can play a significant role in the immiscible displacement of one fluid by another (Engelberts and Klinkenberg, 1951). Peters (1979) developed a dimensionless stability number, N_s, which defined stable flow as occurring below a critical value. He showed experimentally that the number of fingers increased with velocity, thereby increasing instability. Demetre et al. (1982) studied immiscible displacement at various superficial velocities in cylindrical cores with different lengths and diameters, for water-wet and oil-wet systems. Their results showed that geometric similarity between model and prototype is not important, provided the displacement is either stable ($N_s < 13.56$) or pseudo-stable ($N_s > 900$) and that neither the linear nor the radial scaling groups were, by themselves, adequate as correlating parameters in the transition zone between stable and pseudo-stable displacement ($13.56 < N_s < 900$).

Extending the works of Peters and Demetre, Bentsen (1985) proposed a new approach to instability theory in porous media, suggesting

that the type of displacement which takes place depends on the balance existing between capillary, gravitational and viscous forces. If the combined forces of gravity and capillarity are greater than the viscous forces, the displacement will be stable. The displacement will be unstable if the reverse is true. Bentsen defined an instability number proportional to the one proposed by Peters, the constant of proportionality being a function of the mobility ratio. This additional factor arises because water fingers are wider than oil fingers.

Bentsen showed that recovery is independent of the stability number for stable and pseudo-stable displacements, the displacement efficiency being much lower in the latter. In the transition region, the recovery efficiency is dependent on the stability number, and fingers having different wavelengths may dominate the displacement. His calculations showed that changing from a field-size to a laboratory-size system resulted in a stable flow regime in the laboratory compared to a pseudo-stable regime in the field. He concluded that many of the relative permeability curves measured in the laboratory are not determined under conditions representative of the field. Islam and Bentsen (1986) suggested that effective permeabilities were unique functions of saturation only if the displacement was steady state or stable and stabilized, but not when the displacement was unstable, due to the larger impact of local heterogeneities.

Welge (1952) first proposed a method to calculate the ratio of two

phase relative permeabilities from displacement experiments. He showed that the oil fraction in the outlet stream could be determined from the slope of the production history curve and the relative permeability ratio calculated therefrom. The Johnson et al. (1959) method, commonly known as the JBN method, extended Welge's technique to calculate individual phase relative permeabilities. In addition to the production history, the slope of the relative injectivity curve (inversely proportional to pressure drop history) is used to decouple the permeabilities. Calculation steps to determine slopes analytically from best fits to experimental data and to calculate relative permeabilities are given in Appendix B.

Jones and Roszelle (1978) developed graphical techniques to determine these slopes as an alternative to the JBN method. Despite being easy to use, all unsteady state methods apply only under negligible capillary pressure conditions and results should be interpreted with great care. Because of these idealized assumptions, several workers (Archer and Wong, 1973; Sigmund and McCaffery, 1979) resorted to an optimization technique for obtaining relative permeability curves by matching laboratory displacement experiments using a numerical reservoir model.

2.1.2 Theoretical Description

The simplest model of permeability is based on flow through a bundle of straight parallel capillaries, which correlates capillary pressure with pore size distribution (Purcell, 1949; Burdine et

al., 1950). The most widely accepted model is the Kozeny-Carman model that considers the porous medium as an ensemble of flow channels of various cross-sections but same length. Wyllie and Gardner (1958) refined the original Kozeny-Carman model and proposed a novel approach by combining the capillary model with a random interconnection of pores, leading to a simple statistical model where the tortuosity is primarily dependent on the pore interconnection probability.

Branching-type models are another extension of capillary models where the fluid flow path may branch and later on, rejoin (Rose and Witherspoon, 1956; Fatt, 1956). A number of investigators have extended the pioneering network approach of Fatt to develop quantitative models to describe the behaviour of fluids in porous media. The most extensive work is that of Dullien (1975) and co-workers at the University of Waterloo. Their approach consisted of measuring the pore size distribution function of a rock specimen in order to construct by analogy a network of capillary tubes reflecting the specimen's pore geometry.

These models have attempted to describe flow of a single fluid through porous media. Empiricism must be resorted to in order to bring the results of capillary models in line with reality. At present, the useful practical mathematical formulations of two phase flow through porous media are basically empirical. Network models have the best potential for understanding and quantitatively describing two phase phenomena in porous media.

Rose (1949) showed that capillary pressure is a measure of fundamental characteristics of a rock and can be used to predict relative permeabilities. The extension of models using parallel capillaries for two phase flow were based on the assumption that the fluid phases flow separately through the porous medium, with one fluid preferentially wetting the rock. Several authors (Gates and Lietz, 1950; Fatt and Dykstra, 1951; Burdine, 1953; Wyllie and Gardner, 1958) obtained expressions of relative permeability based on the Purcell (1949) capillary bundle approach.

Corey (1954) observed that the capillary pressure function $1/P_c^2$ could be approximated linearly in terms of oil saturation. Brooks and Corey (1964) later modified Corey's original capillary pressure-saturation relationship into a two parameter expression for relative permeability. This expression contains a measurement of the maximum pore size and pore size distribution:

$$k_r = k_r (S_e, \epsilon), \tag{2.4}$$

where S_e is the effective wetting phase saturation related to the capillary pressure through the saturation exponent ϵ. The commonly encountered range for ϵ is between 2 and 4 for various sands.

The direction of change of saturation (drainage and imbibition) is an important parameter in multiphase flow through porous media. While the previous expressions can reasonably describe drainage situations, imbibition relative permeability to the non-wetting

phase is generally found to be lower than that predicted mathematically. Naar et al. (1963) developed a mathematical model for consolidated porous media by considering that the advancing wetting phase (imbibition) gradually traps some of the non-wetting phase, making it immobile. Land (1968) developed expressions for imbibition relative permeabilities and provided for trapping of the non-wetting phase, using an empirical relation between initial and residual non-wetting phase saturations.

Fatt (1956) was the first to show that network models can be used to qualitatively describe the undersaturated permeability behaviour of porous media by single-size tube networks and by networks with tube radii distribution. Ehrlich and Crane (1969) mathematically modelled a consolidated porous medium by networks of irregularly interconnected pore channels. They proposed a mechanism for immiscible displacement within a pore channel in which the irregularity and pore channel interconnection are of paramount importance in explaining the drainage-imbibition hysteresis effect, thereby calculating relative permeabilities for both drainage and imbibition. Currently, percolation theory is receiving considerable attention (Larson et al., 1981; Heiba et al., 1982; Chatzis and Dullien, 1982) and this recent application for determining relative permeability curves looks promising. Predictions of relative permeability that are in close qualitative agreement with typical data from two phase systems were obtained and the theory was also extended to three phase relative permeabilities (Heiba et al., 1984).

All the relative permeability models described thus far were derived solely from mathematical considerations and most were tested against experimental data. While two phase relative permeabilities are not easy to obtain experimentally, three phase relative permeabilities are even more difficult to determine (Saraf et al., 1982). Several probability models were proposed to predict the relative permeability of the intermediate wetting phase (oil) in a three phase system from two phase data using empirical definitions (Stone, 1970 and 1973; Dietrich and Bondor, 1976).

Many models or equations were proposed to calculate three phase relative permeabilities: they either rely on the use of two phase experimental data to synthesize three phase relative permeabilities (Stone, 1973; Dietrich and Bondor, 1976), or directly calculate three phase relative permeabilities using variables such as irreducible water saturation or capillary pressure-pore size distribution curves. Usually, in the absence of experimental data, estimation of relative permeability is made from one of the following models: Brooks and Corey (1964) for drainage; Naar et al. (1963) for imbibition; Land (1968) for both drainage and imbibition. These two and three phase relative permeabilities would then be used in reservoir engineering calculations.

2.2 Factors Affecting Relative Permeability

Relative permeability curves depend on the manner in which an experiment is performed. The flow is known as drainage when the

saturation of the wetting phase is decreasing and imbibition when the saturation is increasing. The effect of saturation history in two phase flow has long been recognized (Geffen et al., 1951), as it affects the distribution of fluid phases and causes a hysteresis effect. The magnitude of this hysteresis between drainage and imbibition relative permeabilities is a function of the degree of consolidation of the porous medium (Naar et al., 1962 and 1963) and the pore geometry (Morgan and Gordon, 1970).

Trapping of the non-wetting fluid in the pores during imbibition, which is not found during drainage, also contributes to the hysteresis in relative permeability. Using pore casts and glass micromodels, Wardlaw and Cassan (1979) showed this trapping mechanism to be dependent upon the fluid properties and the characteristics of the pore system, mainly pore-to-throat size ratio, and type and degree of non-random heterogeneity. The wetting phase relative permeability is only marginally affected by the saturation history, whereas the non-wetting phase relative permeability is markedly affected (Craig, 1971).

The relative permeability hysteresis also seems to be directly related to the hysteresis of capillary pressure during imbibition and drainage cycles. The contact angle hysteresis observed during advancing and receding flows provides a partial explanation of the capillary pressure-saturation curve hysteresis. Rose (1972) noted that static capillary pressure measured in the laboratory is different from capillary pressure under dynamic conditions because of

the influence of hydrodynamic forces. The rate of fluid flow has no effect on relative permeability as long as it does not create a saturation gradient caused by inertial effects at higher flow rates and by capillary end effects at lower rates (Geffen et al., 1951; Sandberg et al., 1958; Labastie et al., 1980).

With the increased emphasis on the development of thermal recovery processes, hysteresis becomes important in the case of injection-production cycles in altering the direction of saturation changes of the fluids. Coats et al. (1977) proposed a pressure dependent water relative permeability model, since imbibition is marked by a pressure rise and drainage by a pressure drop. Dietrich (1981) indicated that the effects of hysteresis and variations in effective stress have to be evaluated during laboratory studies of relative permeability if those are to be used in cyclic steam stimulation predictions. He indicated that extreme differences existed between the relative permeability curves estimated by matching field history and those determined experimentally.

2.2.1 Wettability

The relative permeability properties of a porous medium depend on saturation and saturation history, pore size and geometry, and contact angle as discussed earlier. These parameters control the capillary pressure characteristics for a given fluid-liquid-rock system and the microscopic distribution of the fluids in the pore space. By means of the contact angle, which is one measure of the

wetting behaviour of a rock surface, a direct dependence of relative permeability on wettability can be established.

Owens and Archer (1971) studied the effect of contact angle on relative permeability. They found that imbibition relative permeability to both oil and water depends on the contact angle: oil relative permeability is highest and water relative permeability is lowest for water-wet conditions. This seems to suggest that the wetting properties of a rock can be inferred from relative permeability measurements. In his monograph, Craig (1971) gives rules of thumb on the shape of relative permeability curves depending on wettability for strongly water-wet and strongly oil-wet porous media. Usually, rocks are found to have an intermediate wettability (Salathiel, 1973), with no strong preference for either water or oil. Craig suggests that intermediate wettability rocks have some of the relative permeability characteristics of both water-wet and oil-wet formations.

2.2.2 Viscous and Capillary Forces

The measurement of relative permeability is significantly affected by the test environment, which consists not only of the temperature and pressure, but also of the fluids used and the core conditions. Wettability is an important variable and also depends on the experimental procedure and conditions. In addition, the interplay of viscous and capillary forces during the displacement of oil by water must be considered in terms of the fluid properties,

namely viscosity (absolute and/or ratio of non-wetting to wetting phase) and interfacial tension. These parameters are recognized as part of the scaling criteria for displacement processes and are discussed below separately and in combination with other factors affecting relative permeability.

The extension of Darcy's equation to multiphase flow was questioned (Yuster, 1951; Odeh, 1959; Rose 1972) since a slip condition at the fluid-fluid interface would mean a non-zero velocity at that boundary, implying a dependence of relative permeability on viscosity ratio. Odeh (1959) observed that relative permeability to the non-wetting phase increased with viscosity ratio, being greater than unity for higher ratios. He also noted that for an absolute permeability value greater than one darcy, the effect of the viscosity ratio became negligible. Lefebvre du Prey (1973) showed that the viscosity ratio had considerable influence on both relative permeabilities and residual saturations by observing that an increase in the viscosity of one of the liquids decreased the relative permeability to the other liquid.

Relative permeability was found to be independent of flowing fluid viscosities (Sandberg et al., 1958; Donaldson et al., 1966) when similar wetting conditions existed. Ehrlich and Crane (1969) concluded from their theoretical model that relative permeability was independent of viscosity ratio everywhere except near the irreducible wetting phase saturation which itself decreased with an increase in the non-wetting to wetting phase viscosity ratio.

Danis and Jacquin (1983) showed that oil relative permeabilities at residual water saturation may depend on oil viscosity under various conditions and that the influence of viscosity on oil relative permeability seemed to be greater as the porous medium became more complex. This could explain the differences reported by various researchers regarding the effect of viscosity on relative permeability.

An important property which gives rise to capillary pressure in a porous medium is the interfacial tension of the fluids used. An increase in oil recovery resulted from lowering the interfacial tension (Wagner and Leach, 1966; Batycky and McCaffery, 1978) accompanied by a decrease in the hysteresis of the oil/water relative permeability properties which eventually disappeared at the lowest interfacial tension (0.02 mN/m). By reducing the interfacial tension even further, the curvatures of the relative permeability-saturation curves decreased to approach straight lines with an increase in the end point residual saturations to both oil and water (Bardon and Longeron, 1980; Amaefule and Handy, 1982).

A dimensionless group representing the ratio of viscous to capillary forces called the capillary number, N_c, is used in the literature to express the dependence of ultimate recovery on viscous and capillary forces. The formulation for the capillary number varies from author to author, but for an ordinary water flood its typical value is of the order of 10^{-6} (Foster, 1973). Moore and

Slobod (1956), using $N_c = v\mu/\sigma\cos\theta$, showed that breakthrough recovery was a unique function of the capillary number in water-wet porous media. Lefebvre du Prey (1973) preferred to separate the influence of the contact angle, θ, due to the difference in wettability of the fluids and by using $N_c' = v\mu/\sigma$, was able to increase its value by varying each of the parameters. He showed a corresponding increase in relative permeabilities in doing so. Abrams (1975) showed that the viscosity ratio exerted an influence on the residual saturation left by a water flood and expanded the dimensionless scaling group describing the ratio of viscous to interfacial forces to $N_c = (v\mu_w/\sigma_{o-w})\cdot(\mu_w/\mu_o)^{0.4}$ by including viscosity effects.

Melrose and Brandner (1974) defined a microscopic displacement efficiency, E_m, which they correlated with the capillary number. They obtained a critical value for N_c which, when exceeded, permitted the microscopic displacement efficiency to increase to unity. Below this critical point, however, E_m was independent of the capillary number, as observed earlier (Lefebvre du Prey, 1973; Foster, 1973). Based on the premise that the critical value of N_c is reached when viscous forces begin to compete with capillary forces, they calculated this critical value to be approximately 10^{-3}. From an experimental point of view, the easiest way to significantly increase the capillary number is to lower the interfacial tension. Hence, the effect of capillary number on relative permeability would follow the same trend as that previously reported for interfacial tension.

Fulcher et al. (1985) studied the effect of capillary number and its constituents on two phase relative permeabilities. Based on experimental and computational observations, they concluded that non-wetting (oil) relative permeabilities were functions of the interfacial tension and viscosity individually, rather than the capillary number. On the other hand, wetting phase (brine) relative permeabilities behaved as functions of the capillary number but were better modelled using individual variables. Further observations regarding the effect of the individual constituents of the capillary number (interfacial tension, viscosity, and velocity) did not significantly differ from previous reports.

2.2.3 Pressure and Temperature

Laboratory measurements of relative permeability are used to represent and scale field conditions. With the increasing development of thermal recovery processes, the effects of pressure and temperature on relative permeability must be included in any study simulating in situ conditions along with the other parameters discussed above. Due to the paucity of the data available, the dependence of relative permeability on the pressure gradient is unclear (Fatt, 1953). External pressure may however have an effect on the relative permeability as overburden pressure was found to change the porosity and absolute permeability of rock samples (Gobran et al., 1981).

Temperature effects, on the other hand, have received much more attention since the [illegible]0s. Contradictory results were obtained, mainly because different systems were used, and this issue is still highly controversial. Tables 2.1 and 2.2 present a summary of the observations reported in the literature for unconsolidated and consolidated porous media, respectively. Nakornthap and Evans (1986) summarized the most commonly observed temperature effects in proposing a theoretical model. The following general trends emerged:

- Residual oil saturation decreases and irreducible water saturation increases with increasing temperature. This shift in saturation also affects relative permeability.
- At a constant saturation, there is a considerable increase in relative permeability to oil and a decrease in relative permeability to water with an increase in temperature.
- The water/oil relative permeability ratio increases with temperature in unconsolidated sand, whereas it decreases in consolidated rocks. These differences could be explained by the fact that low residual oil saturations exist in the former, while the reverse is true for the latter.

Two recent studies performed in clean unconsolidated sand cores using white mineral oils (Sufi et al., 1982; Miller and Ramey, 1985) showed that residual saturations and relative permeability relationships were virtually unaffected by temperature. The main conclusion of these studies was that previously reported results

Table 2.1 : Summary of Temperature Effects on Relative Permeability Studies in Unconsolidated Porous Media

oil type	core type	temperature range (°C)	temperature effects on end point saturations	temperature effects on relative permeabilities	comments	reference of publication
			Steady State Measurements			
refined	extracted	20 - 80	yes	N/A	-convex oil curve for high μ_o	Combarnous and Pavan (1968)
			Dynamic Displacement Measurements			
refined	extracted	24 - 282	N/A	yes	-μ_o adjusted for dissolved water	Davidson (1969)
refined	extracted	24 - 135	yes	yes	-water wetness increases with T	Poston et al. (1970)
refined	extracted	21 - 86	no	no	-homogeneous system	Sufi et al.(1982)
crude	preserved	20 - 272	yes	yes	-very low k_{rw} at low T	Maini and Batycky (1983)
refined	extracted	21 - 146	no	no	-no T effect on k_o	Miller and Ramey (1985)
crude	extracted/ preserved	27 - 220	yes	yes	-k_{rw} much lower for extracted core	Bennion et al. (1985)
crude	extracted	21 - 200	no	yes	-fixed end points -effect on k_{ro} unclear -k_{rwro} increases greatly	Maini and Okazawa (1986)

Table 2.2 : Summary of Temperature Effects on Relative Permeability Studies in Consolidated Porous Media

oil type	core type	temperature range (°C)	temperature effects on end point saturations	temperature effects on relative permeabilities	comments	reference of publication
			Steady State Measurements			
refined	extracted	29 and 71	no	no	-no change in μ_r	Wilson (1956)
refined	extracted	25 - 149	yes	yes	-no effect for const. μ_r -some oil curves convex	Lo and Mungan (1973)
refined	extracted	22 - 175	yes	yes	-oil chosen to minimize μ_r effect -more hysteresis at low T	Torabzadeh and Handy (1984)
			Dynamic Displacement Measurements			
refined/ crude	extracted	24 - 260/ 24 - 149	yes	yes	-k_r ratio independent of T when same μ_r	Edmondson (1965)
refined	extracted	22 and 79	yes	yes	-k_o decreases as T increases -oil curve nearly linear	Weinbrandt et al. (1975)
crude	preserved	20 - 200	yes	yes	-40% increase in E_d	Abasov et al.(1976)
refined	extracted	21 - 146	no	no	-use k_o as base for k_r	Miller and Ramey (1985)
			from Capillary Pressure Measurements			
refined	extracted	21 - 163	yes	yes	-more hysteresis at low T	Sinnokrot (1971)

for unconsolidated sands may have been affected by viscous instabilities, capillary end effects, and/or difficulties in maintaining material balances. The authors noted that there was no way to evaluate such problems in others' works. They did not prove that temperature effects were non-existent for real reservoir rocks and fluids, but only implied that such effects were probably unrelated to fundamental flow properties.

2.3 Published Heavy Oil Relative Permeability Data

Due to the experimental difficulties encountered in determining relative permeabilities, a suitable laboratory procedure that eliminates inlet and outlet end effects and the resulting saturation gradients must be used. Usually, experimental conditions are idealized and simplified by the use of small core plugs or reconstituted sand cores, and refined oils rather than native reservoir materials. Thus, very few experimental data on relative permeability involving heavy oil or bitumen are reported in the literature. This section contains published relative permeability data for the oil sand and heavy oil deposits of Alberta. The data presented were either determined experimentally or obtained from history matching, and are grouped according to the location of the deposit.

Earlier experimental studies conducted at the Alberta Research Council were aimed at determining relative permeability curves for the Athabasca oil sands as a function of temperature. The work

concentrated on obtaining end point saturations and permeabilities using the steady state method. The first set of experiments involved cores packed with mined Athabasca oil sand; the test procedure and results were reported by Polikar (1980). Bitumen was first displaced from the cores with hot water, and some were subsequently flooded with bitumen to irreducible water saturation. A lack of reproducibility of the results between 55 and 250°C was attributed to the heterogeneity of the oil sand samples.

Leung (1982) reported end point data and relative permeability curves obtained by history matching the performance of a well for Athabasca bitumen recovered by steam stimulation, and did not take into account temperature effects on the end points for his numerical evaluation. Edmunds (1984) used two phase oil/water and oil/gas relative permeability data in developing a model of the steam drag effect in oil sands. The effective oil permeability at connate water saturation with no gas present was the base permeability for his data. He did not consider temperature effects. The relative permeability curves he used were representative of a clean unconsolidated sand but were adjusted to fit Stone's (1973) model for three phase data.

In situ thermal recovery processes in Alberta were first applied in Cold Lake oil sands. There are more field data available for this than for any other Canadian heavy oil/oil sand deposit but no experimental relative permeability data were published to date. Coats (1976) reported relative permeability data he used in a

three dimensional numerical model for simulating steam injection processes where he derived the relative permeabilities from field production data presented a decade earlier (Samoil, 1966). These data were used in their unaltered form by Stone and Malcolm (1985) to history match large scale experiments with Athabasca oil sands.

Settari and Raisbeck (1981) used oil/water relative permeability data in modelling hydraulic fracturing during cyclic steam stimulation of Cold Lake oil sands. Their data were also derived from a field pilot's production history. Dietrich (1983) analyzed cyclic steam stimulation above the fracturing pressure using a numerical model. He used power law expressions for the relative permeability functions, taking into account imbibition and drainage hysteresis effects, and included the effect of temperature on end point saturations and water relative permeabilities.

Lloydminster heavy oil has received a lot of attention because of its lower viscosity at reservoir conditions. Most reported experimental data originate from the Petroleum Recovery Institute (PRI) in Calgary. Sayegh and Maini (1983) carried out laboratory tests with field heavy oil and brine, preparing their core with unconsolidated sand from a fresh core sample. The stock tank oil was cleaned by centrifugation to remove water and suspended fines. Relative permeabilities were determined under reservoir conditions using a computer history match of the production and pressure drop data obtained during unsteady state displacements. The end point water saturation was extrapolated to a higher value as some oil

was still being produced after two pore volumes of water injection. From experimental curves, these authors derived empirical expressions between the effective permeabilities and saturations.

Maini and Batycky (1983) measured oil/water relative permeabilities with preserved core materials under simulated downhole conditions of confinement, pore pressure and temperature, and used stock tank heavy oil from the same pool. Their experiments were conducted between 23 and 272°C, on horizontally and vertically drilled core plugs. The results indicated a shift towards higher water saturations and a decrease in the oil/water relative permeability ratio with increasing temperatures. They also measured very low end point water relative permeabilities, especially at lower temperatures. These effects were less marked in the horizontally drilled core plugs than in the vertical plugs. Subsequent work in the same laboratory was performed on clean unconsolidated sands with a crude and a refined oil (Maini et al., 1985). Temperature effects were found to be absent in the mineral oil but present in the crude oil. However, caution should be applied to the interpretation of these results as the experiments were not performed in the same manner for both oils.

Bennion et al. (1985) measured relative permeabilities for a preserved core from the Sparky sand of the Lloydminster area at reservoir and steamflood temperatures. They compared their results with those obtained for an extracted core from the same formation. The latter exhibited much lower irreducible water saturation than

found in the field and had an effective water permeability at residual oil saturation much higher than that measured for stressed preserved cores and actual reservoir fluids. They subsequently showed that preserved core relative permeabilities gave a much closer match to field data than those from extracted cores. Besides the experimental data reported, Adams (1981) presented end point saturations and relative permeabilities for three different Lloydminster fields.

Waxman et al. (1980) conducted Peace River tar flow experiments under in situ conditions and reported steady state relative permeability data for only one core in which they used deasphalted tar which yielded steady state pressure drops across the core for constant tar/brine flow. Closmann et al. (1985) reported steady state tar/brine relative permeabilities at 196°C for undisturbed core samples. They used three types of Peace River tar: (1) unaltered tar, (2) thermally-altered tar, and (3) deasphalted tar. Most of their flow measurements were made with the unaltered tar obtained by cold solvent extraction from core material. A few measurements were also made with the thermally-altered (field-produced) and deasphalted unaltered tars. The relative permeabilities reported for the thermally unaltered tar were in a region of water saturation comparatively lower than was expected. Considerably different results were obtained with the other two tars. They also found that the limited oil and water relative permeability values measured for the thermally-altered tar agreed with the numerical simulation curves used in their Peace River studies.

Ehrlich (1977) presented results of displacement studies in Wabasca Grand Rapids "A" cores. Residual oil saturations of 25-30% pore volume were observed in hot water floods (93-149°C), regardless of the initial oil saturation whereas steam at 204°C left a residual oil saturation of about 20%. Fewer pore volumes were required to reach the steam residual due to lower effective mobility of steam compared to hot water. Relative permeabilities were measured using a modified Penn State method with high flow rates to minimize capillary end effects. Reported data include water/oil relative permeability ratio curves for brine and caustic solutions displacing heavy oil at 149°C. Gas and water relative permeabilities and corresponding water saturations as a function of steam quality were reported for steam displacement runs in an initially water flooded core.

2.3.1 Observations

As heavy oil/water systems were studied in great depth, this discussion is limited to the end points of the relative permeability curves. An examination of the relative permeability data reported in the previous section led to the following observations:

- The typical range encountered for connate water saturation is between 10 and 40%. However, laboratory measured connate water saturations in unconsolidated sand packs can be lower. As temperature increases, the connate water saturation approaches the upper limit of the 10-40% range.

- Residual oil saturations have been reported to be as high as 50% of the pore space. This can be explained by the fact that fingering can occur when water displaces a viscous oil, leaving a large residual oil saturation. With increasing temperature and a subsequent decrease in the oil-to-water viscosity ratio, residual oil saturations have been found to decrease to as low as 10%.
- End point relative permeabilities, based on the absolute permeability of the porous medium, are generally greater than 0.6 and smaller than 0.3 for oil at connate water saturation and water at residual oil saturation, respectively. The ratio of oil-to-water end point relative permeabilities was generally found to be larger than about 2.5, which agrees with the values reported by Craig (1971) for water-wet systems. It is worth noting that the end point water relative permeability was, in most cases, higher for imbibition than for drainage.

An examination of the published data reveals that researchers used a variety of curves for relative permeability. No direct comparison is undertaken here between experimentally (laboratory) and theoretically (numerical simulation) determined relative permeability relationships. A single set of curves does not seem to exist for any of the Alberta heavy oil/oil sand deposits.

3. EXPERIMENTAL APPARATUS AND PROCEDURES

3.1 Apparatus

The experimental apparatus was designed to perform displacement studies in cores under isothermal conditions up to 300°C, and to measure two phase steady state relative permeabilities. A schematic diagram is shown in Figure 3.1. Any modifications to the apparatus will be reported as they occur.

3.1.1 Core Holder

The core was packed inside a copper sleeve, which in turn was contained in a steel pressure vessel, and constant overburden pressure was applied in the annular space between the pressure vessel and the sleeve using water. A detailed schematic of the core holder is shown in Figure 3.2. The body was about 23 cm long, with an internal diameter (ID) of 4.23 cm.

The copper sleeve was flared at both ends and held between flange joints to seal the internal fluids from the overburden fluid. Copper was chosen for its machinability and for its compatible thermal expansion coefficient with mild steel. To fabricate the sleeve, the wall thickness of a 3.88 cm ID copper tubing was machined down from 0.13 to approximately 0.03 cm. The copper was then softened by heating to 510°C in a muffle oven for 15 minutes

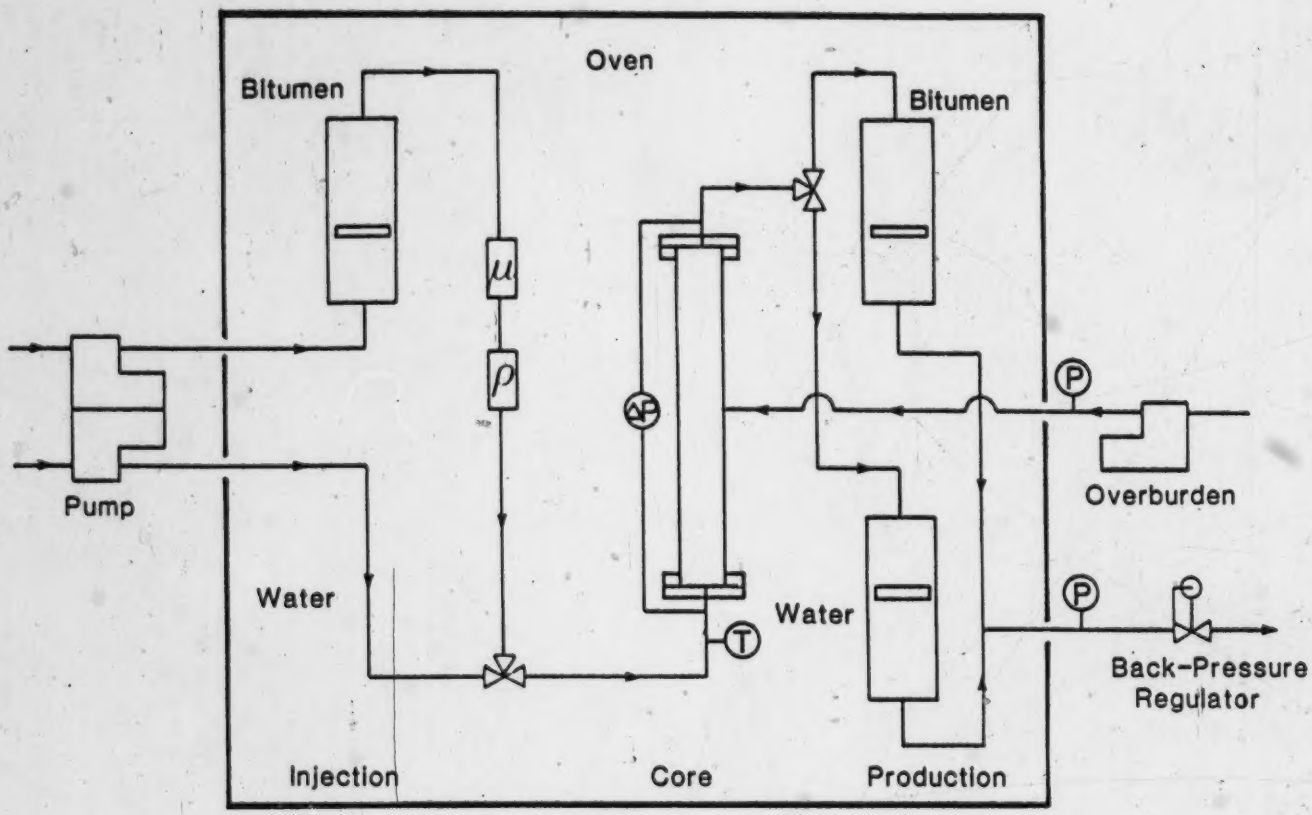

Figure 3.1 : Schematic Diagram of Relative Permeability Apparatus

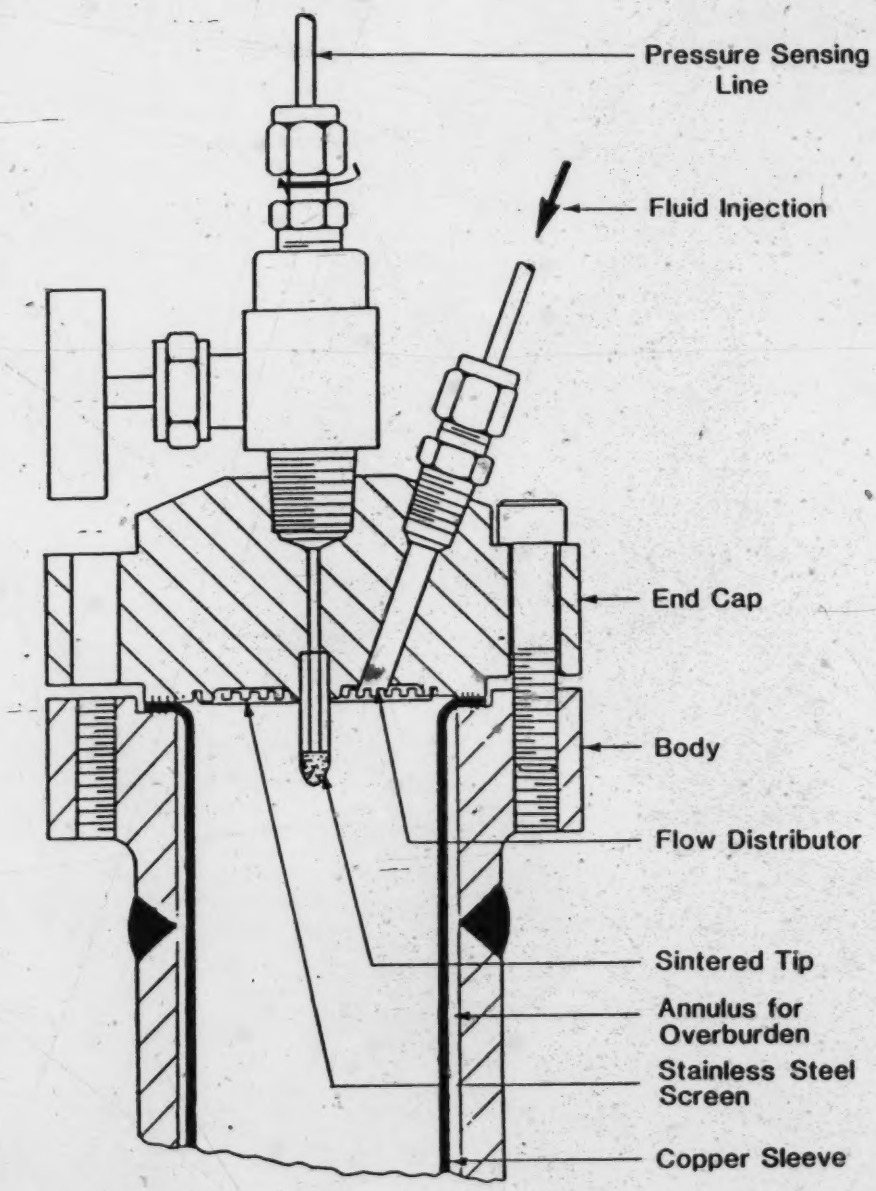

Figure 3.2 : Core Holder (end cap detail)

with subsequent quenching. It then provided a leak-proof sleeve capable of operating at temperatures up to 250°C with 14 MPa net confining pressure under flow conditions, and compared favorably with a lead sleeve by providing close contact between the sand grains and the sleeve.

The end caps were equipped with flow distributors for even distribution of injected or produced fluids over their entire cross-section. A 400 mesh stainless steel screen was spot welded onto the flow distributor to prevent any fine sand from plugging the flow lines. The central portion of each end cap was equipped with a pressure probe connected to the pressure sensing lines, and a sintered tip for keeping the fine sand out of the lines was attached to the end of these probes.

3.1.2 Injection Equipment

A positive displacement pump controlled the rate of flow of the injected fluids. The fluids were located in a main oven and heated to the experimental temperature for the duration of each run. Water was contained in tubing; bitumen in an accumulator equipped with a floating piston. The residence time of the fluids was long enough to reach the experimental temperature before entering the core. Most of the valves could be operated from outside the oven and a pressure relief valve was placed in the injection line to the core.

To minimize its decomposition above 175°C, the bitumen was pre-heated in a small oven to approximately 90°C. A capillary tube viscometer and a pycnometer, located in the bitumen injection line, were used to measure bitumen viscosity and density, respectively, at operating conditions.

3.1.3 Production Equipment

Accumulators with floating pistons were used to collect production fluids. Separate accumulators were used for each portion of the flooding sequence, and were initially filled with water. They were kept in the small oven at 90°C, unless the experiment was conducted below 200°C (same arrangement as for injection). As production fluids were collected, the water was pushed out through a back-pressure regulator located outside the main oven which maintained a constant discharge flow pressure.

3.1.4 Pressure Measurement

Pressures and temperatures were monitored throughout the system as indicated in Figure 3.1. Three differential pressure transducers to record the pressure drop across the core were placed in parallel so that the appropriate and most sensitive range could be used during any measurement. A separate transducer was used for the viscometer.

3.2 Materials

3.2.1 Sand

The cores were prepared from clean, unconsolidated Ottawa sand. Large batches of F-140 sand were sieved, and the fraction smaller than 140 mesh was used for packing (see Section 3.3). An example of the fractional grain size distribution is given in Appendix C. Because of variations in the original sand, each batch of sieved sand had a slightly different grain size distribution, resulting in a slightly different average grain size. However, in every case, more than 70% of the sand was in the 170-230 mesh fraction. This narrow distribution resulted in homogeneous packing that gave reproducible core properties for each batch.

Several native oil sand samples were taken during the summer from the mine site of the Suncor, Inc. plant (Fort McMurray, Alberta). Samples were cored manually from a high grade Athabasca oil sand face after removing the weathered surface layer. Core barrels, having the same internal diameter as the copper sleeves, were pushed into the sand face to a depth of approximately 30 cm and removed by rotation to avoid further disturbance of the sample and surrounding area. The cores were immediately frozen in dry ice to preserve the natural distribution of the fluids. A dozen samples were cored, one next to the other, by following the dipping in the depositional pattern. Flow experiments were conducted on these

samples shortly after the coring to minimize the drying of the water film surrounding the sand grains while in a frozen state.

The samples used in the experiments contained, on the average, 88.2 wt % sand, 11.6 wt % bitumen and 0.2 wt % water, which corresponds to an initial oil saturation of 0.98. Despite the precautions taken, the initial water content of these samples was very low. The grain size distribution of the dried sand is presented in Appendix C. In comparison to the Ottawa sand, this sand is poorly sorted and extremely coarse, as can be seen in Figure 3.3, and contains a considerable amount of fines (in excess of 5 wt %).

3.2.2 Water and Brine

Deionized water was used in all experiments. The viscosity and density data for water were taken from steam tables by Schmidt (1979), and intermediate values were interpolated using a cubic spline. The water properties used in the calculations are reported in Appendix D.

An aqueous solution of 0.0704 molal sodium sulphate was used for two experiments at 150°C to study the effect of brine (see Section 5.1.3). The viscosity and density of this solution at the experimental conditions were estimated from the data of Korosi and Fabuss (1968) who measured the density and viscosity of several solutions as a function of solute concentration near atmospheric pressure up to 150°C. Their data have been linearly interpolated

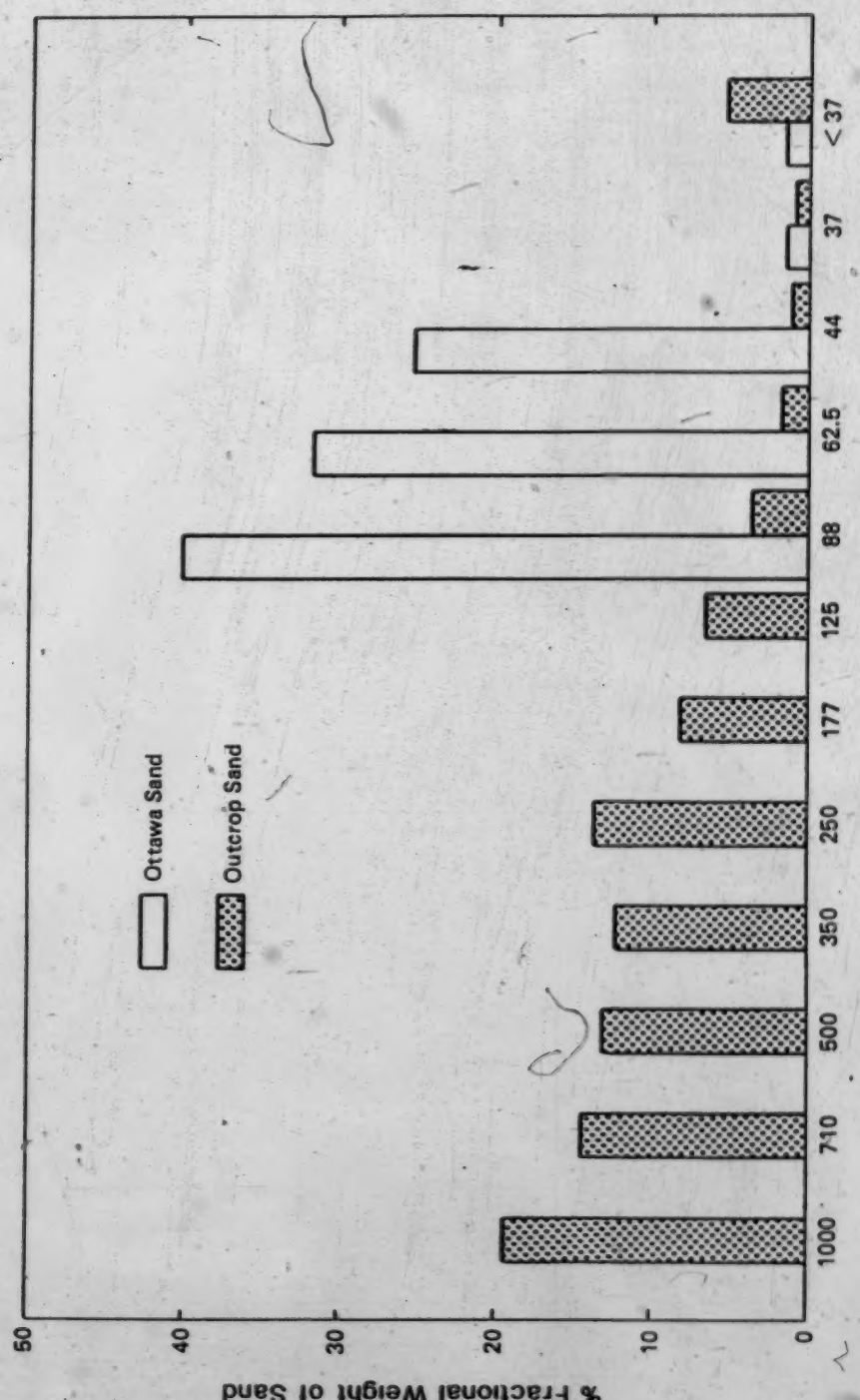

Figure 3.3 : Comparison of Particle Size Analysis (clean versus outcrop sand)

for concentration at fixed temperatures and pressures and the estimation of the properties of a 0.0704 molal sodium sulphate solution at the prevailing experimental conditions was possible (see Appendix D). The pressure correction for viscosity and density of the dilute sodium sulphate solution was assumed to be the same as for water.

Sodium chloride brine having a concentration of 0.05 M was chosen for the outcrop sand experiments, as the previously used sodium sulphate was found to react with the clay minerals. Ion exchange between sodium from the brine and calcium from the clays resulted in calcium sulphate precipitation (Gunter, 1986). The relative viscosity and density of this brine were calculated from the correlations of Numbere et al. (1977), as presented in Appendix B.

3.2.3 Bitumen

The bitumen used in this study was solvent-extracted from high grade Athabasca oil sand. A large batch of this bitumen was homogenized by mixing overnight in a large rotating flask at 30°C. To preserve the homogeneity of each batch, the bitumen was then stored in a refrigerator. Three such 10 L batches were used in the experiments. The measured physical properties of these bitumen batches fall within the typical range reported for the Athabasca deposit (see Appendix D), and were consistent for all bitumen batches. However, in order to take into account differences between batches, the viscosity and density of bitumen were measured

during each flooding experiment at the prevailing experimental conditions.

3.2.4 Kaydol

Kaydol is a USP-grade heavy white mineral oil manufactured by Witco Chemical. The manufacturer specifies a specific gravity range of 0.869-0.884 at 25°C and a kinematic viscosity range of 64.5-68.5 cs at 40°C. As done for bitumen, the density and viscosity of this oil was determined at experimental conditions. Among equivalent mineral oils is Chevron's #15 white mineral oil that has been extensively used for relative permeability determinations reported in the literature. Kaydol was used for comparing the results of the present study with published works, and it allowed a different temperature range for similar viscosity values when compared to bitumen.

3.3 Core Packing Procedure

A major purpose of this study, in addition to relative permeability experiments, was to develop a reproducible packing procedure for clean unconsolidated sand cores to simulate oil sand cores. This packing technique was primarily used to prepare cores for relative permeability measurements, but found also favour in other core-size displacement experiments conducted in the laboratories of the Alberta Research Council.

The following approach was used to determine the optimal packing procedure. A transparent lucite tube having the same dimensions as the cores to be used in the relative permeability experiments was built for visualizing the packing procedure, with no provision for applying overburden pressure. Clean Ottawa sand was screened into its various size fractions, and the lucite tube was packed by allowing a given sand fraction contained in a separatory funnel to fall freely into the vertically positioned core which was vibrated during the packing operation. Figure 3.4 shows a schematic of the packing apparatus. Both dry and wet packing were attempted. For the latter, the water level was maintained approximately 2.5 cm above that of the sand in the core at all times.

Target porosities of less than 35% and absolute permeabilities of 1.5 to 2 Darcies (d) were sought, based on the available data from various Alberta oil sand deposits (Carrigy, 1967). A uniform packing density was also desired.

All packing experiments were carried out at room temperature. Porosity was determined from the volume of the sand packed into the core holders's known volume. Using Darcy's equation, absolute permeability was calculated from the pressure drop observed during the upward flow of water through the core (see Appendix B).

The following parameters were considered in determining the best possible packing procedure:

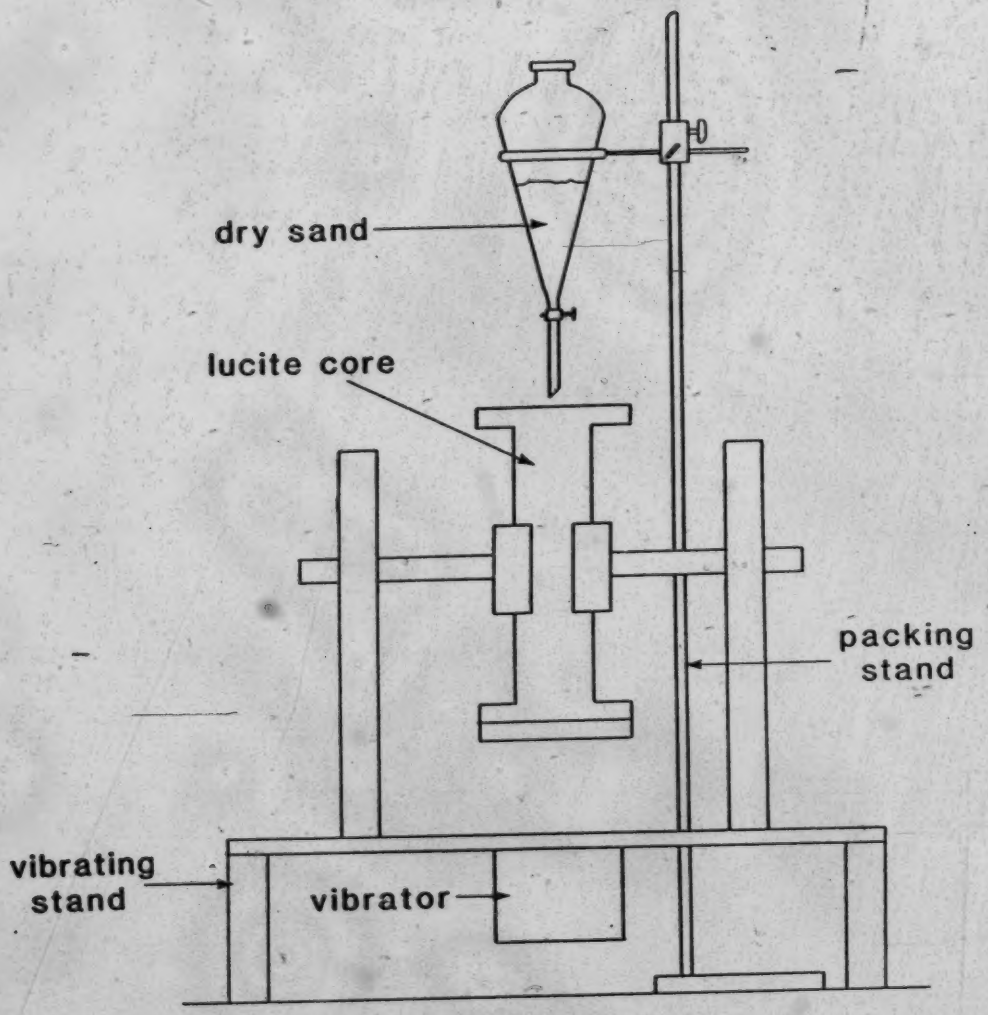

Figure 3.4 : Schematic of the Packing Apparatus

1. sand grain size distribution
2. type of packing
3. sand fall rate
4. vibration setting and duration.

3.3.1 Preliminary Packing Experiments

The observations of Naar and Wygal (1962) were used as the basis for the core packing procedure. They indicated that for a narrow grain size distribution, porosity and pore geometry are independent of the grain size. Also, all such uniform size packs have the same porosity of 36.2% and permeability varies with the square of the grain size. However, for aggregates composed of only two sizes of particles, the porosity and permeability of these binary mixtures must be determined experimentally, and depend on the proportion and arrangement of the finer and coarser grains.

Initially, a large batch of clean 70-140 nominal mesh size Ottawa sand was sieved into various fractions. Most of the sand particles were larger than 105 μm, with an average particle diameter of approximately 142 μm, as shown in Appendix C.

The various grain size fractions were used individually or in predetermined proportions for preliminary trials. The results of these experiments are detailed in Appendix A. An equal mixture of 60-80 and 120-140 mesh sand, both in the dry and wet modes, were used in the first nine packing tests. In two cases, wet sand was

dried and reused. This gave rise to fairly high porosities and absolute permeabilities; it was then decided to use only the original sand. On average, the dry packing method resulted in porosity and permeability values lower than those obtained by the wet packing method but these values were still outside the desired range.

To achieve lower values of porosity and permeability, a finer size sand was needed for mixing with the coarser sand. To extend the range of grain sizes below 230 mesh, F-140 mesh Ottawa sand was found to have an average particle size of 90 μm. Only the fraction of this sand finer than 140 mesh (labelled L-140 sand), with an average particle size of 72 μm, was used in subsequent experiments. This fraction is referred to as 200 mesh sand and its grain size distribution is given in Appendix C.

Nine other packing experiments were conducted with mixtures of coarse (80-100 mesh fraction of the 70-140 sand) and fine (200 mesh fraction of the F-140 sand) sand in various proportions. As the amount of the coarse sand decreased in the mixture, so did the porosity and absolute permeability of the packs. Porosities of less than 34% and permeabilities of less than 3 d were obtained for the wet packs, and lower values for the dry packs.

Too high a vibrator setting caused very high porosity in the cores, whereas too low a setting did not result in any visible movement of the sand. The final setting of the amplitude of the

transducer attached to the vibrator was made to give slow movement of the sand grains inside the core holder, as observed visually. The setting depended on the total mass of the core holder and sand assembly.

3.3.2 Packing Density

The packing densities of the cores were determined by a one-dimensional x-ray absorption scanning technique (Miles-Dixon et al., 1982). An example of packing density variation is shown in Figure 3.5. The bottom portion of core A was more tightly packed than the top. By continuing vibration for an additional hour after the packing operation, the density variation decreased (core B). The x-ray absorption technique can be used to determine the porosity of a core; however, the x-ray scan of a wet core gives lower counts than that of a dry one because of the added attenuation due to the presence of water. Porosity is calculated from the difference of the dry and wet scans. This method was used to confirm the porosities obtained from the core parameters.

Cores packed in the presence of slight excess of water had distinct layering which disappeared when the core was initially at least half filled with water. Despite the visually observed layers, the pressure drops across these cores were always very steady during water flow required for the measurement of absolute permeability. The dry packs did not display layering.

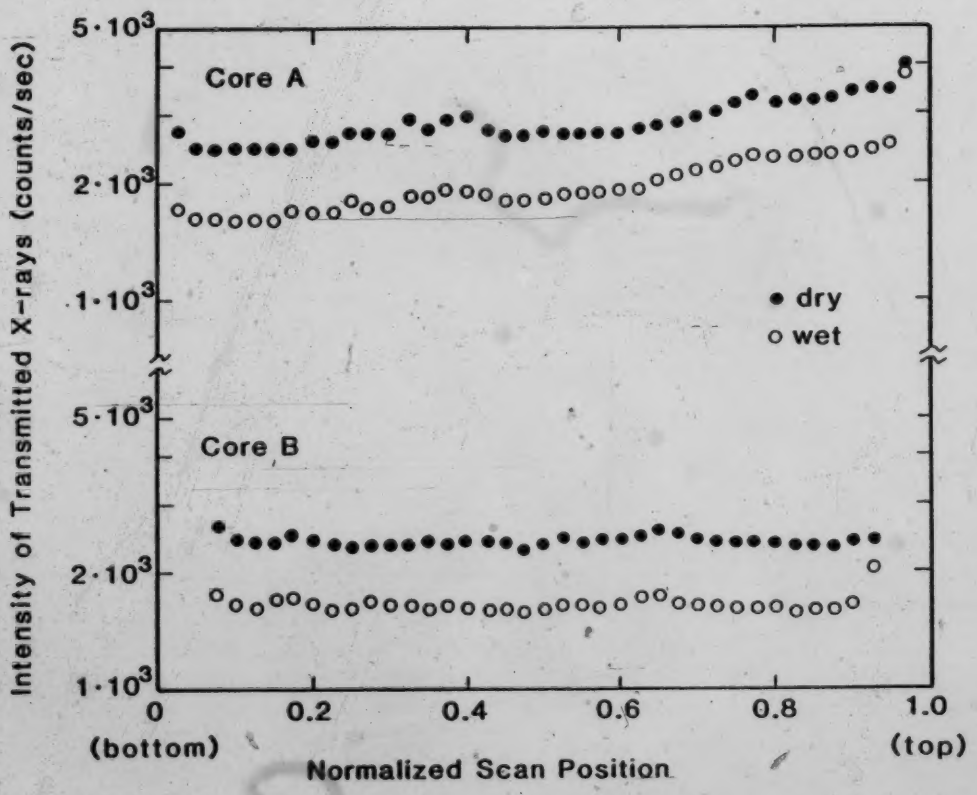

Figure 3.5 : Packing Density along the Length of the Core

3.3.3 Packing Procedure

On the basis of the preliminary packing experiments and observations described above, a dry packing procedure with 200 mesh sand was developed. Dry packing has the advantage of determining porosity directly without having to dry the core.

The packing was performed at a sand fall rate of about 10 g/min under constant vibration. The vibration of the core was continued for twice the duration of the packing, resulting in a total vibration time of 1.5-2.0 hours.

The porosity of the core was first determined from the packing parameters (see Appendix B). The dry core was then subjected to an overburden pressure of 34.5 MPa for at least 24 hours to seal the sand pack in the copper sleeve. Before the start of an experiment, this pressure was reduced to the desired value of 17.5 MPa, corresponding to 10.5 MPa of net confining pressure.

The absolute permeability of the core remained nearly constant upon any further increase of confining pressure. The measured pore volume changed by approximately 10% after the application of the confining pressure, as determined at the end of each experiment, corresponding to a decrease of about 2% in porosity. The packing procedure described above was used for all cores prepared for relative permeability measurements.

3.3.4 Cleaning Procedure for Reuse of Cores

A solvent cleaning procedure was devised to reuse the cores for subsequent experiments. Toluene was used to remove the bitumen, followed by a series of more polar compounds to restore the original water-wet behaviour of the oil sand (Cottrell, 1963; Takamura, 1982). First, the sequence methanol-acetone-nitrogen-water was tried. This left a bitumen residue in the core. Then, isopropanol-water-superheated steam-water was used. This sequence proved effective in cleaning the core, but was rejected because of the gradual but persistent decrease in absolute permeability after each experiment. This decrease was attributed to the migration of fines under the influence of locally created pressure gradients during steam injection and the change in wettability of the sand pack due to the use of organic solvents. Therefore, the core cleaning approach was eventually abandoned in favour of packing a new core for each experiment.

3.3.5 Packing of Reservoir Oil Sand

A press was initially used for the transfer of the frozen cores from the core barrel to the core holder but compressed the oil sand to the extent of damaging the sleeve while not completely filling the core holder. To avoid compaction of the oil sand, the frozen core was cut into several plugs after having removed the core barrel, and packed end to end into the sleeve. Both ends of the original sample were removed before packing and analyzed for

its undisturbed components. After thawing the sample in the core holder, the confining procedure used for the Ottawa sand was applied. The absolute permeability of the sand was determined at the end of the flooding experiments after removing the residual bitumen from the core by solvent-extraction.

3.4 Flooding Sequence

3.4.1 Absolute Permeability Measurements

A dry, clean Ottawa sand core was packed and confined according to the procedure outlined in Section 3.3.3. The core was then evacuated before being wetted with deionized water. In order to saturate the pore space, the water was injected vertically upwards. Usually 3-4 pore volumes (PV) of water were needed at room temperature, at an injection rate of about 0.9 PV/h, to obtain a stable pressure drop across the core, indicating stabilized flow. The absolute permeability of the core was determined from this stabilized pressure drop. The temperature of the system was then increased to the desired level while maintaining a constant back-pressure. The absolute permeability of the core was measured again at the stabilized experimental temperature and pressure drop with the flow of water.

3.4.2 Preparation of Synthetic Oil Sand Cores

Bitumen was injected from the bottom into the water-saturated core at the same nominal flow rate of about 1 PV/h. Injection of 2 PV

of bitumen was usually sufficient for the pressure drop to stabilize. The end point effective permeability to bitumen was then determined from this stabilized pressure drop. At this point a synthetic oil sand core, saturated with bitumen at irreducible water saturation, had been prepared.

3.4.3 Displacement Experiments

Three types of experiments were conducted in the imbibition mode for the displacement of the initial bitumen-in-place from the synthetic oil sand cores. The experimental flooding conditions are presented in Table 3.1 and were not modified during the course of the experiments to avoid introducing variables other than temperature. First, a hot water flood was used to determine end point (residual bitumen) conditions. Then, intermediate point conditions were determined by injecting various mixtures of hot water and bitumen. Finally, long-lasting hot water floods were conducted to study the transient behaviour of the bitumen displacement process.

The same flooding sequence of water-bitumen-water or mixture was used in all experiments. Flow was maintained continuously through the core from the start to the end of each experiment. To ensure that no water vapour was present throughout the system at any temperature, including the heating period, the back-pressure regulator was kept at 7 MPa. This pressure is above the vapour pressure of water at the highest experimental temperature studied.

Table 3.1 : Experimental Flooding Conditions

Discharge Pressure (P_{bpr})	7.0 MPa
Overburden Pressure (P_{ovb})	17.5 MPa
Nominal Flow Rate ($q_{w,pump}$)	80 cm^3/h at room temperature
Temperature Range (T_{exp})	100 - 250°C at 25°C intervals

3.4.3.1 End Point Calculations

The injection rate and direction of flow for the hot water floods were the same as for the bitumen flood used to prepare the synthetic oil sand core. Triplicate experiments were conducted in the temperature range of 100-250°C at 25°C intervals. A steady pressure across the core indicated when the end point was reached. Four PV of hot water injection was usually necessary for stabilization to occur. The end point effective permeability to water was calculated from the steady pressure drop measured.

The same experimental procedures for determining the end points of the Ottawa sand cores were used for the outcrop sand cores, except that brine replaced water. A new core was used for each experiment. The first end point experiment was performed at 150°C with sodium sulphate brine. Four additional end point experiments were later conducted at 100, 125, 150 and 175°C with sodium chloride brine.

During the heating, the brine solution expanded through the core until stabilization of the experimental temperature. Bitumen was then injected to re-establish and determine the initial end point parameters, followed by a hot water flood to reach the final condition. The residual bitumen in the core was solvent-extracted with the toluene-isopropanol-brine sequence to allow the absolute permeability determination at the experimental conditions.

3.4.3.2 Water-Bitumen Mixture Injection

Five water-bitumen mixtures were used to study the saturation range from irreducible water to residual bitumen. The experimental conditions are presented in Table 3.2. The total nominal flow rate for these mixtures varied slightly from one to the other but still corresponded to approximately 1 PV/h. Duplicate experiments were conducted at 125 and 175°C to ascertain the reproducibility of the method.

Preliminary experiments were performed to develop a suitable method by which uniform water-bitumen mixtures could be injected into a core. Attempts to pre-mix water and bitumen in a static mixer before injection led to unstable pressure drops with large pulsations. The use of longer pressure probes on both inlet and outlet ends and an increase in the diameter of the injection lines helped reduce the magnitude of these pulsations. However, the mixing was still non-uniform, resulting in segregated flow. Blobs were visually observed at room temperature during the injection of a mixture of dyed water and refined oil. This mixture had an oil-to-water viscosity ratio of about 300, similar to that of bitumen-to-water at 125°C.

It was then decided to use the inlet end of the sand pack as the mixing medium and to inject the water and bitumen through separate ports. The fluctuations in the pressure drop were eliminated with pressure probes inserted 5 cm into either end of the core, twice

Table 3.2 : Bitumen/Water Mixtures for Steady State Experiments

Experiment #	nominal flow rate (cm^3/h) water	bitumen	total	water/bitumen flow ratio
MID-02,10,11	32.0	48.0	80.0	0.67
MID-01,06,08	64.0	16.0	80.0	4.0
MID-03,12	70.0	4.5	74.5	15.56
MID-04,07,09	80.0	1.25	81.25	64.0
MID-05	80.0	0.5	80.5	160.0

as long as the original pressure probes used in the end point experiments. This allowed a long enough mixing zone to obtain a uniform mixture, which was subsequently confirmed during visual inspections of the core at the end of each experiment. Injection was terminated when the pressure drop across the core stabilized. This usually took about 3 PV, and was lowest when the relative amount of bitumen in the mixture was highest. The intermediate relative permeabilities to water and bitumen were calculated from this stabilized pressure drop.

3.4.3.3 Dynamic Displacements

Dynamic displacement experiments were designed to determine the effect of time and water flow rate on bitumen recovery, and to provide a comparison with the previous end point experiments. These experiments were conducted at 125°C using a procedure similar to the end point experiments. Additional accumulators were installed to collect up to four bitumen fractions produced during the uninterrupted hot water floods. The detailed experimental conditions are presented in Table 3.3.

Initially, some minor problems developed during the process of switching from one production accumulator to another. The production accumulators were installed in parallel, each having a valve in their inlet flow line. The outlet flow and pressure were in turn controlled by the back-pressure regulator located downstream of the collection system. When switching from one accumulator to

Table 3.3 : Experimental Conditions for Bitumen Displacement Experiments

Experiment #	Duration of Production Fluid Collection (hr)	Water Flow Rate (cm^3/h)
DIS-1	4, 10, 20	80
DIS-2	4, 10, 20	320
DIS-3	10, 20, 30, 48	80
DIS-4	1, 2.5, 5	80
DIS-5	1, 2.5, 5	80

the next, the valve of the first accumulator was closed only after the valve of the second one was opened. Because the movable piston in the first accumulator was at a higher pressure, opening the second accumulator caused a sudden pressure differential until that piston started moving. This pressure increase was reflected in the pressure drop across the core by an instantaneous surge. These pressure surges were eliminated by replacing the accumulator pistons with a gas-liquid interface where the produced fluids displaced the gaseous phase upwards and through the back-pressure regulator to control the flow. A continuous flow of nitrogen was added to the outlet production stream for a better back-pressure regulation.

3.4.3.4 Sampling and Analysis

At the end of the hot water floods, the core was isolated and rotated to a horizontal position to prevent gravity segregation of the fluids. The core was then allowed to cool to room temperature. The sand was removed from one end of the copper sleeve, and any abnormalities in its appearance were recorded. The sleeve was then washed with toluene to recover any oil and sand left on it. The average residual bitumen saturation at the end of the water flood was calculated from the total amount of bitumen recovered from the core.

Production fluids were collected at experimental conditions in a single accumulator for each flood, except if described otherwise.

They were allowed to cool and depressurize with the rest of the system, and were also analyzed for bitumen content. The initial average bitumen saturation of the reconstituted oil sand core was then calculated from the measured residual saturation and the total bitumen produced during each water flood. In the case of the water-bitumen mixture experiments, the amount of bitumen injected was subtracted from the produced fluids.

Analyses of the oil sand (core) and production fluids were performed using the Dean and Stark extraction method that separates bitumen, water and sand fractions. The filter paper method was used to determine the amount of bitumen in each sample. The detailed procedure for these analyses was reported by Koots (1983) as OSRD Methods 1.05 and 2.05, respectively. The uncertainties introduced by the analytical procedures are not greater than 0.5% absolute, provided no errors were introduced during the sampling (Wallace, 1984).

3.4.4 Kaydol Experiments

Several experiments were carried out with Kaydol-saturated cores, where Kaydol is a less viscous heavy oil than bitumen. Synthetic Kaydol oil sand cores were prepared in the same manner as described previously for bitumen. The Kaydol was subsequently displaced by a water flood in the dynamic displacement mode. Both short and long-lasting experiments were performed at 20 and 100°C. These temperatures were selected to reproduce the viscosity conditions

of bitumen in the temperature range studied. Detailed experimental conditions are given in Table 3.4.

Instead of collecting the produced fluids in three or four accumulators, a visual fraction-collector was installed at the outlet end of the core for continuous production monitoring. This fraction collector was initially filled with deionized water containing a chemical de-emulsifier to help break any emulsions formed during the displacement of Kaydol by water.

The sampling procedure for Kaydol at the end of a flood was somewhat different from that used for bitumen. The volume of the produced fluids was directly measured at experimental conditions in the visual fraction collector during the water floods. The Kaydol remaining in the core at the end of the displacement was washed by mineral spirits. The refractive index for the Kaydol-mineral spirit mixtures was found to be a linear function of the weight percent of Kaydol in the mixture. The calibration curve is given in Appendix G. The solvent-filled core was first allowed to soak overnight and then, under vacuum, was subjected to washing in stages until no more Kaydol was detected in the washings by measuring the refractive index. For each washing, about 250 cm^3 of solvent was used and the core was evacuated almost to complete dryness. After separating the organic and aqueous phases, the weight of the Kaydol in the organic phase was determined from the measured refractive index. The volume of the residual Kaydol was calculated from the density measured at experimental conditions.

Table 3.4 : Experimental Conditions for Kaydol Displacement Experiments

Experiment #	Temperature (°C)	Total Water Injected (PV)
KAY-1	20	3.00
KAY-2	20	3.06
KAY-3	100	3.23
KAY-4	20	41.95
KAY-5	100	42.76

4. SAND PACK AND HEAVY OIL PROPERTIES

The relative permeability experiments in this study utilized a combination of unconsolidated sand, water or brine, and heavy oil. The individual properties of water were taken from steam tables or calculated from analytical expressions, whereas those of sand and oil were determined experimentally and are presented below.

4.1 Ottawa Sand Pack Properties

Fifty-three cores were prepared using the procedure described in Section 3.3.3. All but two of the cores were packed with the 200 mesh silica sand, these two being packed with coarser 100-120 mesh and 20-45 mesh sand. The porosity and absolute permeability of each core were measured at the experimental conditions. The packing procedure was found reliable on the basis of the reproducible results obtained for cores packed under similar situations.

4.1.1 Porosity

To take into account changes which occurred on applying the confining pressure, the pore volume of each core was determined at the end of each experiment, and the porosity calculated therefrom. The detailed results are presented in Appendix C. The porosity values ranged from 31.8 to 35.8%, with an average value of 34.0 ± 1.0%. The average pore volume for all the cores was found to be

approximately 90 cm^3. With time, the packing became more consistent, resulting in a narrower porosity range for the later cores.

Porosities were determined at room temperature by comparing the volume of the packed sand to the total volume available in the copper sleeve. For each core, the confining pressure reduced the pore volume by approximately 10% from its original value. The observed differences in porosity from one core to another were attributed to variations in the grain size distribution of the sand batches. This was also true for the absolute permeability. Packing variations arising out of different orientations of the sand grains were present despite a reproducible packing procedure.

4.1.2 Absolute Permeability

The absolute permeability to water of each core was first determined at room temperature (k_o), and again at the experimental temperature (k_o) before the start of a bitumen flood. The detailed experimental results are presented in Appendix C.

With the exception of the two cores packed with coarser sand, the room temperature absolute permeabilities ranged from 0.959 to 2.069 d. These values are similar to those reported for rich Athabasca oil sands. There appeared to be a direct relationship between the average values of porosity and permeability: the lower the porosity, the lower the permeability. The room temperature for these measurements varied from one day to another, with an

average of 21.6°C.

The absolute permeability of each core was also determined at the experimental temperature and ranged from 0.907 to 2.028 d for the 200 mesh sand. With the exception of three measurements, absolute permeability was always found to be lower at the higher temperature. In general, this decrease in absolute permeability was less than 10% below 175°C, and more than 10% above 175°C, as indicated in Table 4.1.

4.1.3 Effect of Temperature on Absolute Permeability

Table 4.1 presents the average core parameters calculated from the experimental results. An analysis of variance showed that the room temperature absolute permeabilities of the cores were not statistically different (see Appendix H). To evaluate the effect of temperature and account for variations in the initial measurement, each experimental absolute permeability was normalized with respect to its room temperature value. The temperature dependence of the normalized absolute permeability ratio is shown in Figure 4.1. The average value, standard deviation and number of experiments are indicated for each temperature.

Two distinct regions, with a boundary between 175 and 200°C, appear in Figure 4.1. The absolute permeability ratio is fairly constant in both regions, but has a higher value below 175°C than above 175°C. The average is 0.947 for the "low" temperature range

Table 4.1 : Average Core Parameters as a Function of Temperature

Run Temp. (°C)	No. of Cores	Porosity ϕ (%)	Absolute Permeability Ratio (k_o/k_o)	% Decrease in Absolute Permeability
100	5	32.8	0.936 ± 0.024	6.4
125	23	34.3	0.953 ± 0.050	4.7
150	4	34.7	0.969 ± 0.023	3.1
175	9	34.4	0.927 ± 0.052	7.3
200	3	34.1	0.857 ± 0.038	14.3
225	3	33.1	0.861 ± 0.028	13.9
250	3	33.4	0.838 ± 0.032	16.1
Overall	50	34.0	0.930 ± 0.057	7.0

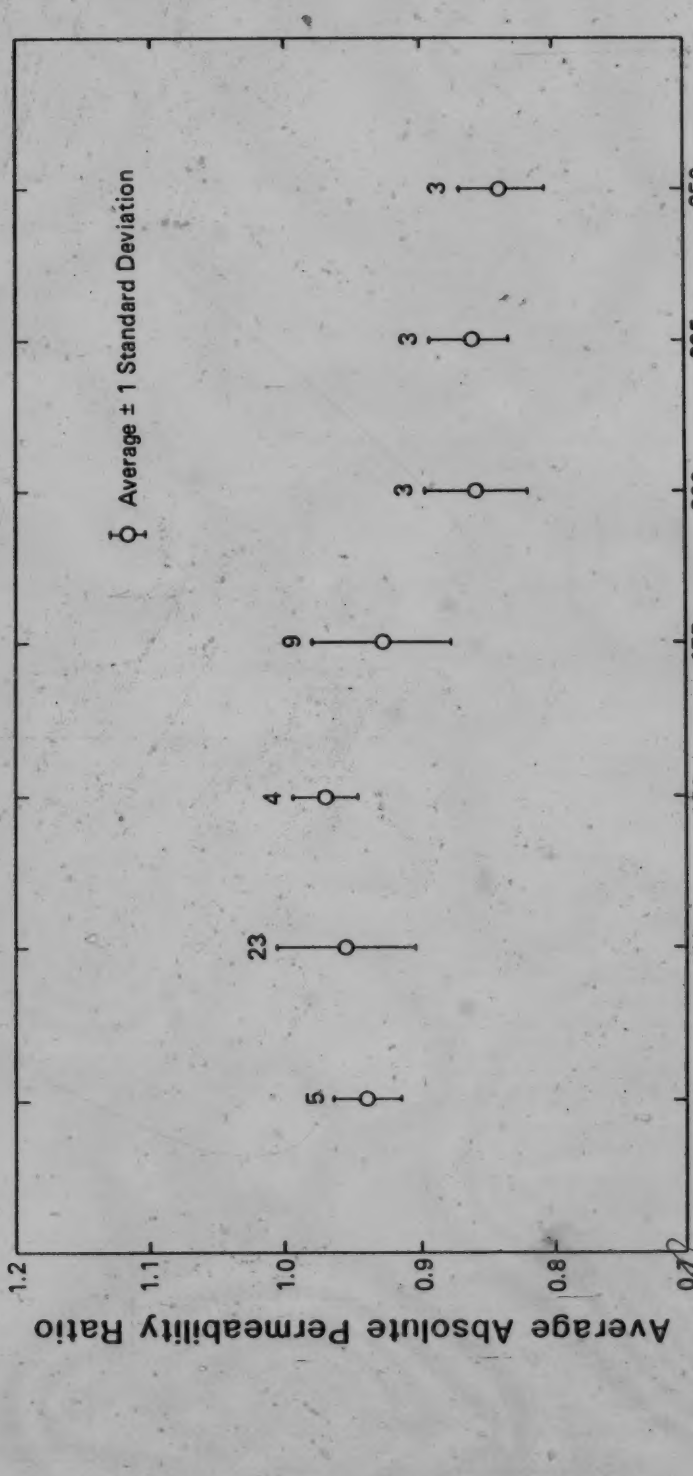

Figure 4.1 : Temperature Dependence of Absolute Permeability

and 0.852 for the "high" temperature range. The overall absolute permeability ratio average is 0.930, which is approximately the average of the 175°C measurements. At that temperature, the features of both the "low" and "high" temperature measurements are present.

The percentage decrease in absolute permeability from the room temperature measurement also shows the same trends as the absolute permeability ratio. This percentage jumps from approximately 6 to 15% between 175 and 200°C. The overall average is similar to that at 175°C as well.

To assess the significance of the effect of temperature on absolute permeability, a statistical F-test was conducted. This test was performed to determine if the variation between populations was greater than the variation due to random error within a population. A calculated F-value larger than the tabulated F*-value would indicate a significant statistical difference between these populations (see Appendix H).

The relevant parameters for 95% confidence limits are presented in Table 4.2. The results of the F-test showed that mean absolute permeability ratios at each temperature were not all equal in the temperature range 100° to 250°C. From a statistical point of view, the absolute permeabilities of the sand packs above 175°C were significantly different from the overall average. Considering the decrease in absolute permeability from room temperature to

Table 4.2 : Statistical Parameters for Temperature Dependence of Absolute Permeability

Temp. Level	Number of Cores	Absolute Permeability Ratio	95% Confidence Interval	F-factor (F*-value)
all (100-250°C)	50	0.930	0.014	-
100°C	5	0.936	0.040	
125°C	23	0.953	0.019	
150°C	4	0.969	0.045	6.11
175°C	9	0.927	0.030	(2.32)
200°C	3	0.857	0.052	
225°C	3	0.861	0.052	
250°C	3	0.838	0.052	
low (100-175°C)	41	0.947	0.012	33.52
high (200-250°C)	9	0.852	0.019	(4.07)
100°C	5	0.936	0.040	
125°C	23	0.953	0.019	1.05
150°C	4	0.969	0.045	(2.86)
175°C	9	0.927	0.030	
200°C	3	0.857	0.052	0.42
225°C	3	0.861	0.052	(5.14)
250°C	3	0.838	0.052	

experimental temperature, it is apparent that the temperature effect was less marked at the lower temperatures and was within experimental error.

By using only two temperature levels for absolute permeability (low and high) the temperature effect was statistically significant, as indicated in Table 4.2, even though the average values between 100 and 175°C and between 200 and 250°C were not significantly different. The stepwise decrease observed around 175°C could be a result of the relative expansion of the sand grains as compared to the water in a confined system, therefore decreasing the permeability. More measurements are needed to confirm these findings and to determine a functional relationship between temperature and absolute permeability for clean unconsolidated Ottawa sand packs.

4.2 Reservoir Sand Pack Properties

Table 4.3 lists the experimental core properties of the reservoir sand packs determined at the end of each experiment. Porosities ranged from 23.4 to 30.8%, and this indicated that the original samples contained void spaces and were compressed further during the confining procedure. Absolute permeabilities to brine were determined after solvent-extraction of the residual bitumen from the core. The permeabilities were in the range expected for high grade oil sands, but did not follow any particular trend with increasing temperature, except that lower values were obtained at

Table 4.3 : Experimental Core Parameters for Reservoir Sand Samples

Core/Run No.	Temperature (°C)	Porosity (%)	Permeability (d)
OCS-01*	150.0	22.4	0.633
OCS-02	149.8	23.4	0.934
OCS-03	174.8	28.0	0.511
OCS-04	99.6	30.6	1.275
OCS-05	123.2	30.8	1.678

* experiment with sodium sulphate brine

higher temperatures. It is not known whether permeability damage due to fines movement and/or clay alteration occurred as a result of the procedure utilized.

4.3 Heavy Oil Properties

4.3.1. Bitumen Viscosity

The viscosity of bitumen was measured for different experimental conditions of temperature at constant pressure. The average values of viscosity at 7 MPa are reported in Table 4.4 as a function of temperature, with the detailed viscosity values presented in Appendix D. The viscosity data were correlated using a semi-logarithmic regression scheme (see Table 4.4). Also, the standard deviation on the measured properties was found to be comparatively higher when more than one batch of bitumen was used at any one temperature. Bitumen that had been used at a given temperature was reused only at a higher temperature because of the possibility of thermal degradation.

Bitumen-to-water viscosity ratios were also calculated from the experimental measurements. They ranged from 786 at 100°C to 31 at 250°C, and followed a trend similar to that of bitumen viscosity versus temperature. The viscosity ratio variation is presented in Figure 4.2.

Table 4.4 : Viscosity of Bitumen Measured at 7 MPa

Temperature (°C)	Viscosity - (mPa·s)	Viscosity Ratio	# of Measurements	# of Batches
100	222.4 ± 13.2	786.0	3	1
125	69.8 ± 6.8	311.8	23	3
150	30.3 ± 1.4	162.5	4	1
175	14.5 ± 1.3	92.8	9	3
200	8.2 ± 0.1	60.6	3	2
225	5.0 ± 0.3	41.8	3	1
250	3.3 ± 0.2	30.9	3	1

Linear regression correlations:

- viscosity : $\ln \mu_b = 7.751 - 0.027\ T$ ($r^2 = 0.9701$)

- viscosity ratio : $\ln (\mu_{b/w}) = 8.435 - 0.021\ T$ ($r^2 = 0.9647$)

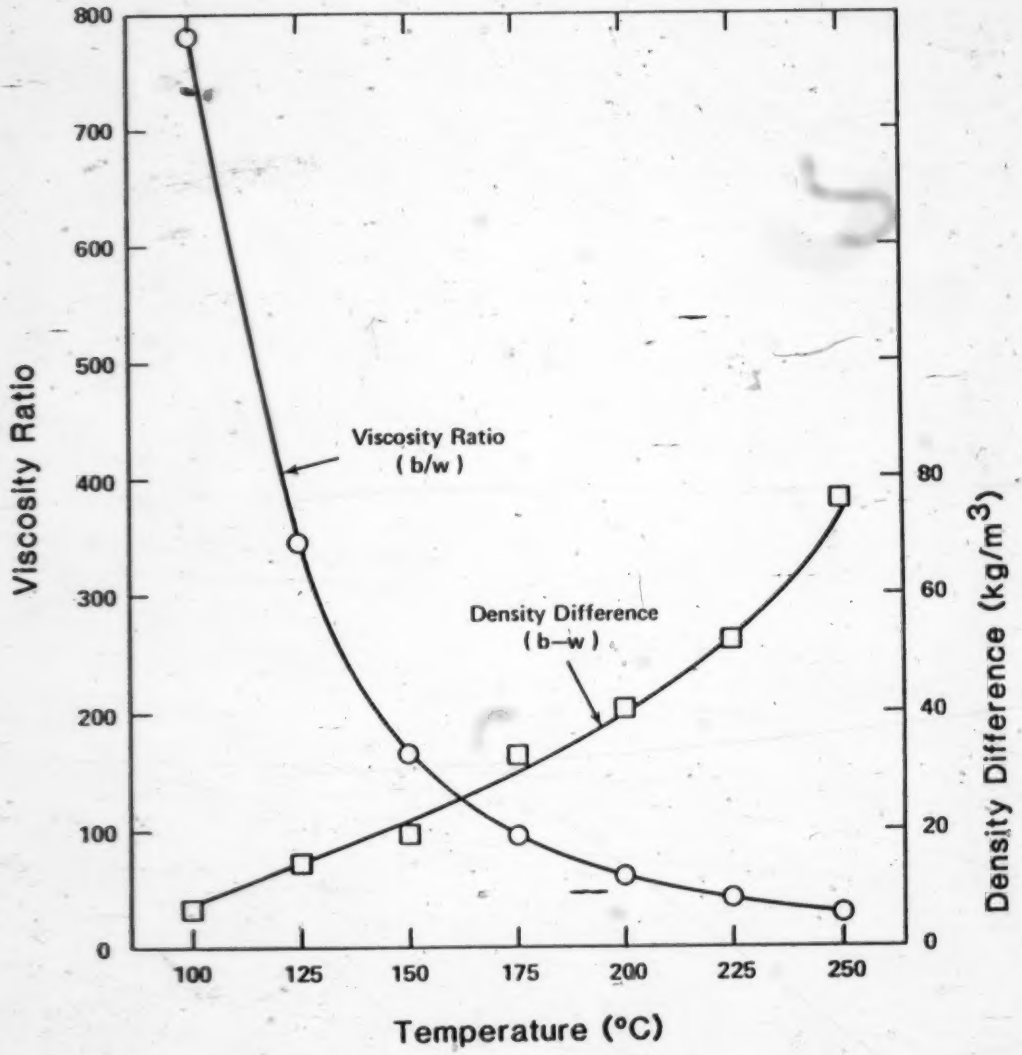

Figure 4.2 : Fluid Properties in Displacement Experiments

4.3.2 Bitumen Density

Bitumen density was determined at the prevailing experimental conditions. The average values are reported as a function of temperature in Table 4.5, and correlated by linear regression. The same trends as in the viscosity data also appeared in the standard deviation of the measured densities.

The bitumen-to-water density difference was calculated from the measured data. At any temperature in the range studied, this difference was positive and increased with temperature, from less than 1% at 100°C to 8% at 250°C. The absolute density difference is illustrated in Figure 4.2.

4.3.3 Property Correlations

The average bitumen viscosity and density values at each experimental temperature have been presented to indicate the trends that were found with increasing temperature. However, these properties varied within each batch. Some other properties such as asphaltene content, API gravity and residual solvent were also specific to each batch, and are reported in Appendix D.

Strausz (1977) reported a dependence of the viscosity of bitumen on its asphaltene content. Wallace (1979-83) indicated that specific gravity and carbon residue appeared to increase with increasing asphaltene content. The residual solvent content is also

Table 4.5 : Density of Bitumen Measured at 7 MPa

Temperature (°C)	Density (kg/m^3)	Density Difference	# of Measurements	# of Batches
100	968.1 ± 0.6	6.85	3	1
125	951.1 ± 7.1	8.90	23	3
150	940.2 ± 0.6	19.90	4	1
175	925.4 ± 8.9	29.10	9	3
200	909.3 ± 8.6	39.90	3	2
225	890.2 ± 3.5	52.50	3	1
250	879.1 ± 3.0	77.00	3	1

Linear regression correlations:

- density : $\rho_b = 1028.3 - 0.600\ T$ ($r^2 = 0.9962$)

- density difference : $\Delta\rho_{b-w} = -45.96 + 0.454\ T$ ($r^2 = 0.9449$)

known to influence the bitumen properties.

Bitumen from batch #1 was used for about one half of the measurements, with the other two batches making up the remaining in equal proportions. Comparisons were limited to three of the temperatures when two or three batches were used. It was therefore not possible to correlate the viscosity of bitumen versus its density because of the variations between these batches.

4.3.4 Kaydol Properties

Kaydol experiments were conducted at only two temperatures under a pore pressure of 7 MPa. At 20°C, the average viscosity from three measurements was 191.7 mPa·s, with an average oil-to-water viscosity ratio of 190.2. For two experiments at 100°C, these parameters were 5.95 mPa·s and 21.1, respectively. Both the absolute viscosity and viscosity ratio values were in the range of those determined for the bitumen-water system.

The average density of this oil was 892.9 and 854.4 kg/m^3, for the low and high temperatures, respectively. The oil was considerably less dense than water, contrary to the case of bitumen.

The Kaydol was reused after the first temperature cycle. The second time, its density value at both temperatures was significantly higher, although the viscosity was almost unaffected. It is not known if this temperature cycling affected its properties.

5. EXPERIMENTAL RESULTS

5.1 End Points

Steady state end point relative permeabilities and their respective residual saturations for bitumen and water floods were measured between 100°C and 250°C, at 25°C intervals. Average results are presented in Table 5.1. At each temperature, experiments were performed at least three times to examine the reproducibility of the experimental procedure. The experimental flooding conditions used in the 31 experiments are presented in Table 3.5. These conditions were not modified during the course of the experimental series to avoid introducing variations other than those due to temperature. In addition to establishing the effect of temperature on the end points, the effects of brine, sand grain size and overburden pressure were examined.

As fluid properties such as viscosity, density and interfacial tension all change with temperature, these changes were taken into account for the end point calculations. The detailed results for each end point are given in Appendix E.

5.1.1 End Point Criterion

The end point was assumed to have been reached when the pressure drop across the core stabilized for the period of time required to

Table 5.1 : Average Bitumen-Water End Point Results as a Function of Temperature

T(°C)	k_{rbiw}	k_{rwrb}	S_{bi}	S_{wi}	S_{br}	E_d^*
100	0.762	0.053	0.966	0.034	0.554	0.426
125	0.758	0.075	0.930	0.070	0.529	0.432
150	0.791	0.129	0.927	0.073	0.462	0.501
175	0.736	0.119	0.912	0.088	0.445	0.513
200	0.766	0.274	0.917	0.083	0.505	0.450
225	0.654	0.136	0.932	0.068	0.515	0.449
250	0.726	0.022	0.992	0.008	0.544	0.452
Average	0.752	0.108	0.932	0.068	0.501	0.464

* $E_d = \dfrac{S_{bi} - S_{br}}{S_{bi}}$

inject one pore volume of fluid. This criterion achieves a practical end point but may not represent the "true" end point, particularly with respect to water flooding where the displacement viscosity ratio was unfavorable as illustrated in Figure 4.2 (large bitumen-to-water viscosity ratio). Production of bitumen might still occur at this stage, but at a rate too low to be indicated by the pressure drop measurement. However, reproducible results were obtained with this criterion for the end point experiments at each temperature.

5.1.2 Bitumen Floods

In the majority of the experiments, the resulting initial bitumen saturation from bitumen flooding was in excess of 88% PV, with an overall average of 93% PV. These saturations were established by injecting bitumen at a favorable bitumen-to-water viscosity ratio ranging from approximately 785 at 100°C to approximately 30 at 250°C. The average irreducible water saturation was then determined after the final flood, when the core had been sampled and analyzed. Excluding the results at 100°C (very high viscosity ratio) and 250°C (possible drying out of the core), the average irreducible water saturation (or initial bitumen saturation) values obtained in these experiments were consistent with the range of 6 to 13% reported in the literature (Morrow, 1970; Bentsen and Saeedi, 1979).

Usually less than 3 PV of bitumen injection were sufficient to reach the steady state condition although difficulties were encountered in obtaining a stable pressure drop for the experiments conducted at the higher temperatures. At 225°C, a stable pressure drop was obtained in only one of the experiments. For the runs conducted at 250°C, the pressure drop reached a stable value when the amount of bitumen injected was around 2-3 PV. However, upon further injection of bitumen, the pressure drop started to increase, with no tendency to stabilize. This continued injection also affected the end point saturation. The pressure drop increase could be due to the deposition and filtration of asphaltenes at the higher temperatures, as observed with thermally-altered Peace River tar around 200°C (Waxman et al., 1980).

5.1.3 Hot Water and Brine Floods

All hot water floods were conducted with deionized water, with the exception of two runs where brine was injected. For the brine floods, the sodium ion concentration was approximately 0.07M (0.99 wt%), in the range indicated by Takamura (1982) for ensuring maximum water film stability in oil sands. Aqueous sodium sulphate rather than sodium chloride was used to avoid corrosion. The two brine experiments were conducted at 150°C for the purpose of comparison with the hot water floods. Good agreement was found for the brine floods, with a slight improvement in displacement efficiency, E_d, over the hot water floods.

In the hot water floods, stabilized conditions were observed after 3.5 to 5.5 PV of water injection. There were no visible trends with respect to temperature. The scatter observed in the end point water relative permeabilities at 225°C (see Appendix E) was attributed to difficulties encountered during the bitumen flood. Also, results of the bitumen analyses for two of the experiments conducted at 100°C were incomplete due to analytical difficulties.

5.1.4 Effect of Sand Grain Size and Overburden

Two end point experiments were performed with coarse sand to investigate the effect of the sand grain size. Both batches of sand had a fairly narrow size range: 100-120 and 20-45 mesh. The absolute permeabilities of these cores were approximately three and a hundred times higher, respectively, than the average permeability of the 200 mesh sand, although porosities remained in the same range. Despite this large variation in absolute permeabilities, the end point results obtained were within the range of all the other end points measured between 100 and 250°C.

A core with reduced overburden pressure exhibited the same end points as a "similar" core subjected to the usual overburden pressure. This indicated that the high level of confining pressure used for the experiments would not conceal an eventual temperature effect, but rather amplify it if present (Gobran et al., 1981).

5.1.5 Effect of Temperature

The average end point values are summarized as a function of temperature in Table 5.1. The temperature variations of the end point relative permeabilities and residual saturations are shown in Figures 5.1 and 5.2, respectively. For each temperature, the range of occurrence, the average value and the number of experiments are indicated. The overall average for each variable is also shown as a dashed line independent of temperature. The statistical parameters for each individual end point are presented in Table 5.2.

The individual average end point bitumen relative permeabilities, k_{rbiw}, for each temperature straddle the overall k_{rbiw} average line. An F-test indicated that all averages were not significantly different. The same cannot be said of the end point water relative permeabilities, k_{rwrb}. Their average values at each temperature gradually increased up to 175°C. No trend was evident in their variation with temperature at the higher temperatures. At 200°C the measured values were highest, whereas at 250°C they were lowest. The values obtained might have been affected by experimental difficulties during the bitumen flood at temperatures higher than 200°C, as mentioned earlier. The respective magnitudes of relative permeability at the end points are indicative of a water-wet system (Craig, 1971). This is generally accepted as a characteristic of Athabasca oil sands (Takamura, 1982).

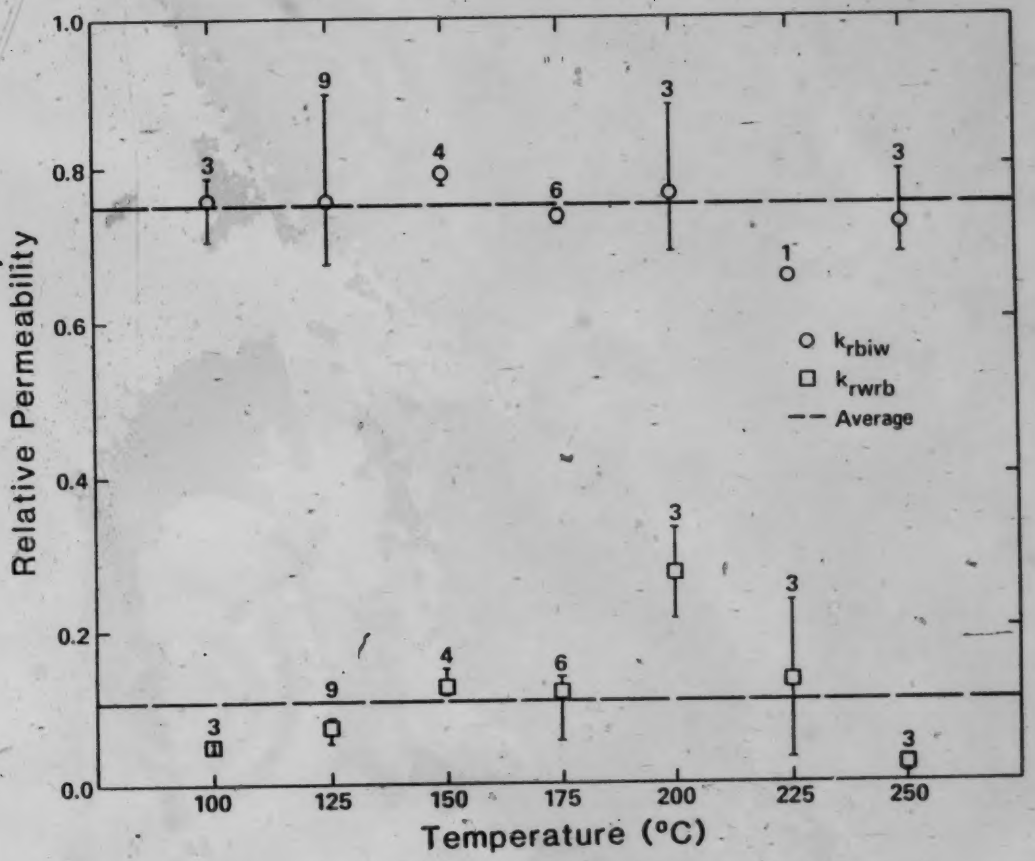

Figure 5.1 : Bitumen-Water End Point Relative Permeabilities as a Function of Temperature

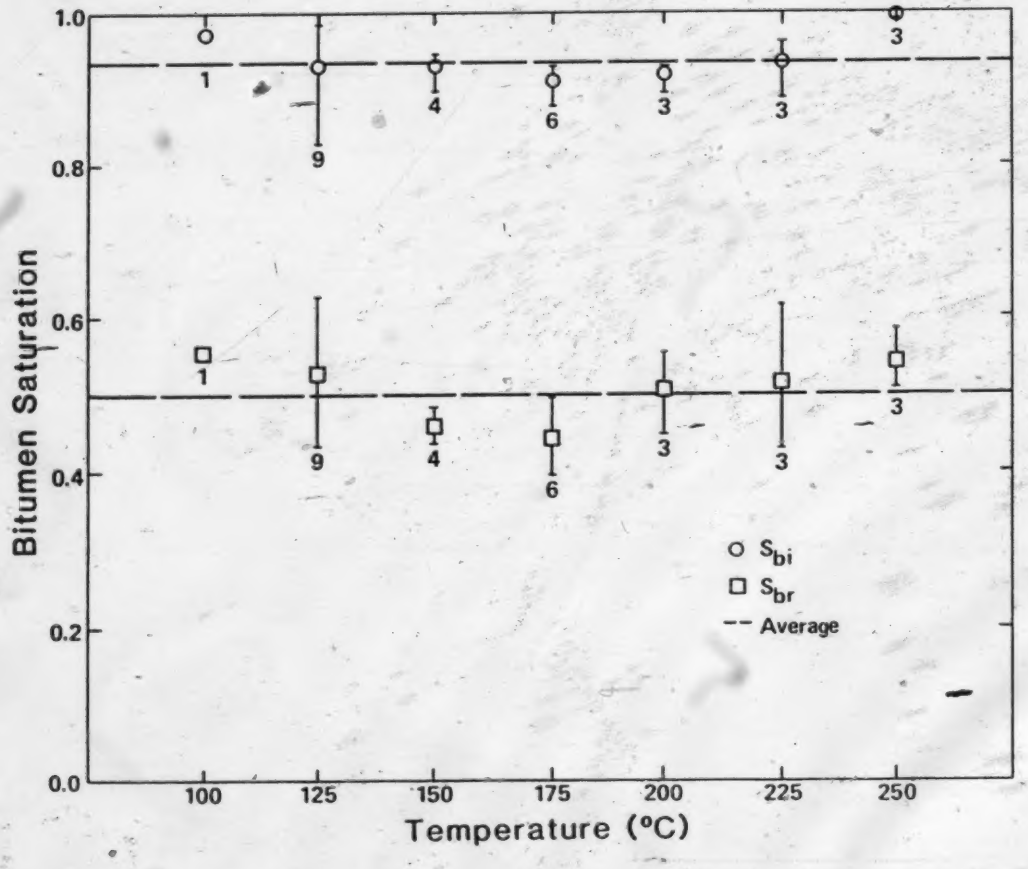

Figure 5.2 : Initial and Residual Bitumen Saturations as a Function of Temperature

Table 5.2 : Statistical Analysis of End Point Results

Temperature (°C)	Average Value	Standard Deviation	95% Confidence Interval	F-Factor
		k_{rbiw}		
100	0.762	0.047	0.071	
125	0.758	0.074	0.041	
150	0.791	0.012	0.061	
175	0.736	0.009	0.050	0.97
200	0.766	0.102	0.071	
225	0.654	*	0.123	
250	0.726	0.061	0.071	
all	0.752	0.059	0.019	2.55
		k_{rwrb}		
100	0.053	0.040	0.046	
125	0.075	0.012	0.027	
150	0.129	0.017	0.040	
175	0.119	0.032	0.033	14.35
200	0.274	0.060	0.046	
225	0.136	0.104	0.046	
250	0.022	0.009	0.046	
all	0.108	0.074	0.023	2.51
		S_{bi}		
100	0.966	*	0.071	
125	0.930	0.047	0.024	
150	0.927	0.027	0.036	
175	0.912	0.019	0.029	2.14
200	0.917	0.020	0.041	
225	0.932	0.040	0.041	
250	0.992	0.005	0.041	
all	0.932	0.037	0.012	2.55
		S_{br}		
100	0.554	*	0.105	
125	0.529	0.060	0.035	
150	0.462	0.027	0.053	
175	0.445	0.033	0.043	2.68
200	0.505	0.053	0.061	
225	0.515	0.078	0.061	
250	0.544	0.038	0.061	
all	0.501	0.059	0.019	2.55

* one measurement only.

The average initial and residual bitumen saturations, S_{bi} and S_{br}, respectively, showed a similar trend: both S_b versus temperature relationships went through a minimum around 175°C that was more pronounced in the case of the residual bitumen saturations. As a result of the S_{bi} and S_{br} functions, the displacements were found to be most efficient at 175°C (51% recovery), and least efficient at 100-125°C (43% recovery). The F-test results for both S_{bi} and S_{br} values were similar and indicated a weak temperature dependence for the range 100-250°C. However, visual observation of the results from Figure 5.2 showed that the magnitude of this dependence was small.

5.1.6 Fluid Properties and Capillary Number

The properties of the bitumen and water used in these experiments varied greatly with temperature as indicated in Figure 4.2. In the range studied, the inter-fluid properties were monotonic functions of temperature: the bitumen-to-water viscosity ratio, $\mu_{b/w}$, decreased exponentially; and the density difference between bitumen and water, $\Delta\rho_{b-w}$, was always positive and increased almost linearly over the entire temperature range.

Bitumen floods were conducted with favorable and water floods with unfavorable viscosity ratios over the entire temperature range studied. The end point mobility ratio, M_r, defined as:

$$M_r = \frac{\lambda_w}{\lambda_b} = \frac{k_{rwrb}}{\mu_w} \cdot \frac{\mu_b}{k_{rbiw}} \qquad (5.1)$$

varied from approximately 61 at 100°C to approximately 0.5 at 250°C when calculated for each experiment (see Appendix E). The average mobility ratios are given in Table 5.3 as a function of temperature and followed a decreasing trend similar to that of the viscosity ratio. However, they were larger at two temperatures: k_{rwrb} values were higher than their average at 200°C and k_{rbiw} values were lower than their average at 225°C (see Figure 5.1). Both contributed to an increase in the mobility ratio. This phenomenon was attributed to an accumulation of asphaltenes in the sand pack during the bitumen floods. Despite the large variations in the fluid-fluid properties over the temperature range, the end point results were still virtually independent of temperature.

The capillary number, N_c, was calculated from the flow and fluid properties during a water flood as:

$$N_c = \frac{\mu_{w,exp}\ (mPa \cdot s) \cdot q_{exp}\ (m^3/s)}{\phi \cdot A_{co}\ (m^2) \cdot \sigma_{b/w}\ (mN/m)} \qquad (5.2)$$

where the bitumen-water interfacial tension, $\sigma_{b/w}$, was estimated from the experimental data of Isaacs and Smolek (1983). Their results were extrapolated to the maximum temperature according to a linear relationship:

$$\sigma_{b/w}\ (mN/m) = 17.6 - 0.048 \cdot T_{exp}\ (°C) \qquad (5.3)$$

The capillary number was found to vary from $0.98 \cdot 10^{-6}$ to $1.40 \cdot 10^{-6}$ between 100°C and 250°C (see Appendix E). The average value at each temperature given is in Table 5.3. Foster (1973) indicated

Table 5.3 : Average Fluid Properties as a Function of Temperature in End Point Experiments

T (°C)	$\mu_{b/w}$	M_r	$\sigma_{b/w}$ (mN/m)	N_c	$Lv\mu_w$ ($cm^2 \cdot cp/min$)
100	785.9	55.0	12.79	$1.35 \cdot 10^{-6}$	0.750
125	334.4	31.8	11.59	$1.10 \cdot 10^{-6}$ *	0.600 *
150	162.5	26.5	10.38	$1.09 \cdot 10^{-6}$	0.523
175	81.3	15.0	9.22	$1.03 \cdot 10^{-6}$	0.440
200	60.6	21.6	8.02	$1.12 \cdot 10^{-6}$	0.415
225	41.8	16.2 +	6.79	$1.22 \cdot 10^{-6}$	0.376
250	30.9	0.9	5.58	$1.38 \cdot 10^{-6}$	0.352

* does not include run END-26 where the flow rate was three times higher

\+ one measurement only

that this order of magnitude is typical for high tension relative water floods and showed that a further increase in N_c by about two orders of magnitude is required to reduce the residual oil saturation from its nominal water flood value. The variation of the capillary number for these experiments as a function of temperature is therefore not significant.

5.1.7 Stabilization Criterion

The scaling coefficient $Lv\mu_w$ proposed by Rapoport and Leas (1953) was calculated for the water floods and varied from approximately 0.76 $cm^2 \cdot cp/min$ at 100°C to approximately 0.35 $cm^2 \cdot cp/min$ at 250°C when calculated for each experiment (see Appendix E). The average values of the scaling coefficient are given in Table 5.3 as a function of temperature. These are in the range of critical scaling coefficients for stabilized flow as reported by Rapoport and Leas (1953). In addition to stabilized flow, end effects were minimized by using pressure probes inserted into the sand pack.

5.1.8 Reservoir Sand Experiments

Five experiments were conducted with the reservoir oil sand samples. End point effective, and relative permeabilities are presented in Table 5.4 as a function of temperature. The 150°C and 175°C experiments behaved similarly, with measured effective permeability values of the same order of magnitude as Ottawa sand. For these three experiments, the end point bitumen relative

Table 5.4 : End Point Results for Reservoir Sand

Run Temp (°C)	Effective / (Relative) Permeability to water	to bitumen	Bitumen Saturation initial	final	Displac. Eff. (%)
100	0.094 (0.074)	3.444 (2.701)	0.968	0.528	0.455
125	0.015 (0.009)	0.732 (0.436)	0.822	0.538	0.345
150*	0.109 (0.172)	0.943 (1.490)	0.907	0.490	0.460
150	0.078 (0.083)	1.058 (1.133)	0.989	0.535	0.459
175	0.079 (0.155)	0.746 (1.460)	0.781	0.422	0.460

* experiment with sodium sulphate brine

permeabilities ranged from 1.13 to 1.49 while the end point water permeabilities compared favorably with the clean sand results. The results at 100°C and 125°C were much more erratic. The end point bitumen relative permeability was exceedingly high (2.70) at 100°C. At 125°C, the end point relative permeability to water was extremely low (0.009) and the end point relative permeability to bitumen was also the lowest (0.436). This was the only experiment to exhibit an absolute permeability greater than the effective permeability to bitumen at irreducible water saturation. Clay movement could be the cause for the observed permeability decrease as a result of solvent-extraction. The end point bitumen-to-water relative permeability ratios could not be correlated with temperature, and followed a pattern similar to the absolute permeabilities (see Section 4.2).

Initial and final bitumen saturations in the reservoir sand cores, obtained from a material balance of the produced and extracted bitumen, are also presented in Table 5.4. No trends with respect to temperature could be inferred from either the initial or final saturations. The displacement efficiencies in all but one experiment were the same and equal to that of clean sand. The efficiency was significantly lower for the core having the lowest effective water permeability. The core having the lowest absolute permeability exhibited the lowest initial bitumen saturation, but this did not affect the displacement efficiency.

The major clay mineral component of the high grade Athabasca oil

sand samples used was found to be kaolinite, a non-swelling clay. Hydrothermal transformation of the kaolinite clay was not expected in the temperature range studied and for the duration of these experiments (Bird, 1986), and could not be the cause for the differences seen between the various results. With the exception of one core sample that behaved quite differently, the variations in permeability and saturation among the cores were not considered significant and are principally attributable to heterogeneities associated with field samples.

5.2 Relative Permeability Curves

Imbibition relative permeability measurements were made at 125°C and 175°C for bitumen and water using both the steady and unsteady state techniques, and at 20°C and 100°C for Kaydol and water using the unsteady state method. These experiments were conducted in clean unconsolidated sand packs. Relative permeability curves were determined for the two systems based on the JBN calculation procedures outlined in Appendix B.

5.2.1 Initial Oil Sand Core Parameters

Initial oil sand core parameters, namely end point relative permeability to bitumen and initial bitumen saturation, were determined for each core and are listed in detail in Appendix E. Their average values are presented in Table 5.5, and compared with those of the end points reported previously.

Table 5.5 : Comparison of Initial Oil Sand Core Parameters

Oil Sand Experiment Type	Average/(Range) k_{rbiw}	Average/(Range) S_{bi}
	Bitumen	
steady state	0.787 (0.749-0.827)	0.879 (0.736-1.071)
unsteady state	0.673 (0.640-0.726)	0.851 (0.770-0.886)
end points	0.752 (0.654-0.899)	0.932 (0.826-0.989)
	Kaydol	
unsteady state	0.629 (0.535-0.714)	0.943 (0.900-0.966)

The end point bitumen relative permeabilities, k_{rbiw}, for the twelve cores used in the mixture injection experiments ranged from 0.749 to 0.827, with an average value of 0.787. They were determined at 125°C or 175°C, and showed no temperature dependence. All values were within the range measured in the end point study. The initial bitumen saturations, S_{bi}, ranged from 0.736 to 1.071 with an average value of 0.879. These saturations were calculated from a material balance of the injected bitumen and involved taking the difference of two large numbers to obtain a smaller number. A relatively large error was involved in this determination of S_{bi} compared with the previous end point results. With the exception of one value exceeding unity for which no explanation other than analytical error was available, all other S_{bi} values were within the expected range. The initial conditions for the reconstituted oil sand cores used in the steady state measurements were comparable to the cores used previously (see Section 5.1).

A newly packed core was prepared for each of five dynamic displacement experiments conducted at 125°C. The average S_{bi} values (0.851) were not significantly lower for these five cores and fell within the overall average, whereas the average k_{rbiw} values (0.673) were lower (see Table 5.5). Because of the variations in the initial bitumen saturation and corresponding end point bitumen relative permeability, comparisons were made on the basis of these initial core parameters.

Kaydol cores were prepared similar to the bitumen cores. Initial Kaydol saturations and corresponding relative permeabilities to the oil phase were determined as before, and are presented in Table 5.5. On average, the initial Kaydol saturations were about the same as for bitumen (0.943 vs 0.932). However, the end point oil relative permeabilities were significantly lower than the average calculated for bitumen (0.629 vs 0.752). This might indicate a difference in the distribution of the fluids or wetting behaviour of the oil-water-sand system.

5.2.2 Steady State Experiments

Twelve experiments were conducted to obtain steady state bitumen-water relative permeability curves for clean unconsolidated sand. The experiments involved the injection of bitumen-water mixtures into a bitumen saturated core. Nine of these experiments were conducted at 125°C. The remaining three were performed at 175°C to investigate the effect of temperature. All but one of the mixtures was repeated at 125°C, and three of the duplicates were repeated at 175°C. The detailed results are given in Table 5.6.

The data are plotted in Figure 5.3. The left-most points represent the temperature-independent end points at initial bitumen saturation. However, different end point saturations were displayed at the residual bitumen condition, as the displacement was found to be more efficient at 175°C than at 125°C (see Table 5.1). This differentiation was done by extending the saturation range

Table 5.6 : Intermediate Data for Relative Permeability Curves (steady state)

Temp. (°C)	k_{rbiw}	S_{bi}	w/b ratio	S_w	k_{rb}	k_{rw}
125	0.764	0.874	4.0	0.317	0.484	0.007
125	0.760	0.800	0.67	0.218	0.591	0.001
125	0.810	0.911	15.56	0.359	0.446	0.024
125	0.759	0.893	64.0	0.454	0.243	0.055
125	0.771	0.914	160.0	0.474	0.123	0.069
175	0.808	0.736	4.0	0.322	0.511	0.023
125	0.772	0.925	64.0	0.437	0.243	0.053
125	0.749	0.906	4.0	0.287	0.486	0.007
175	0.817	0.883	64.0	0.520	0.241	0.174
175	0.826	0.800	0.67	0.227	0.658	0.005
125	0.776	0.831	0.67	0.214	0.560	0.001
125	0.827	1.071	15.56	0.367	0.520	0.023

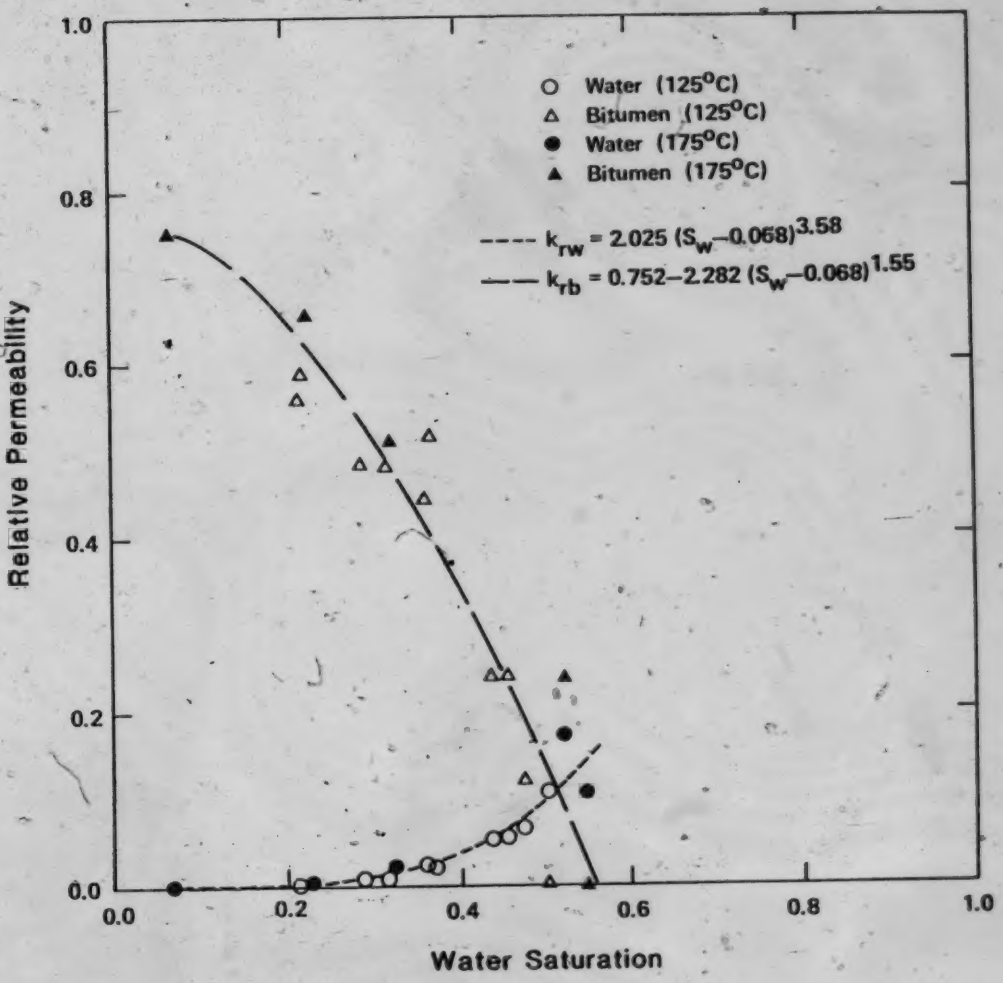

Figure 5.3 : Bitumen-Water Relative Permeability Curves (steady state)

for the 175°C experiments, and is shown by the right-most points in Figure 5.3. The residual bitumen saturation at 125°C was taken as 0.50, the average value determined in the end point study. For both temperatures, the temperature-independent value of water relative permeability was used.

The steady state relative permeability data thus obtained were fitted with power law functions using all the data points. The only parameters used in these functional representations were the end point bitumen relative permeability and the irreducible water saturation. The scatter in the experimental data was attributed to experimental error, as the temperature effect was insignificant. All the data points were then considered to be temperature-independent. To determine the individual phase relative permeabilities, the following functional forms were used:

$$\text{bitumen:} \quad k_{rb} = k_{rbiw} + a_b \cdot (S_w - S_{wi})^{e_b} \tag{5.4}$$

$$\text{water:} \quad k_{rw} = a_w \cdot (S_w - S_{wi})^{e_w} \tag{5.5}$$

where the parameters a and e were determined from the experimental data for bitumen and water. The best fit results are presented in Table 5.7, with the fitted curves shown in Figure 5.3.

Often, relative permeability curves are presented in a normalized form in numerical simulators, both for saturation and permeability. Perkins and Collins (1960) suggested normalizing each curve

Table 5.7 : Best Fit Results for Steady State Relative Permeability

	Non-Normalized Curves			Normalized Curves		
Phase	a	e	r^2	a*	e*	r^2
bitumen	-2.282	1.55	0.9797	0.995	0.495	0.9923
water	2.025	3.58	0.9254	0.998	4.14	0.9767

with respect to its own end point relative permeability. This procedure was followed here. The normalized curves are shown in Figure 5.4, along with the normalized data points, and are of the form (the superscript * refers to normalized variables):

$$k^*_{rb} = a^*_b \cdot (1 - S^*_w)^{e^*_b} \tag{5.6}$$

$$k^*_{rw} = a^*_w \cdot (S^*_w)^{e^*_w} \tag{5.7}$$

$$S^*_w = \frac{S_w - S_{wi}}{1 - S_{br} - S_{wi}} \tag{5.8}$$

where the a^* and e^* parameters are also presented in Table 5.7.

The shape of the fitted curves deserves some attention. The water curve is concave as usually reported in the literature. An exponent of about 3.6, which is not uncommon and widely accepted in the literature (e.g. Brooks and Corey, 1964), is required to fit the experimental data using Equation (5.5). The bitumen curve, on the other hand, is convex and the fit to Equation (5.4) has an exponent of approximately 1.6.

A convex curvature was also reported by Combarnous and Pavan (1968) for a mineral oil-brine-unconsolidated silica sand system. Their relative permeabilities were measured by the steady state method at 40°C. The mineral oil-to-brine viscosity ratio was estimated to be higher than 70. In the experiments reported herein, the bitumen-to-water viscosity ratio ranged from approximately

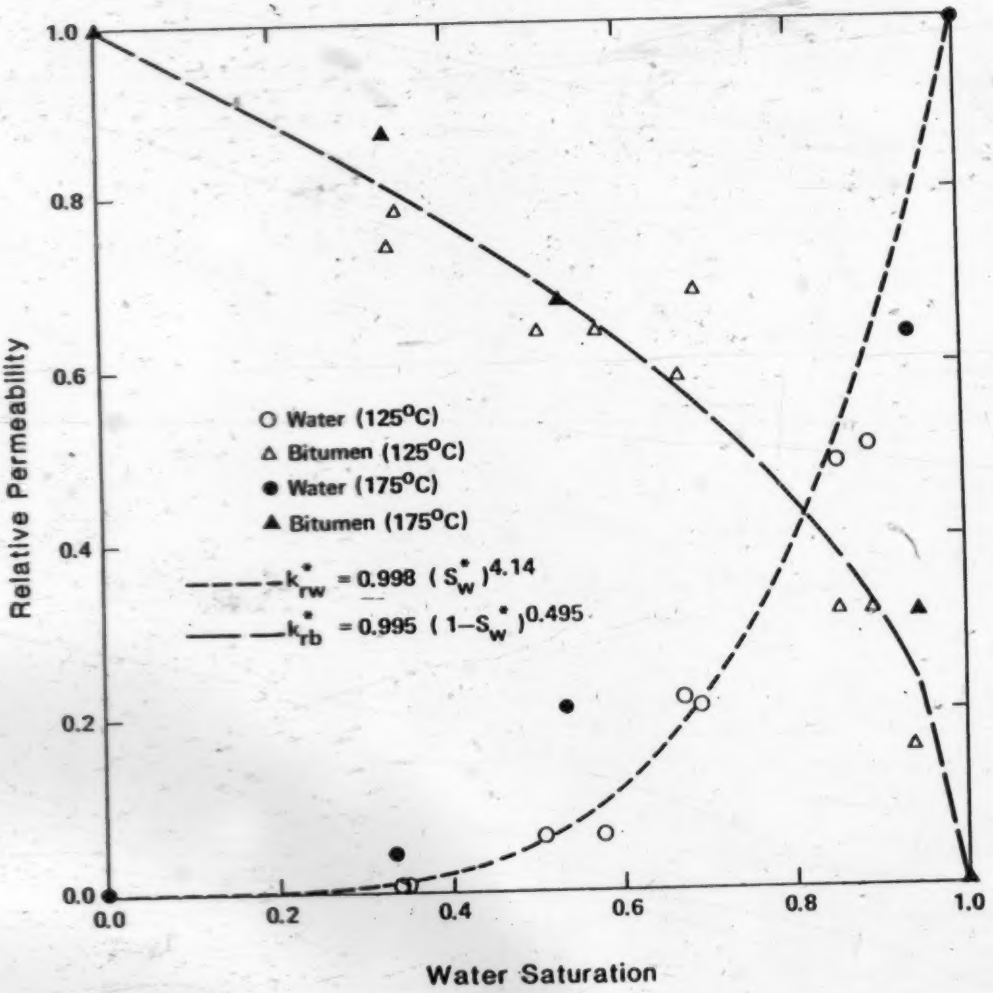

Figure 5.4 : Normalized Bitumen-Water Relative Permeability Curves (steady state)

90 to 300 for the temperatures studied. It should also be mentioned that Combarnous and Pavan obtained a concave oil relative permeability curve with a less viscous mineral oil (viscosity ratio estimated at approximately 20) as did Closmann et al. (1985) at 196°C with unaltered Peace River bitumen (viscosity ratio of approximately 60). It appears, therefore, that the viscosity ratio may influence the shape of the steady state oil relative permeability curve in an oil-water-unconsolidated sand system.

5.2.3 Dynamic Displacement Experiments

The Johnson-Bossler-Naumann (JBN) method (1959) was used to calculate two phase oil-water relative permeability curves from dynamic displacement experiments as outlined in Appendix B. Smoothing was performed using a linear regression analysis to choose a single functional representation of the entire range of data because the JBN approach requires the differentiation of the data (Tao and Watson, 1984). Recovery and injectivity data were empirically correlated to the logarithm of the cumulative pore volumes of water injected, W_i, using polynomial functions as suggested by Miller and Ramey (1985) for the determination of relative permeability relationships. The results for the bitumen-water and Kaydol-water systems are presented below.

5.2.3.1 Bitumen-Water Curves

The results of five water displacement experiments at 125°C are

presented in Table 5.8 with detailed results given in Appendix F. The comparison of the bitumen recovery by hot water injection is in terms of displacement efficiency, E_d, defined in Table 5.1, to account for the variations in initial bitumen saturations (see Section 5.2.1).

The recovery data as a function of pore volumes of water injected are shown in Figure 5.5 for all five experiments. As indicated in the figure, a single recovery curve can be fitted to all experimental data points and has an asymptotic nature: most of the bitumen recovery occurred in the early stages of the water flood.

The experimental results indicate that a four-fold increase in the water injection rate, as in experiment DIS-2, did not have a significant effect on recovery. Comparing experiments DIS-1 and DIS-2, recoveries after 20 PV of water were injected were approximately the same. This would indicate that the nature of the displacement was not significantly altered. After 4 PV of water injection, the recovery for both these experiments was around 42% of the original-oil-in-place (OOIP), which compares favorably with the results of the end point experiments (average recovery at 125°C: E_d = 0.43). The injection of additional water increased the recovery to approximately 57.5%.

Experiment DIS-3 was of even longer duration, and the recovery reached 61% after 48.7 PV of water injection. Intermediate recovery values at 10 and 20 PV injected were significantly lower than

Table 5.8 : Bitumen Displacement Results

Experiment #	Pore Volume Injected	Displacement Efficiency	Relative Injectivity*
DIS-4	1.17	0.330	13.27
DIS-5	1.33	0.337	13.86
DIS-4	2.33	0.391	17.01
DIS-5	2.50	0.396	17.11
DIS-1	3.93	0.412	27.81
DIS-2	4.21	0.418	31.84
DIS-4	4.76	0.456	19.32
DIS-5	4.87	0.454	18.82
DIS-3	9.45	0.465	55.16
DIS-1	9.65	0.502	37.78
DIS-2	9.88	0.517	37.12
DIS-3	18.88	0.533	70.21
DIS-1	19.32	0.565	42.38
DIS-2	19.44	0.588	33.38
DIS-3	29.88	0.577	94.90
DIS-3	48.66	0.611	126.29

* defined in Equation (B.39)

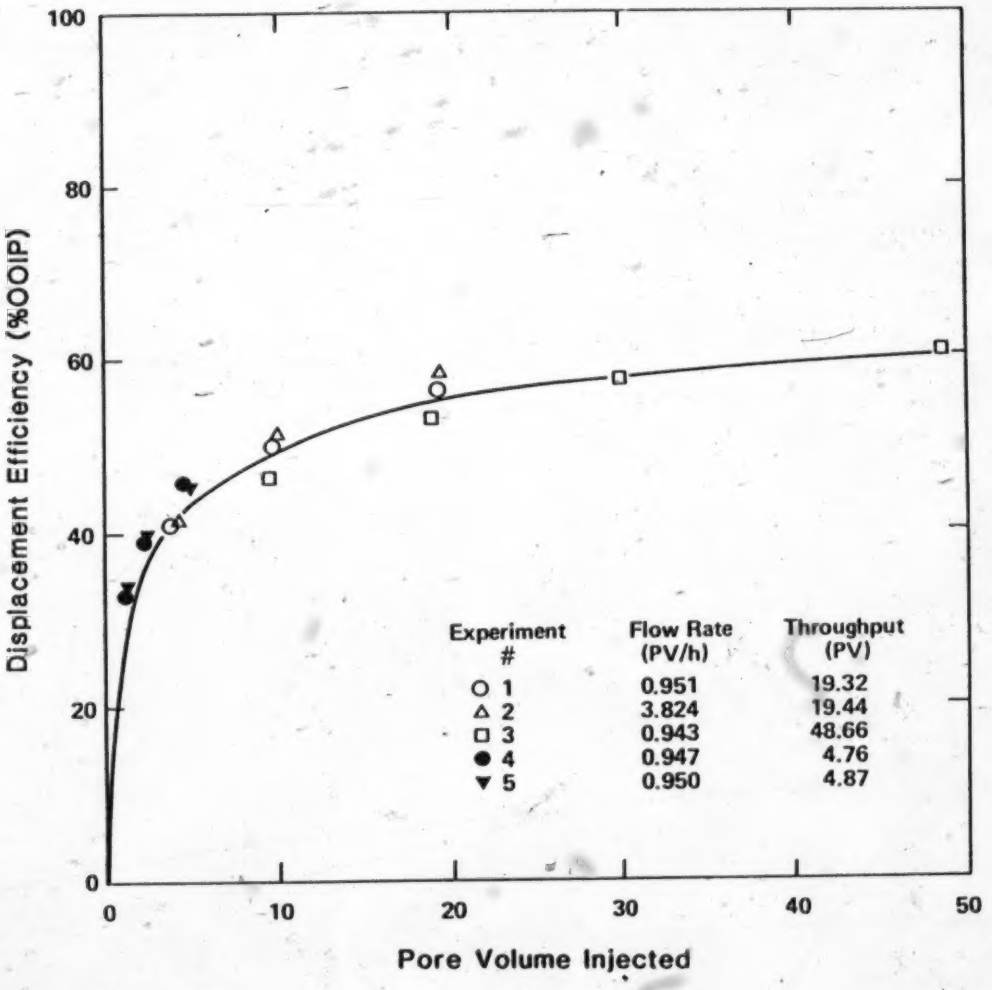

Figure 5.5 : Bitumen Recovery Data at 125°C

for experiments DIS-1 and DIS-2. A recovery of 57.5% was only reached at 30 PV of water injection in experiment DIS-3.

Experiments DIS-4 and DIS-5 were carried out after some improvements to the procedure used for the first three experiments (see Section 3.5.3.3). Bitumen recoveries at each stage of the procedure were very similar, as shown in Figure 5.5, indicating good reproducibility between these two experiments. These results indicate that it is important to minimize pressure disturbances to achieve reproducible recovery results. After approximately 5 PV of water injected, these last two water flood experiments were more efficient than the first three as indicated by higher recoveries of around 45% as compared to 42%.

It is believed that the production recorded in each accumulator during the last two experiments is a better representation of the recovery as shown by the good agreement between experiments DIS-4 and DIS-5 in comparison to experiments DIS-1 and DIS-3. This can be illustrated on a semi-logarithmic plot of recovery versus pore volume injected shown in Figure 5.6, where the post-breakthrough recovery is represented as a linear function of the logarithm of pore volumes injected.

The pressure drop in this series of experiments decreased as more water was injected for all experiments except one. In experiment DIS-2 the pressure drop first decreased and then increased. This anomalous trend cannot be explained by experimental disturbances

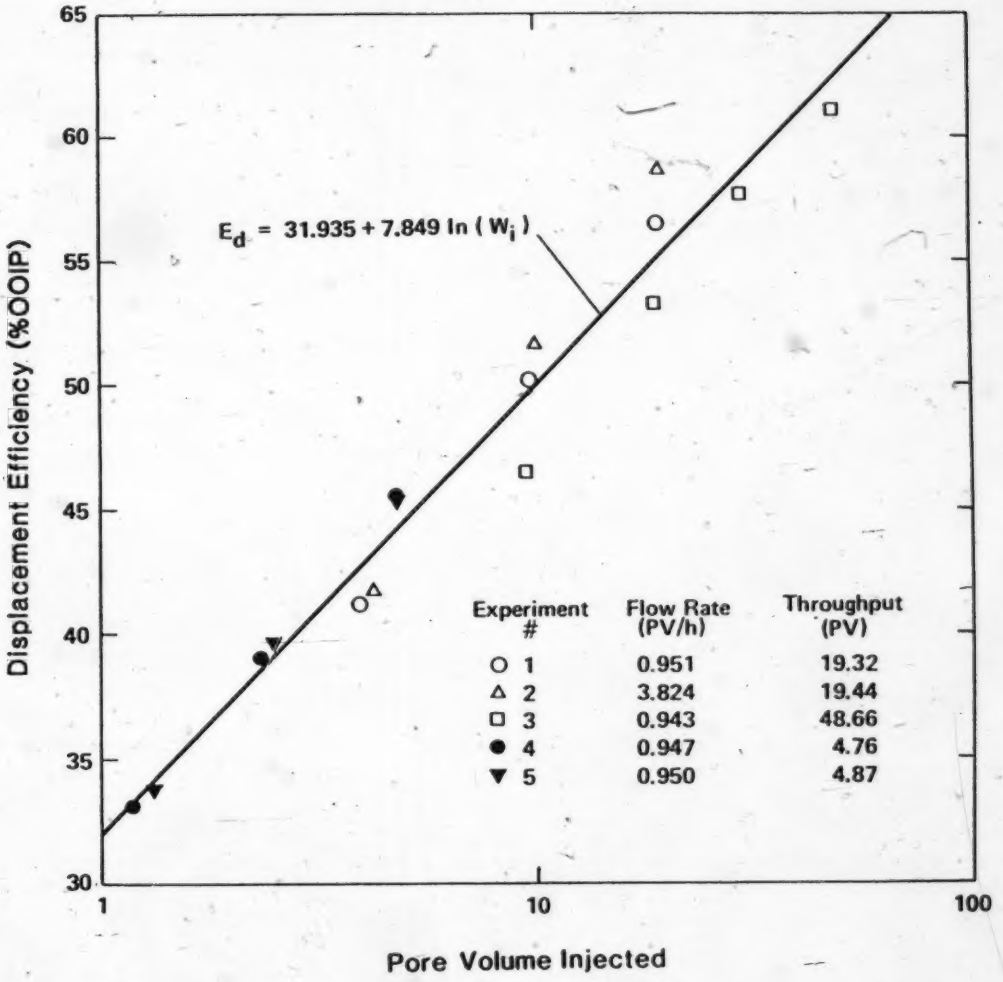

Figure 5.6 : Bitumen Recovery Function (semi-logarithmic)

alone, and its cause is unknown. Also, the pressure drops were two to three times higher per unit flow rate for experiments DIS-4 and DIS-5 than for the other three experiments. The higher the pressure drop, the higher the bitumen recovery in hot waterfloods.

As indicated earlier, the results of all five dynamic displacement experiments can be represented by a single recovery curve. Despite the scatter in the pressure drop data used in the relative injectivity computations, a single set of relative permeability curves could also represent all five experiments. Best fits were obtained with a third order polynomial for the recovery data (E_d vs $\ln\{W_i\}$, r^2=0.9675) and a second order polynomial for the relative injectivity data ($\ln\{W_i I_r\}$ vs $\ln\{W_i\}$, r^2=0.9793). The fitting parameters are detailed in Table 5.9 for each function.

The resulting bitumen-water relative permeability curves are shown in Figure 5.7, with detailed relative permeabilities given in Appendix F. The end point relative permeabilities to bitumen and corresponding initial water saturations were taken as the average of the five experiments. It can be seen from the figure that the residual bitumen condition was not achieved after almost 49 pore volumes of hot water injected.

5.2.3.2 Kaydol Experiments

Five experiments were performed using Kaydol to compare with the bitumen-saturated core results. The temperatures used were chosen

Table 5.9 : Fitting Parameters for JBN Calculations

Experiment #	a_0	a_1	a_2	a_3	r^2
		recovery data			
bitumen	0.27352	0.05375	0.01099	-0.00217	0.9675
KAY-1	0.22458	0.05153	0.00062	0.00540	0.9986
KAY-2	0.28119	0.06960	0.00755	-0.00284	0.9985
KAY-3	0.46446	0.08005	-0.00740	-0.00440	0.9988
KAY-4	0.33679	0.07734	0.00143	0.00083	0.9998
KAY-5	0.46318	0.11408	-0.01948	0.00065	0.9966
		injectivity data			
bitumen	2.5503	1.3198	0.0631		0.9793
KAY-1	2.6949	1.5642	-0.0335		0.9999
KAY-2	2.6609	1.6544	-0.1010		0.9997
KAY-3	1.5388	1.2873	-0.0397		0.9999
KAY-4	2.5737	1.7800	-0.0710		0.9998
KAY-5	1.3815	1.2991	-0.0338		0.9999

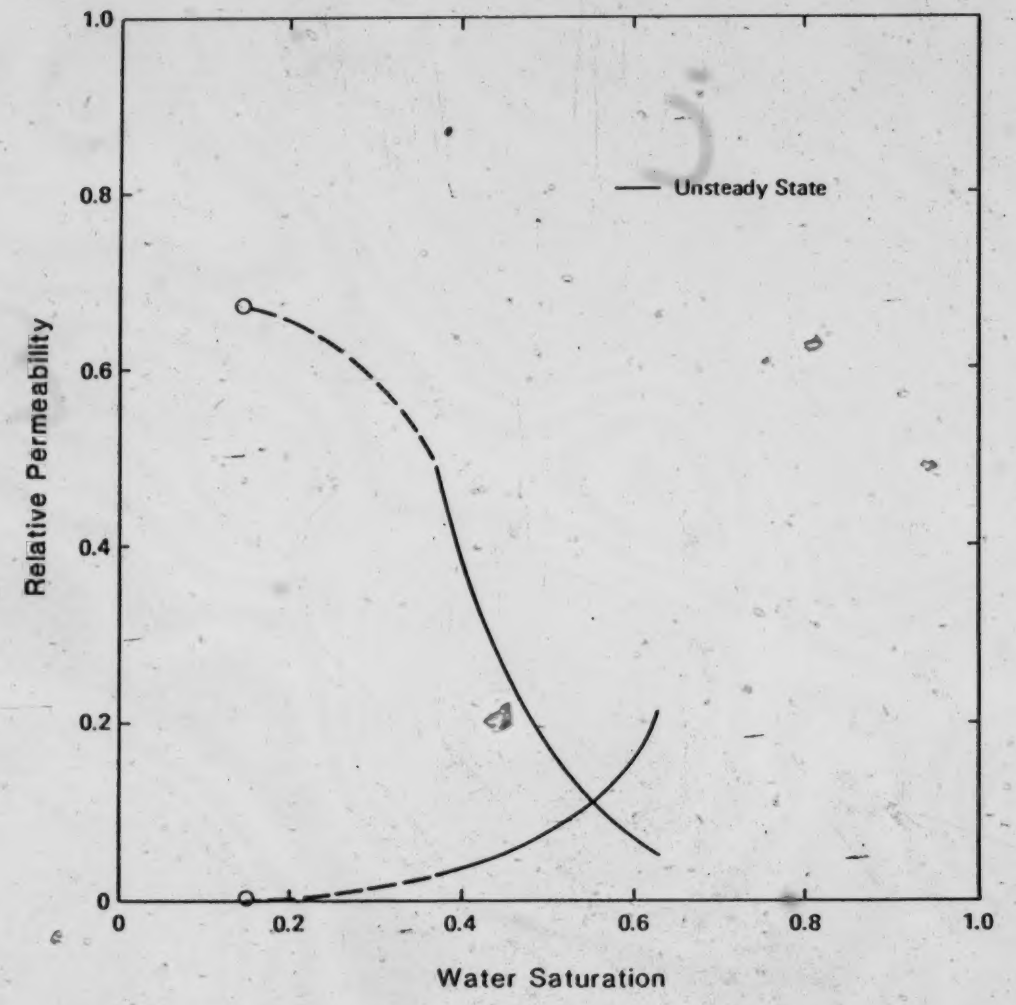

Figure 5.7 : Bitumen-Water Relative Permeability Curves (from dynamic displacement experiments)

to simulate the absolute viscosities and viscosity ratios encountered in the bitumen experiments. The apparatus was modified to collect the necessary information for determining relative permeabilities from a single experiment. Liquid holdup in the lines prior to water flooding necessitated a correction to the measured data which resulted in shifting the starting time of the water flood and the corresponding oil production. The corrected data are given in Appendix G for all five experiments.

Recovery

The first three experiments (two at 20°C, one at 100°C) were conducted for a short period of time in terms of water injection. The two low temperature water floods (viscosity ratio of 190) resulted in approximately 35% oil recovery after injection of 3 PV of water whereas the high temperature flood (viscosity ratio of 21) recovered 57% of the Kaydol in the same time period. Two subsequent experiments (one each at 20°C and 100°C) were carried out with 42 PV of water, and both resulted in similar recoveries of nearly 70% of OOIP. However, their recovery curves differed considerably from each other as shown in Figure 5.8.

The recovery pattern for all Kaydol experiments conducted at the same temperature was similar: rapid recovery in the initial stages of the water flood for the high temperature/low viscosity runs and a more gradual recovery curve for the low temperature/high viscosity runs. At any time during the water flood, the displacement

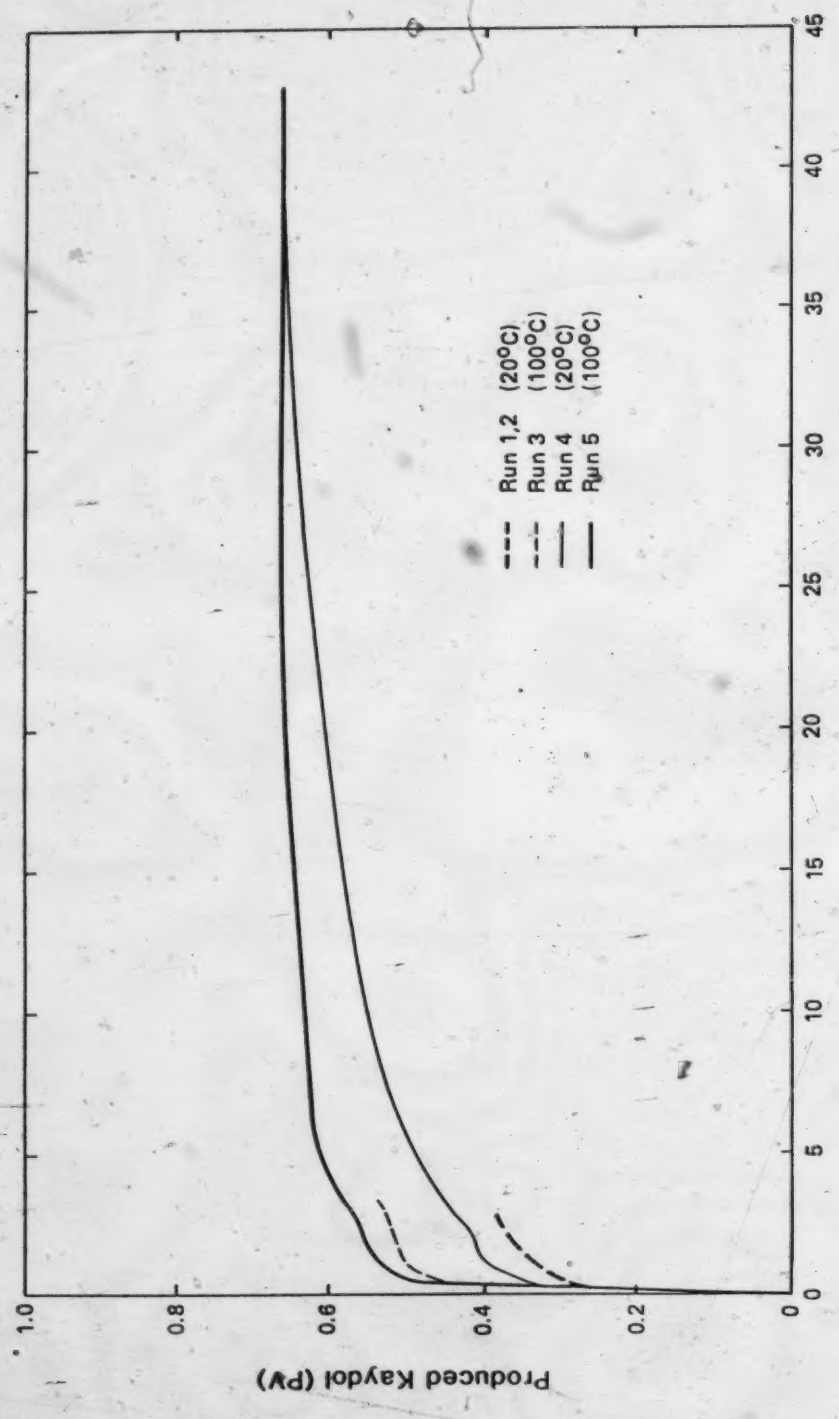

Figure 5.8 : Recovery Curves for Kaydol Experiments

efficiency was greater at the higher temperature when compared to the lower temperature. However, if the experiments were conducted for a long enough period of time, the recovery tended to reach an "ultimate" value regardless of the temperature/viscosity conditions. Despite a change of direction in the pressure drop behaviour (described below) which developed during the long low temperature experiment (KAY-4), the final recovery was not affected.

Pressure Drop

The pressure drop observed during the water floods depended on the viscosity of the displaced fluid: the higher the viscosity, the higher the pressure drop. Qualitative examination of the data indicated that the recovery increased with larger pressure drop. Comparisons are then only meaningful for similar temperatures.

The normal pressure drop behaviour for this type of experiment is a gradual decrease as more oil is recovered. This was observed in every case throughout the duration of the experiments, except in run KAY-4 where the pressure drop initially decreased, then started to increase after 10-12 PV of water were injected. This occurred at night while the experiment was unattended. A similar phenomenon occurred earlier in one of the bitumen displacement experiments (DIS-2), and the reason for this change in pressure drop behaviour also remains unexplained. For this reason, only the portion of the water flood that behaved "normally" was used in the calculation of relative permeability for this experiment.

Relative Permeability

As with the bitumen experiments, dynamic relative permeabilities for the Kaydol displacement experiments were calculated using the JBN procedure. With the modifications made to the experimental procedure, enough data were collected during each water flooding experiment to make calculations for each separately. The relative permeability calculations were based on the absolute permeability of each core.

The breakthrough point was estimated from the production data by considering the oil produced versus water injected ratio. The first few points immediately after breakthrough were disregarded on the basis that they were not representative of the post-breakthrough trend (Miller and Ramey, 1985). Best polynomial fits of post-breakthrough recovery and relative injectivity functions were determined from the experimental data. These were plotted to examine anomalies in the experimental data and trends in the slopes of the fitted functions (see Appendix G).

All five relative injectivity functions exhibited decreasing slopes with increasing W_i. However, these slopes were lower at all times for the high temperature experiments. The slopes of the recovery functions were distinctly different: they increased for the low temperature experiments and decreased for the high temperature experiments with increasing W_i. Because of these differences observed in the recovery data as a function of temperature

(see also Figure 5.8), the relative permeability relationships were considered separately for 20°C and 100°C. The fitting parameters are presented in Table 5.9. Detailed relative permeability values are given in Appendix G.

The first two Kaydol experiments conducted at room temperature were short. In both cases, the calculated saturation range was very small (approximately 0.3). In the second room temperature experiment (KAY-4), more than 10 PV of water were injected, but many more pore volumes of water would be needed to reach the residual oil saturation because of the high oil-to-water viscosity ratio. Even though the residual oil saturation was not achieved, an outline of the relative permeability curves could be drawn in the middle saturation range. These curves are presented in Figure 5.9. Differences in their shape are due to the saturation range available for determining the best fit functions and the accuracy of these fits.

The curves obtained in this study were also compared to those measured by Sufi (1982) for a similar oil-water-sand system at room temperature (see Figure 5.9). By injecting 154 PV of water at a flow rate ten times higher than these experiments into a core having an initial water saturation, S_{wi}, of 0.064, Sufi recovered 87% of the oil-in-place to reach a residual oil saturation of 0.125. His curves can be thought of as an extension of those determined here for run KAY-4.

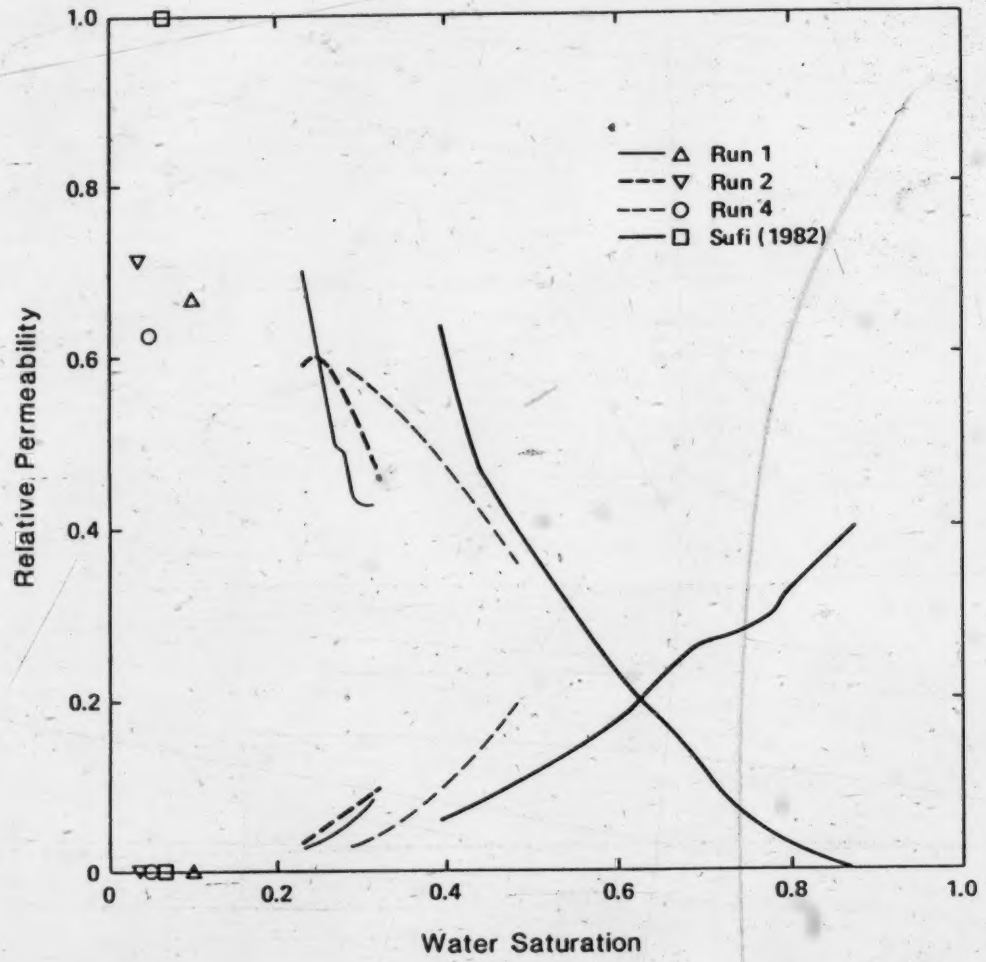

Figure 5.9 : Kaydol-Water Relative Permeability Curves (low temperature)

Two Kaydol experiments of different durations were conducted at 100°C. The number of pore volumes of water injected in reaching the residual oil saturation was again large: 42 PV were found sufficient for the experimental flow conditions in run KAY-5. The two sets of relative permeability curves for these experiments are shown in Figure 5.10 and are similar for both experiments.

The anomalous shapes described earlier for the Kaydol relative permeabilities were seen for the two short low temperature/high viscosity experiments (see Figure 5.9) and did not occur for the short high temperature/low viscosity experiment. The reasons for this anomaly were thought to come from the interpretation of the experimental data. The JBN calculations are sensitive to the saturation range resulting from water flood experiments for high viscosity oils. This sensitivity decreases with a decrease in oil viscosity or an increase in saturation range. Since the experiments were conducted in different cores under conditions which were similar except for temperature, different flow patterns might occur due to packing and/or temperature variations. As the magnitude of these variations are not known, the effect of temperature on the Kaydol-water relative permeability relations is difficult to interpret.

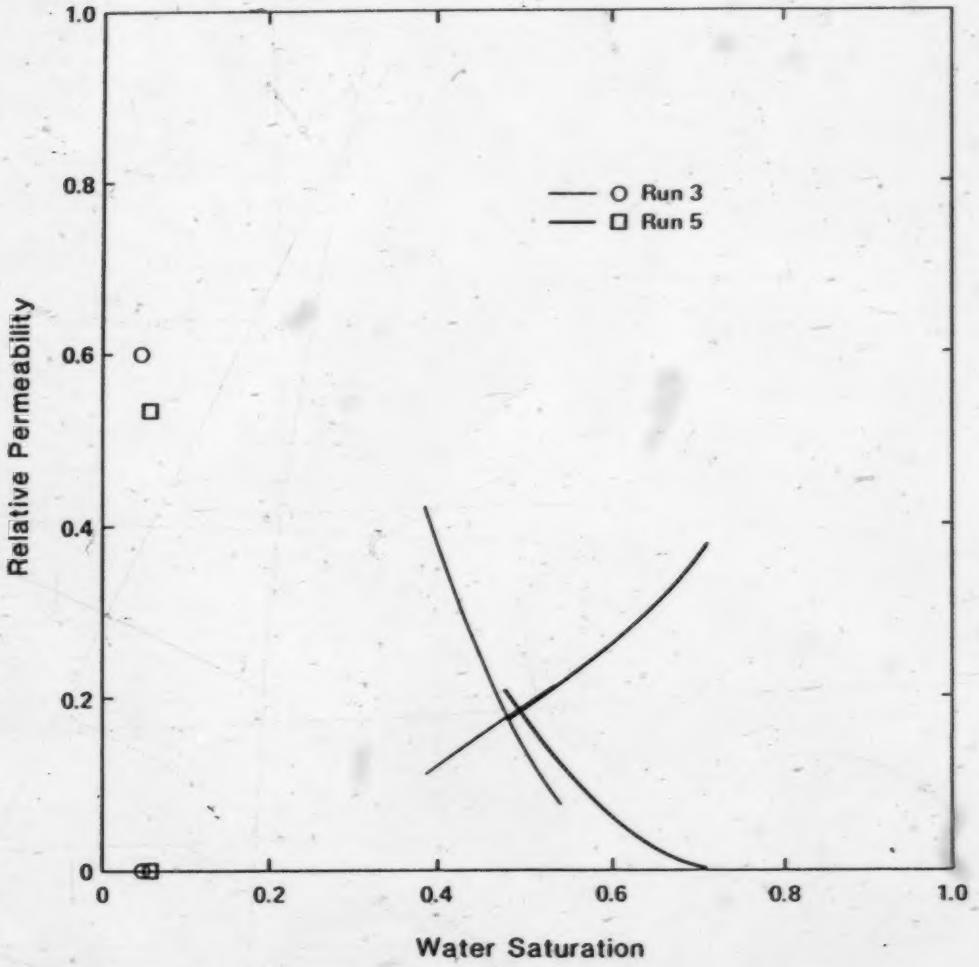

Figure 5.10 : Kaydol-Water Relative Permeability Curves (high temperature)

6. DISCUSSION

The purpose of this study was to examine the effects of temperature on two phase oil-water relative permeability relations and to broaden the relative permeability data base for Alberta heavy oils and oil sands. The experimental results raised as many questions as they answered. The following discussion is intended to explain the observed effects in terms of fundamental properties and to indicate the range of applicability of the measured curves.

6.1 Effect of Temperature on Relative Permeability

6.1.1 Review of Theoretical Models

Theoretical models of relative permeability are traditionally used for performance prediction calculations in the absence of experimental data. Most models represent the porous medium as a set of capillaries ranging from straight capillaries having the same dimensions to randomly distributed interconnected capillaries with various diameters. However, in all cases, the expressions for relative permeability obtained from these models are representative of idealized systems.

In general, two phase oil-water capillary models assume that the porous medium is preferentially water-wet: water only flows in the smaller capillaries and either oil, or oil and water flow in the larger ones. When both fluids are flowing simultaneously, water

exists in the annular region. Flow through capillaries is governed by Poiseuille's equation. The tortuosity concept, usually determined empirically to approximate experimental data, has sometimes been used to take into account the tortuous path of the flow channels as opposed to the concept of parallel capillary tubes.

Theoretical relative permeability relations are usually expressed as a function of the wetting phase saturation and some basic property of the porous medium such as porosity, capillary pressure, tortuosity factor, pore size distribution factor or irreducible wetting phase saturation. Presented in integral form, these all contain a capillary pressure term that could be expressed in terms of the wetting phase saturation. In their basic form, none of these models incorporate explicitly an easily measurable fluid property. However, when considering both the wetting and non-wetting phases flowing in the capillaries, the models give rise to a viscosity ratio (non-wetting fluid to wetting fluid) term in the non-wetting phase relative permeability expression. The result is that the relative permeability would increase with an increase in the viscosity ratio and could explain the convex oil relative permeability seen in this study and curves reported in the literature for water-wet systems (Combarnous and Pavan, 1968). On the other hand, the wetting phase relative permeability equation remains unchanged because of the assumption of a continuous wetting phase throughout the porous medium.

Few models have directly incorporated the effect of temperature on relative permeability. Ehrlich (1970) presented a simple geometrical model to approximate the effect of variation in wettability as characterized by the contact angle, θ. The effect of increasing temperature would decrease the contact angle, resulting in a more water-wet porous medium, although this would be a function of the oil polarity and composition as adsorption on the rock surface would depend on these factors. For an oil-wet system, Ehrlich reported that the relative permeability ratio was insensitive to contact angle variations, hence temperature variations. He also showed that residual oil saturation would decrease and water relative permeability would increase with decreasing contact angle for a water-wet system. Some of the experimentally observed temperature effects indicated a shift of the relative permeability curves towards higher water saturations (Poston et al., 1970). These have been attributed to possible wettability changes due either to a decrease in the contact angle, or to clay migration, or to core-cleaning procedures.

Although the latter two effects can reflect experimental difficulties and could be the cause of observed temperature effects, the first one cannot explain the temperature effects. An increase in the adhesion tension expressed as the product of the oil-water interfacial tension and of the cosine of the contact angle with temperature increase would mean an increase in water wetness. The contact angle decreases with temperature and so does the interfacial tension, tending to offset any increase in cos θ, as the

change of contact angle with temperature is smaller than that of interfacial tension. Calculations of adhesion tension as a function of temperature would indicate a decrease with temperature increase and invalidate some of the models mentioned earlier.

Nakornthap and Evans (1986) postulated an analytical theory and formulated a mathematical model to describe the variation of relative permeability with temperature in an oil-water system. They developed analytical equations for temperature-dependent relative permeabilities in terms of water saturation, irreducible water saturation and differential change in irreducible water saturation with temperature. The entire model assumes that irreducible water saturation increases with temperature and therefore predicts temperature-dependent relative permeabilities. The change in irreducible water saturation with temperature was based on experimental evidence that is widely reported but not always observed, as is the case in this study. This is, then, one of the controversial issues regarding temperature effects on relative permeability and should not be incorporated as such in a theoretical model without full proof of its validity.

Temperature also affects fluid and rock properties, such as viscosity and wettability. The effect of absolute fluid viscosity and viscosity ratio is still being debated. In the literature, there is experimental evidence pointing to both its presence and absence. Although Lefebvre du Prey (1973) observed it in all his experiments, Odeh (1959) reported that viscosity ratio did not

affect relative permeability if the porous medium had an absolute permeability greater than 1 d. Danis and Jacquin (1983) concluded on the basis of their numerical and experimental results that the influence of viscosity on oil relative permeability seemed to increase as the porous medium geometry became more complex. Their resulting oil relative permeability curves were convex and in some instances, they reported end point oil relative permeabilities greater than unity.

Wettability has been incorporated in some of the relative permeability models, either by contact angle considerations or by a fractional wettability factor. In contrast to fluid viscosity, wettability is not an easy property to measure, especially under in situ conditions. Contact angles are usually determined in a static mode and for a "representative" rock sample. The microscopic wetting behaviour cannot be precisely determined and is therefore assumed. This has led to the concept of dual or fractional wettability where both oil-wet and water-wet regions coexist in the porous medium. Reznik et al. (1967) developed such a model, but its application to actual reservoirs would be limited because this simplified model did not incorporate actual pore-size distribution to define pore geometry. This model indicated that optimum oil recovery was achieved when the wettability tended towards oil-wetness, and the oil relative permeability curves changed from a convex to a concave curvature.

Theoretical models of relative permeability are thus mainly based on a description of fluid flow through a more or less complex arrangement of capillaries and can therefore only represent ideal porous systems. The resulting relations are usually expressed in terms of saturation and some basic property of the porous medium. This dependence is not based on intrinsic fluid or rock properties but on a combination of these that might vary with the system that is being considered. Directly measurable quantities, such as fluid properties, rarely appear in their formulation. Therefore, it is impossible to predict theoretically what effect increasing temperature would have on relative permeabilities. Carefully conducted experiments would shed some light on the matter but will be specific to the fluid-fluid-solid system studied as has been the case for all reports published in the literature to date.

6.1.2 Experimental Studies

The effect of temperature on irreducible water and residual oil saturations and relative permeability has been studied extensively by many researchers. Summaries of the experimental observations reported in the literature were presented earlier in Tables 2.1 and 2.2 for unconsolidated and consolidated porous media, respectively. Most reported an increase in irreducible water and a decrease in residual oil with increasing temperature, shifting the saturation range to higher water saturations. Contradictory results were obtained for relative permeabilities in many cases because different systems were used.

Most experimental studies were conducted with mineral or refined oils. Extracted rather than preserved cores were used in most cases. The studies reporting no temperature effects were performed in clean sands with both types of oil (Sufi et al., 1982; Miller and Ramey, 1985; this study) or when the viscosity ratio was temperature independent (Wilson, 1956; Lo and Mungan, 1973). Maini and Okazawa (1986) reported temperature effects with clean sand and crude oil. An analysis of their methodology indicated that these effects resulted from interpretation rather than experimental results, which would render their conclusions questionable. From these observations, one might conclude that the cause of temperature effects could be due to the solid-fluid combination and their interaction rather than to the type of solid or fluid.

In this study, no significant temperature effects were found for the Athabasca bitumen-water-clean unconsolidated sand system, and this is attributed to the use of a clean porous network containing virtually no clays. The type of oil is not the determining factor as similar results have been obtained with various crude and mineral oils: Cold Lake bitumen (Henning and Polikar, 1986), Kaydol (Sufi et al., 1982) and Blandol (Miller and Ramey, 1985). An ideal system, although not directly related to field operations, is more representative and useful for establishing the methodology for such complex measurements and obtaining reproducible and reliable results.

Experiments with reservoir oil sand samples failed to show any temperature variations in the end points. This by no means indicates that temperature effects are absent when dealing with heterogeneous systems. Possible alterations in cores could be of geochemical (clay-brine interactions) and/or mechanical nature (plugging due to clay movement) when clay minerals are present. The reactive nature of such systems could, in turn, depend on various factors such as temperature, flow rate, brine concentration. The reservoir sand samples behaved like non-reactive materials, and temperature effects on their relative permeability relationships cannot be considered to be significant.

The reactive nature of the fluid-fluid-solid system has not been addressed by any study until now and is the critical factor for defining temperature effects. Only a comparison between ideal (clean) and real (reservoir) systems as undertaken in this study will provide answers to the effect of temperature on relative permeability relations. Maini and Batycky (1983) indicated temperature effects to be less marked in horizontally drilled preserved core plugs than in vertical plugs and attributed the differences to the occurrence of clay lenses and clay migration. Bennion et al. (1985) reported much lower water relative permeabilities for preserved cores and reservoir fluids than for extracted cores and mineral oil. It seems that in both the above cases the reactivity of the system studied is responsible for the observed effects.

The effect of temperature on Kaydol-water relative permeability curves in clean sand is more difficult to interpret. Recovery functions seemed to depend on the absolute oil viscosity: the higher the viscosity, the longer the hot water flood to reach residual conditions. This factor could have caused the observed differences because the temperature range for the Kaydol experiments was not the same as that for the bitumen experiments. Another cause of the observed effect could be viscous instabilities that were not directly accounted for in the calculations, although Sufi et al. (1982) found the curves to be insensitive to viscous fingering.

Because of practical considerations, all bitumen experiments were conducted at elevated temperatures (100°C and higher). The Kaydol experiments started at room temperature to obtain comparable viscosities and viscosity ratios to bitumen, and the temperature range for Kaydol could explain the differences between bitumen and Kaydol results: heating in itself affects fluid and rock properties. Most literature reports relative permeability studies starting at or near room temperature and ranging up to 280°C, and temperature induced changes can vary greatly from one system to another. In light of the results obtained in this study with both oils, one can conclude that temperature effects on relative permeabilities are insignificant in a clean sand despite the large variation encountered in the fluid properties; however, these effects could exist for actual field systems.

6.2 Comparison of Steady and Unsteady State Results

The experimentally measured average initial water saturation was not found to be the same for steady and unsteady state bitumen-water relative permeability curves (see Table 5.5). There is a shift to higher water saturations in the unsteady state data. A comparison between the two sets of curves, both obtained at 125°C, is nevertheless possible and is presented in Figure 6.1, where the magnitude of the saturation difference is indicated. It should be noted that the smooth curves shown in Figure 6.1 were obtained from fitting the calculated (steady state) and the experimental (unsteady state) data. The similarities and differences are discussed below.

6.2.1 Shape of the Relative Permeability Curves

The water relative permeability curves exhibit the same shape but overlap: the unsteady state values are initially higher and then lower than the steady state values. The bitumen relative permeability curves are less alike and in this case, the steady state values are lower for most of the saturation range. Both curves have a convex curvature at low water saturations but the curvature of the unsteady state function changes from convex to concave as the water saturation increases. This results in an S-shaped unsteady state bitumen relative permeability curve having a tail at high water saturations. This tail results from the much larger fluid throughput needed to reach the actual residual saturation

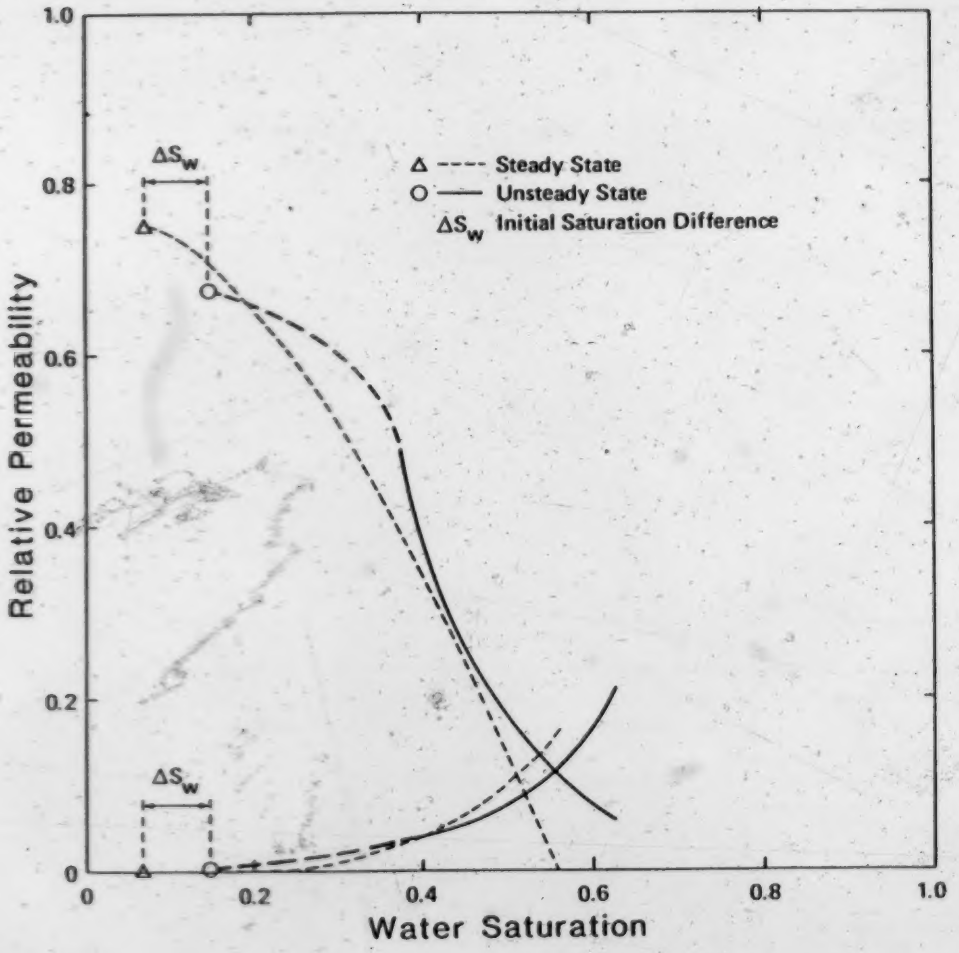

Figure 6.1 : Bitumen-Water Relative Permeability Curves
(steady versus unsteady state)

condition, which was not the case in the steady state experiments reported in this study. However, a tail was observed in some steady state experiments with a large water throughput (Henning and Polikar, 1986), indicating that the recovery of viscous oils by hot water could take an infinitely long time.

Relative permeability curves may have various shapes, depending on the dominant mechanisms controlling the multiphase flow through porous media. They are typically presented with concave curvatures for both the oil and water branches, as shown in Figure 2.1. This representation might not be totally justified for heavy oils in view of the oil recovery mechanism that these curves describe. The experimental results of this study showed that oil was recovered rapidly in the initial stages of the hot water flood, with further production tapering off rapidly. Convex oil relative permeability at low water saturations would represent such a recovery behaviour. There is increasing evidence in the literature, based on theoretical as well as experimental reports, that the shape of the oil curve is convex rather concave (Sahimi et al., 1986).

To further examine differences and similarities of the experimental results, the water-to-bitumen relative permeability ratios are presented in Figure 6.2 on a semi-logarithmic plot as a function of the water saturation. All the relative permeability ratios fall on a single curve. A higher water-to-bitumen relative permeability ratio at constant saturation would indicate that the water

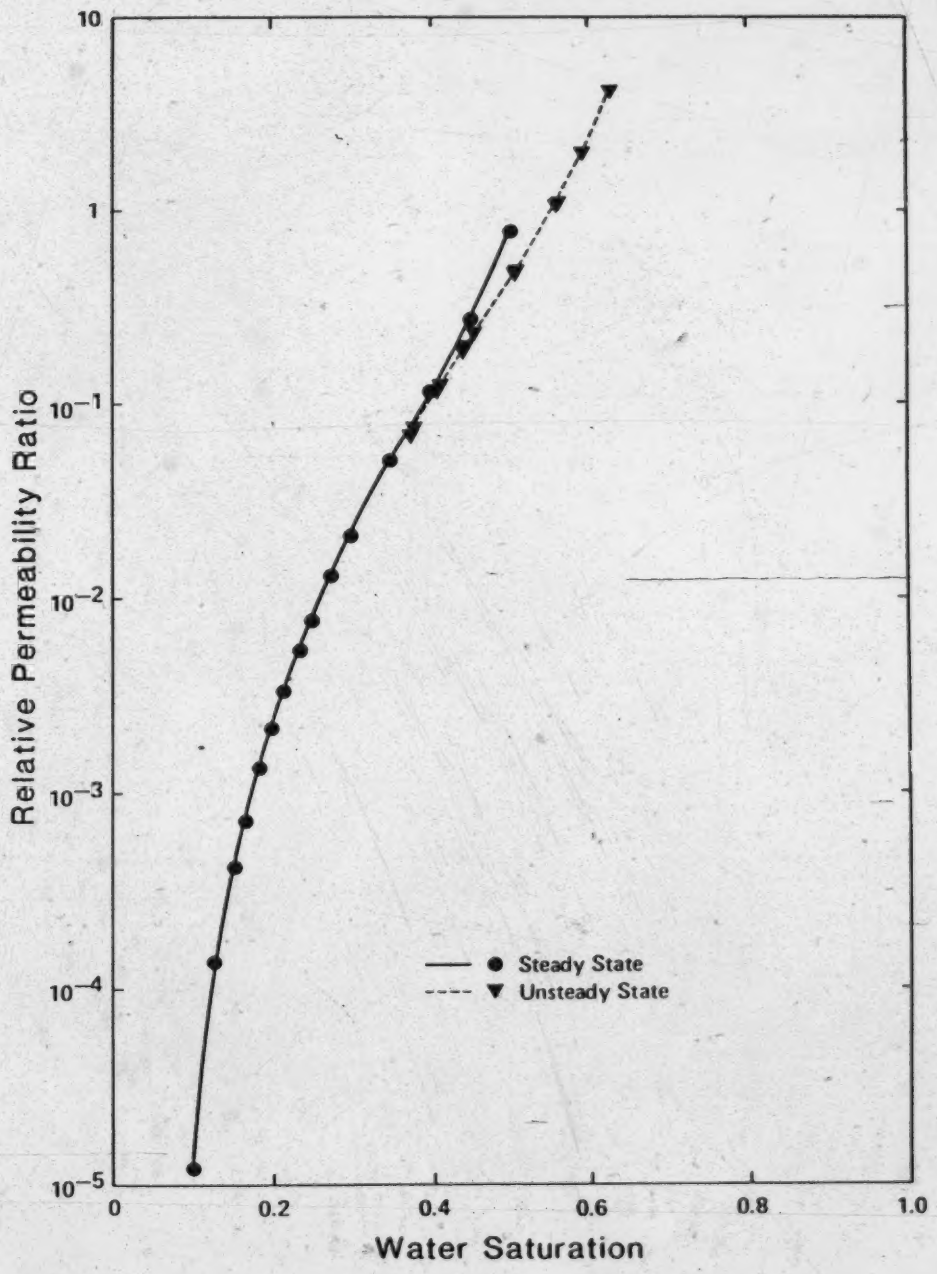

Figure 6.2 : Bitumen-Water Relative Permeability Ratio Functions

flood is less efficient due to a change in the wettability (less water-wet), all other variables being constant (Mungan, 1966). Such a behaviour has been reported by Handy and Datta (1966) and Amaefule and Handy (1982), showing different phase distributions for steady and unsteady state water floods, where the latter were less efficient than the former.

The fractional flow of water, f_w, was calculated under the assumption of negligible capillary pressure (high pressure drop) and gravitational components (very small density difference). Its mathematical expression is

$$f_w = \left[1 + \frac{k_{rb}}{k_{rw}} \cdot \frac{\mu_w}{\mu_b} \right]^{-1} \qquad (6.1)$$

The fractional flow curves for the steady and unsteady state cases are shown in Figure 6.3. Although data were incomplete for the lower water saturations in the dynamic displacement experiments, all the values can be represented by a single curve. It should be noted that the fractional flow curve is quite steep and covers a relatively narrow saturation range, indicating that most of the bitumen displacement by hot water under isothermal conditions occurred in the initial stages of the flood.

6.2.2 Stability Analysis

Rapoport and Leas (1953) defined a scaling coefficient $Lv\mu_w$ based

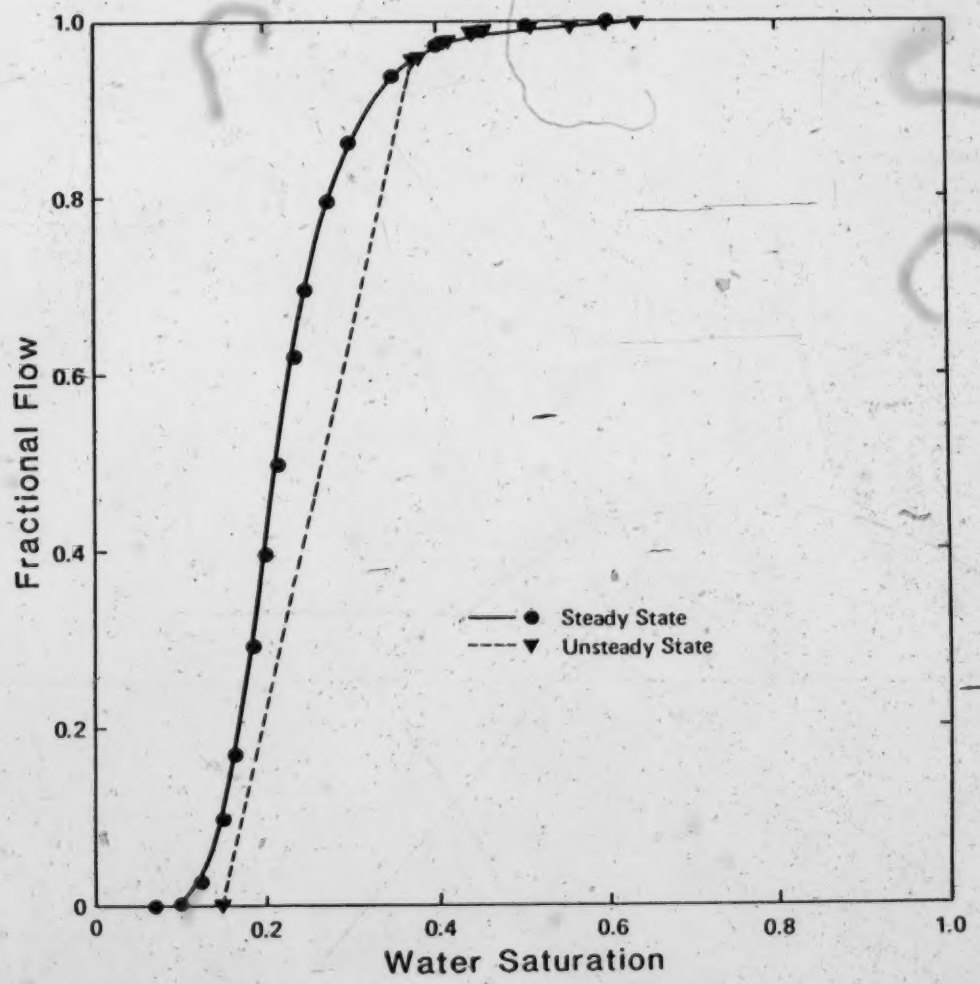

Figure 6.3 : Fractional Flow Curves for Bitumen-Water

on the length of the system, the rate of injection and the viscosity of the displacing phase. They experimentally determined a critical value above which capillary end effects were negligible and floods were stabilized: breakthrough recoveries became independent of the scaling coefficient above this critical value. They reported that, in oil-wet porous media, fairly small end effects usually resulted for a value of $Lv\mu_w$ greater or equal to 1.0 $cm^2 \cdot cp/min$. They also reported values both smaller and larger than unity for various sandstones, indicating a transition region between stabilized and unstabilized flow. In the dynamic displacement experiments considered here, the scaling coefficient was calculated to be 0.62 $cm^2 \cdot cp/min$ for a nominal flow rate of 80 cm^3/h (1 PV/h) at 125°C, which is in the range of critical scaling coefficients for stabilized flow. The use of the JBN method based on the assumption of stabilized flow may then be justified in calculating two phase relative permeabilities for our experiments.

All experiments were conducted vertically upwards for both steady state and dynamic displacement experiments. An initial injection rate of 1 PV/h (superficial velocity of 2 m/d) was chosen to minimize capillary forces with respect to viscous forces. The criterion for stabilized flow postulated by Kyte and Rapoport (1958), that the imposed total pressure drop be 345 kPa (50 psi) or greater regardless of the length of the core, was not met in any of the water floods. Even a seven-fold increase in the initial injection rate did not satisfy the Kyte and Rapoport criterion (Miles-Dixon et al., 1985), although the saturation profiles measured with an

x-ray attenuation scanning device during the water floods indicated a steady state condition.

The stability theory of Bentsen (1985) suggests that the type of displacement which takes place in a porous medium depends on the balance which exists between capillary, gravitational and viscous forces. If the combined forces of gravity and capillarity are greater than the viscous forces, the displacement will be stable. If, however, the reverse is true, the displacement will be unstable. In all the water flood experiments described in this study, gravity slightly destabilized the upward water flow during the displacement of bitumen because the density of the displacing phase was less than 1% lower than that of the displaced phase (Marle, 1981).

Bentsen (1985) presented a dimensionless instability number for rectangular systems that is proportional to the one proposed by Peters and Flock (1981) by a function of the end point mobility ratio, $f(M_r)$. The criteria used to determine the onset of instability utilize the concept of an effective interfacial tension within the porous medium, σ_e, that depends on the characteristics of the porous medium and the bulk interfacial tension. The instability number for a cylindrical system, I_{sc}, will be of the following form when combining the Bentsen and Peters-Flock equations:

$$I_{sc} = \frac{(M_r-1)\cdot(v-v_{crit})\cdot\mu_w\cdot D^2}{\sigma_e\cdot k_{wor}} \cdot f(M_r) \qquad (6.2)$$

The critical value of I_{sc} for the onset of instability is 13.56. Peters and Flock (1981) used a wettability number, C*, to define the effective interfacial tension ($\sigma_e = C^* \cdot \sigma_{o/w}$) which they determined experimentally from the wavelength (or diameter) of the fastest growing finger. Recently, Bentsen (1986) suggested the use of capillary pressure data to estimate the effective or pseudointerfacial tension, σ_e, which he defined in terms of the area under the capillary pressure curve. However, insufficient data are available at the present time for directly calculating an instability number based on the theories of Bentsen or Peters and Flock for these core-size experiments.

The scaling coefficient for stabilized flow (Rapoport and Leas, 1953) and the instability number (Bentsen, 1985; Peters and Flock, 1981) are both proportional to the flooding rate. If a high flow rate is necessary to overcome capillary end effects for satisfying the stabilized flow requirement, this high flow rate will be in conflict with the requirement to prevent viscous fingering. Thus, in many heavy oil systems, it may be impossible to generate stable and stabilized flows.

A flow stability analysis is not of concern to the steady state experiments, which were conducted until no further changes were observed in the pressure drop behaviour across the core. At this stage, changes in production were assumed to be negligible and the Darcy equation was used separately for each flowing phase to calculate the individual relative permeabilities at the prevailing

saturation conditions. Since the steady state experiments do not involve the displacement of one fluid by another, the resulting relative permeability curves are not affected by instability and may therefore be considered to be the true curves for the system.

The steady state experimental results were consistent with the findings of Foster (1973): the residual bitumen saturations obtained in the temperature range of 100°C to 250°C, like their corresponding capillary numbers, were all similar. These residuals averaged only 0.50 (average displacement efficiency of 46.4%). This relatively high saturation value could be explained by the adverse mobility ratio encountered during the water floods, giving rise to fingering. Some cores were sampled sectionally at the end of a water flood and the residual bitumen saturation was found to be fairly uniform along the length of the core, with a slight increase on the production side, beyond the tip of the pressure probe. This uniform sweep, however, was not an indication that the displacement was complete.

The unsteady state experiments showed that a higher recovery could be achieved by increasing the duration of the hot water flood. The results indicated that a ten-fold increase in the volume of water injected decreased the final bitumen saturation from about 50% to 40% PV. This "stripping" process is extremely slow due to the adverse mobility ratio of the fluids and would take a very long, if not infinite time to reach the true residual saturation. The tail of the bitumen relative permeability curve at large water

saturations reflects the recovery process that is taking place under the unfavorable conditions. Otherwise, the few differences between steady and unsteady state relative permeability curves indicate that the level of stability is similar in both cases.

Peters and Khataniar (1985) studied the effect of instability on oil-water relative permeability curves obtained by the dynamic displacement method. They compared curves determined from steady and unsteady state experiments at several levels of instability. At a given saturation, the unsteady state relative permeabilities to oil were always lower and those to water were always higher than their steady state counterparts. The differences increased as the displacements became more unstable. The steady state oil relative permeability curve was convex and all unsteady state oil curves had an S-shaped curvature, similar to the results of the present study.

The stability numbers for the Peters and Khataniar experiments ranged from 34 to 30,360 and were divided into three broad groups of mild (less than 50), intermediate (50 to 10,000) and severe (greater than 10,000) instability. The sensitivity of relative permeability curves to the degree of instability was found to be minimal for the first and third groups and significant for the second group. Their results showed that for the mildly unstable displacements, the relative permeability curves approached the steady state curves.

The steady and unsteady state bitumen-water curves showed the same trends as those of Peters and Khataniar but did not differ much from one another, indicating a very mild level of instability. Using the Peters and Flock (1981) stability criterion for cylindrical systems and assuming their wettability constant of 306.25 to hold for the bitumen-water system examined in this study, this number for our experiments was estimated to be approximately 723 for the bitumen experiments, which is not consistent with their results.

In using the method proposed by Bentsen (1986) to calculate a pseudointerfacial tension, a determination of the capillary pressure curve representing the bitumen-water-sand system used in these experiments is necessary. The pseudointerfacial tension is then calculated from the area under this capillary pressure curve, A_c, using:

$$\sigma_e = A_c \cdot \phi \cdot \frac{(1-S_{wi}-S_{or})}{2/\bar{r}_m}, \qquad (6.3)$$

where $2/\bar{r}_m=1$. The pseudointerfacial tension is a function of both the pore size distribution of the sand and the wetting behaviour of the fluids. In the absence of capillary pressure data, the pseudointerfacial tension, and therefore the instability number by using Equation (6.2), can only be estimated from available data for other oil-water-sand systems. Sarma and Bentsen (1986) have reported data for the area under the capillary pressure curve of various mineral oil-distilled water-80 to 120 mesh Ottawa sand

systems. Based on these data and assuming that the function of the end point mobility ratio, expressed as:

$$f(M_r) = \frac{(M_r^{5/3} + 1)}{(M_r + 1)\cdot(M_r^{1/3} + 1)^2} \qquad (6.4)$$

is the same for cylindrical and rectangular geometries, the instability number was estimated to be about 742.

Using both the Peters and Flock (1981) and Bentsen (1985) criteria, the instability number for the bitumen-water experiments was estimated, and found to be larger than its critical value for stable flow. Unsteady state imbibition relative permeability functions for bitumen and water were nevertheless calculated by the JBN method as the flow was stabilized during the displacement of bitumen by hot water. Therefore, the relative permeabilities calculated in these core flood experiments may not be applicable to other systems having different levels of stability.

During the dynamic displacement experiments, the pressure drop and production data were collected while changes were still taking place inside the core. The interpretation of these displacement data to obtain relative permeability versus saturation functions should reflect the phenomena occurring during the displacement process. Because of differences in methodology and interpretation of the measured data between the steady and unsteady state experiments, the resulting relative permeability curves could be different. However, on the basis of relative permeability ratios and

fractional flow curves discussed above, these differences are small and do not represent a change in stability or phase distributions during the hot water flood process.

6.3 Relative Permeability Curves for Alberta Heavy Oils

Relative permeability is a macroscopic parameter describing the average behaviour of fluids over several pore throat diameters. It averages various microscopic phenomena such as advection, dispersion and capillarity without differentiating between the individual contribution of each one. Due to heterogeneity and interfacial effects present in the reservoir, the dominating features may vary with the location. Therefore, a single set of relative permeability curves may not describe an entire reservoir, as they do a homogeneous core. A range of relative permeability curves may be necessary to describe the recovery of heavy oils, even for a given deposit, as indicated in the following comparative study for Alberta heavy oils and bitumens.

A graphical comparison was undertaken of published data on Alberta heavy oil-water relative permeabilities to determine their range of applicability. Hirasaki (1975) found that the shape of normalized relative permeability curves and the end point mobility ratio were important adjustable parameters during history matching of an oil displacement process. All relative permeability curves were brought to the same scale by normalizing the water saturation, and the oil and water relative permeabilities (see Section 5.2.2).

Published data for experimentally determined heavy oil-water relative permeabilities are compared in Figure 6.4. The steady state curves of this study along with representative curves chosen from the latest available published works make up this comparison. A wide variation was found in the relative permeabilities for these heavy oil-water systems. The relative permeability curves compared were determined experimentally in clean, extracted or native sand cores, with a heavy oil or bitumen and water or brine as the flowing fluids.

The saturation range for the non-normalized curves never exceeded 0.5 in all cases, indicating that final recovery under the experimental conditions would not reach 50% of OOIP in the laboratory. The curves, however, differ considerably. The two heavy oil curves obtained by the steady state method are the highest (this study) and the lowest (Closmann et al., 1985), and their corresponding water curves are the lowest ones. The present study was conducted in clean unconsolidated sand and the other one used native sand. The remaining curves were all obtained by history matching of dynamic displacement experiments. Thus, the shapes of the latter curves were dictated by the history matching procedure which incorporated concave curves as these are most commonly found in the literature (Kerig and Watson, 1985).

Figure 6.5 presents the results of the comparison for data used in numerical simulation. A wide variation was found, similar to that of the experimental curves (Figure 6.4), since most data were

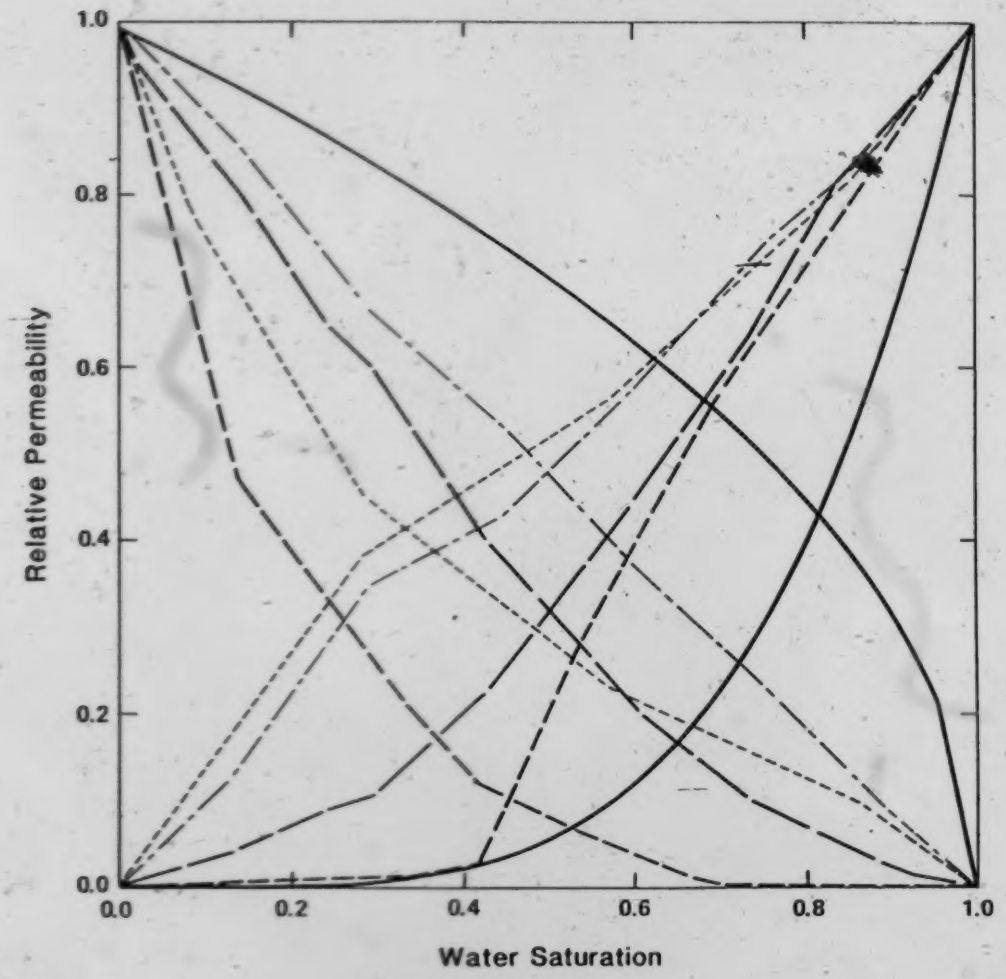

Figure 6.4 : Comparison of Experimental Heavy Oil-Water Relative Permeability Curves (normalized)

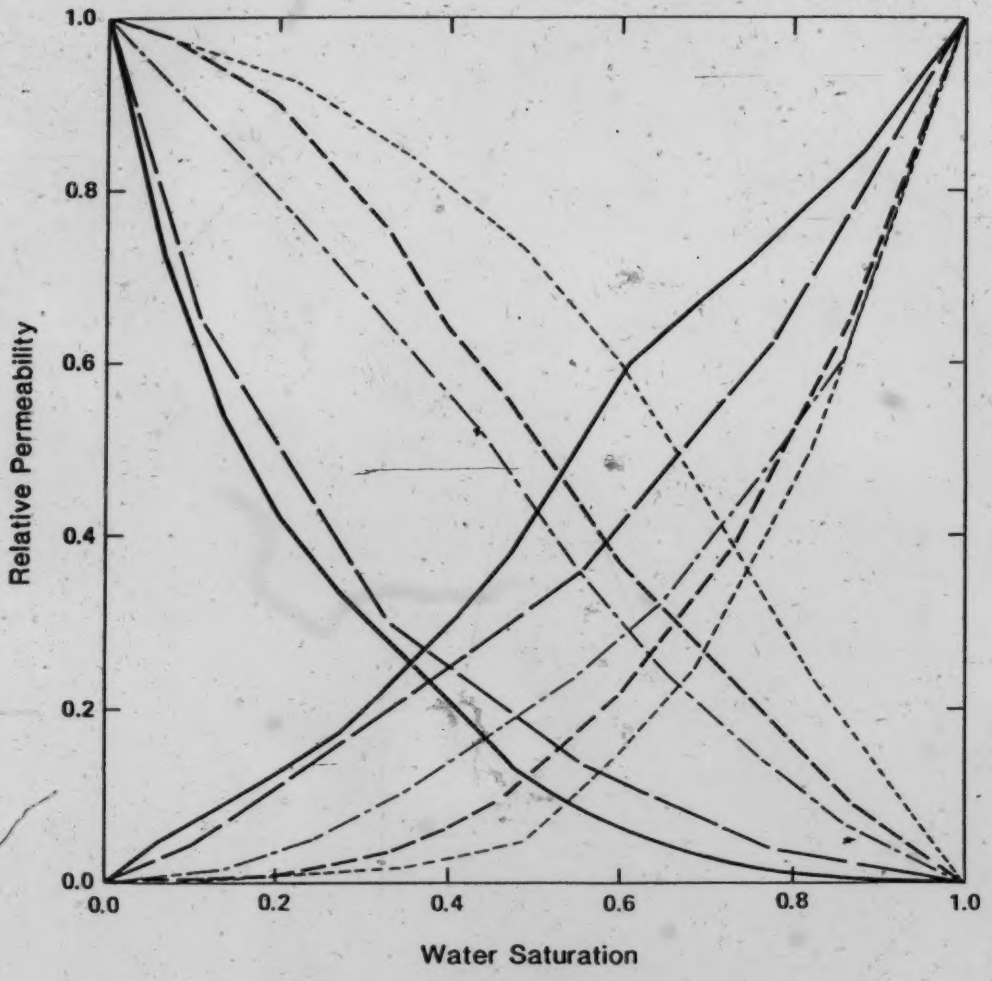

Figure 6.5 : Comparison of Normalized Oil-Water Relative Permeability Curves

obtained by history matching the production performance of individual fields. A common trend also emerged from these graphical comparisons: the higher the oil curve, the lower the water curve in most cases. Although some of the oil curves were convex, the water curves seldom exhibited such behaviour.

When normalized with respect to saturation and end point relative permeabilities, the bitumen-water relative permeability curves obtained in this study retain their basic shape. Both sets of normalized curves fall within the range presented for the various Alberta heavy oil and oil sand deposits (see Figures 6.4 and 6.5). The large variation found in the comparative study can be attributed to the manner in which those curves were determined. Some were obtained by history matching field data, others were derived from dynamic displacement experiments, and the remaining were measured by the steady state method.

Laboratory-determined relative permeability relations must account for the mechanisms of the displacement process and be representative of the porous medium when used in field applications. Controlled experimental conditions that best reproduce the field must be used in the laboratory. The interpretation of the experimental data should be performed in conjunction with the development of a mechanistic mathematical model that will take into account flow stability, scaling, and reservoir heterogeneity if any of these are dominant factors that will affect the end points and the shape of the relative permeability curves. Ideally, the adjustment of

laboratory curves should not be necessary for their use in reservoir performance prediction, provided the immiscible displacement flow model conceptually represents the physics of multiphase flow in the reservoir. In practice, however, this is not the case: carefully determined laboratory relative permeability curves on a small core sample are used as input parameters to numerical simulators and their shapes are adjusted until a good history match has been achieved for an entire field.

The average end point relative permeability values that were measured in this study for bitumen and water are in the range of those generally encountered in water-wet systems; similar values were recently used in the numerical modelling of a large scale laboratory experiment of bitumen recovery from Athabasca oil sands (Stone and Malcolm, 1985). There was, however, a shift in the saturation range due to the artificial nature of the experimental fluid-fluid-solid system. The initial bitumen saturation in the reconstituted cores was higher than that encountered in field samples. In the laboratory, only half of the bitumen-in-place was recovered by a hot water flood. If the same recovery were true for the field, these end point saturation results could be used directly in numerical simulators that predict reservoir performance, provided the saturation range is adjusted to reflect the irreducible water saturation in the reservoir.

7. CONCLUSIONS

To date, very little information is available on the effect of temperature on bitumen-water relative permeability relationships. This is the first extensive study undertaken to determine bitumen-water relative permeability functions over a large temperature range (100°C to 250°C).

An apparatus was developed and successfully tested for the determination of two phase oil-water relative permeabilities. It has proven capable of operating at high pressures and temperatures for long periods of time. During the course of this study, several modifications to the apparatus and experimental procedures were made to improve the quality of the data generated.

A reproducible packing procedure was developed for preparing clean unconsolidated Ottawa sand packs to simulate oil sand cores. The cores were homogeneous and yielded reproducible porosities (within 2%) and absolute permeabilities (within 10%) when packed with sand having an average grain size equivalent to 200 mesh. The measured properties were similar to values reported for various Alberta oil sand deposits.

The experiments were conducted with both clean and reservoir sands in order to evaluate differences between ideal and real systems with proven and reliable experimental procedures. These

procedures were then extended to another heavy oil (Kaydol)-water-clean sand system over a lower temperature range (20°C to 100°C). The results of this study support the following conclusions:

1. No significant temperature effects were found for the Athabasca bitumen-water system in clean or field sands due to the lack of reactivity of the fluid-fluid-solid combinations.

2. Bitumen-water relative permeability curves were determined by both the steady and unsteady state methods. Despite different recovery processes, there was little difference between measured steady and unsteady state relative permeability curves, which indicated that the level of displacement stability was similar in both cases.

3. End point experiments done in triplicate with clean sand produced reproducible results, whereas reservoir sand results showed variations that can be attributed to the effects of heterogeneity. New and accurate data have been determined for the Athabasca oil sands.

4. The analysis of dynamic displacement data for the determination of oil-water relative permeability curves is largely dependent on the water throughput. The number of pore volumes needed to reach the residual oil saturation is proportional to the absolute oil viscosity.

5. The relative permeabilities calculated in core flood experiments involving heavy oils may not be applicable to other systems as is shown by the different curves obtained for bitumen-water and Kaydol-water in clean unconsolidated sands. These flow systems may be dominated by viscous fingering.

6. A comparison of normalized relative permeability curves for heavy oils of Alberta, including the results of this study, showed that wide variations exist among the reported data. Therefore, a range of relative permeability curves may be necessary to describe the various recovery mechanisms of heavy oils by hot water from heterogeneous unconsolidated sands.

8. RECOMMENDATIONS

This work has established experimental procedures for determining two phase heavy oil-water relative permeabilities as a function of temperature in ideal systems. An extensive data base has been generated for Athabasca bitumen in the temperature range of 100°C to 250°C. Future work should aim at applying this knowledge to field cores. The effect of temperature and other variables on the end points and the shape of the relative permeability curves will then indicate if and how heterogeneous systems differ from homogeneous systems.

In the future, carefully planned experiments are needed to avoid misleading interpolations because the duration of dynamic displacement experiments under unfavorable viscosity ratio conditions is of prime importance in the accurate interpretation of water flood results. Representative functional forms of the recovery and pressure drop curves over a large saturation range will result in reliable relative permeability relations.

BIBLIOGRAPHY

Abasov, M.T., Tairov, N.D., Abdullaeva, A.A., Alieva, Sh.M. and Mamedov, A.I. (1976): Influence of Temperature on Relative Phase Permeability at High Pressures; Dokl. Akad. Nauk Azerb. SSR., no. 8, pp. 31-34 (in English).

Abrams, A. (1975): The Influence of Fluid Viscosity, Interfacial Tension, and Flow Velocity on Residual Oil Saturation Left by Waterflood; Society of Petroleum Engineers Journal, volume 15(5), pp. 437-447.

Adams, D.M. (1981): Experiences with Waterflooding Lloydminster Heavy Oil Reservoirs; paper SPE 10196 presented at the 56th Annual Technical Conference of the Society of Petroleum Engineers, San Antonio, TX, October 5-7.

Amaefule, J.D. and Handy, L.L. (1982): The Effect of Interfacial Tensions on Relative Oil/Water Permeabilities of Consolidated Porous Media; Society of Petroleum Engineers Journal, volume 22(3), pp. 371-381.

Anderson, W.G. (1986): Wettability Literature Survey-Part 1: Rock-Oil-Brine Interactions, and the Effects of Core Handling on Wettability; Journal of Petroleum Technology, volume 38(11), pp. 1125-1144.

Archer, J.S. and Wong, S.W. (1973): Use of a Reservoir Simulator to Interpret Laboratory Waterflood Data; Society of Petroleum Engineers Journal, volume 13(6), pp. 343-347.

Bardon, C. and Longeron, D.G. (1980): Influence of Very Low Interfacial Tensions on Relative Permeability; Society of Petroleum Engineers Journal, volume 20(5), pp. 391-401.

Batycky, J.P. and McCaffery, F.G (1978): Low Interfacial Tension Displacement Studies; Research Note RN-6, Petroleum Recovery Institute, Calgary, AB.

Bennion, D.W., Moore, R.G. and Thomas, F.B. (1985): Effect of Relative Permeability on the Numerical Simulation of the Steam Stimulation Process; Journal of Canadian Petroleum Technology, volume 24(2), pp. 40-44.

Bentsen, R.G. (1978): Conditions under which the Capillary Term May Be Neglected; Journal of Canadian Petroleum Technology, volume 17(4), pp. 25-30.

Bentsen, R.G. and Saeedi, J. (1979): Liquid-Liquid Immiscible Displacement in Unconsolidated Porous Media; paper no. 79-30-41 presented at the 30th Annual Technical Meeting of the Petroleum Society of CIM, Banff, Alberta, May 8-11.

Bentsen, R.G. (1985): A New Approach to Instability Theory in Porous Media; Society of Petroleum Engineers Journal, volume 25(5), pp. 765-779.

Bentsen, R.G. (1986): Use of Capillary Pressure Data to Estimate the "Pseudointerfacial Tension" for Analysis of Stability of Fluid Flow in Porous Media; AOSTRA Journal of Research, volume 2(4), pp. 213-222.

Bird, G.W. (1986): Personal Communication.

Briggs, J.P. (1985): Preliminary Measurements of Capillary Pressure with a Prototype Centrifuge Cell; AOSTRA/ARC Joint Program, report no. 8586-55, Edmonton, AB.

Brooks, R.H. and Corey, A.T. (1964): Hydraulic Properties of Porous Media; Hydrology Papers no. 3, Colorado State University, Fort Collins, CO (March).

Buckley, S.E. and Leverett, M.C. (1942): Mechanism of Fluid Displacement in Sands; Transactions AIME, volume 146, pp. 107-116.

Burdine, N.T., Gournay, L.S. and Reichertz, P.P. (1950): Pore Size Distribution of Petroleum Reservoir Rocks; Transactions AIME, volume 189, pp. 195-204.

Burdine, N.T. (1953): Relative Permeability Calculations from Pore Size Distribution Data; Transactions AIME, volume 198, pp. 71-77.

Carrigy, M.A. (1967): The Physical and Chemical Nature of a Typical Tar Sand: Bulk Properties and Behaviour; Proceedings, 7th World Petroleum Congress, Elsevier Publishing Co., Amsterdam, volume 3, pp. 573-581.

Chatzis, I. and Dullien, F.A.L. (1982): Mise en Oeuvre de la Theorie de la Percolation pour Modeliser le Drainage des Milieux Poreux et la Permeabilite Relative au Liquide non Mouillant Injecte; Revue de l'Institut Francais du Petrole, volume 37(2), pp. 183-205.

Closmann. P.J., Waxman, M.W. and Deeds, C.T. (1985): Steady-State Tar/Water Relative Permeabilities in Peace River Cores at Elevated Temperature; paper SPE 14227 presented at the 60th Annual Technical Conference of the Society of Petroleum Engineers, Las Vegas, NV, September 22-25.

Coats, K.H. (1976): Simulation of Steam Flooding with Distillation and Solution Gas; Society of Petroleum Engineers Journal, volume 16(5), pp. 235-247.

Coats, K.H., Ramesh, A.B. and Winestock, A.G. (1977): Numerical Modeling of Thermal Reservoir Behavior; The Oil Sands of Canada-Venezuela, D.A. Redford and A.G. Winestock, ed., CIM special volume 17, pp. 399-410.

Combarnous, M. and Pavan, J. (1968): Deplacement par l'eau chaude d'huiles en place dans un milieu poreux; Communication no. 37, III^{e} Colloque A.R.T.F.P., pp. 737-757, Pau, Sep. 23-26 (in French).

Corey, A.T. (1954): The Interrelation between Gas and Oil Relative Permeabilities; Producers Monthly, volume 19(1), pp. 38-41 (November).

Cottrell, J.H. (1963): Development of an Anhydrous Process for Oil Sand Extraction; The K.A. Clarke Volume, M.A. Carrigy, ed., Alberta Research Council, Edmonton, AB, pp. 193-206.

Craig, F.F. Jr. (1971): The Reservoir Engineering Aspects of Waterflooding; Monograph Series, volume 3, Society of Petroleum Engineers, Dallas, TX.

Danis, M. and Jacquin, Ch. (1983): Influence du Contraste de Viscosites sur les Permeabilites Relatives lors du Drainage - Experimentation et Modelisation; Revue de l'Institut Francais du Petrole, volume 38(6), pp. 723-733.

Darcy, H. (1856): Les Fontaines Publiques de la Ville de Dijon; Victor Dalmon, ed., Paris (in French).

Davidson, L.B. (1969): The Effect of Temperature on the Permeability Ratio of Different Fluid Pairs in Two-Phase Systems; Journal of Petroleum Technology, volume 21(8), pp. 1037-1046.

Demetre, G.P., Bentsen, R.G. and Flock, D.L. (1982): A Multi-Dimensional Approach to Scaled Immiscible Fluid Displacement; Journal of Canadian Petroleum Technology, volume 21(4), pp. 49-61.

Dietrich, J.K. and Bondor, P.L. (1976): Three-Phase Oil Relative Permeability Models; paper SPE 6044 presented at the 51st Annual Technical Conference of the Society of Petroleum Engineers, New Orleans, LA, October 3-6.

Dietrich, J.K. (1981): Relative Permeability during Cyclic Steam Stimulation of Heavy-Oil Reservoirs; Journal of Petroleum Technology, volume 31(10), pp. 1987-1989.

Dietrich, J.K. (1983): Cyclic Steaming of Tar Sands through Hydraulically Induced Fractures; paper SPE 11684 presented at the California Regional Meeting of the Society of Petroleum Engineers, Ventura, CA, March 23-25.

Donaldson, E.L., Lorenz, B.P. and Thomas, R.D. (1966): The Effects of Viscosity and Wettability on Oil and Water Relative Permeabilities; paper SPE 1562 presented at the 41st Annual Technical Conference of the Society of Petroleum Engineers, Dallas, TX, October 2-5.

Dullien, F.A.L. (1975): New Network Permeability Model of Porous Media; American Institute of Chemical Engineers Journal, volume 21(2), pp. 299-307.

Edmondson, T.A. (1965): Effect of Temperature on Waterflooding; Journal of Canadian Petroleum Technology, volume 4(4), pp. 236-242.

Edmunds, N.R. (1984): An Analytical Model of the Steam Drag Effect in Oil Sands; Journal of Canadian Petroleum Technology, volume 23(5), pp. 30-39.

Ehrlich, R. and Crane, F.E. (1969): A Model for Two-Phase Flow in Consolidated Materials; Society of Petroleum Engineers Journal, volume 9(2), pp. 221-231.

Ehrlich, R. (1970): The Effect of Temperature on Water-Oil Imbibition Relative Permeability; paper SPE 3214 presented at the Eastern Regional Meeting of the Society of Petroleum Engineers, Pittsburgh, PA, November 5-6.

Ehrlich, R. (1977): Laboratory Investigation of Steam Displacement in the Wabasca Grand Rapids "A" Sand; The Oil Sands of Canada-Venezuela, D.A. Redford and A.G. Winestock, ed., CIM special volume 17, pp.364-379.

Engelberts, W.F. and Klinkenberg, L.J. (1951): Laboratory Experiments on the Displacement of Oil by Water from Packs of Granular Materials; Proceedings, 3rd World Petroleum Congress, The Hague, section II, pp. 544-554.

Fatt, I. and Dykstra, H. (1951): Relative Permeability Studies; Transactions AIME, volume 192, pp. 249-255.

Fatt, I. (1953): The Effect of Overburden Pressure on Relative Permeability; Transactions AIME, volume 198, pp. 325-326.

Fatt, I. (1956): The Network Model of Porous Media - Parts I, II & III; Transactions AIME, volume 207, pp. 144-177.

Foster, W.R. (1973): A Low-Tension Waterflooding Process; Journal of Petroleum Technology, volume 25(2), pp. 205-210.

Fulcher, R.A. Jr., Ertekin, T. and Stahl, C.D. (1985): Effect of Capillary Number and its Constituents on Two-Phase Relative Permeability Curves; Journal of Petroleum Technology, volume 37(2), pp. 249-260.

Gates, J.I. and Lietz, W.T. (1950): Relative Permeabilities of California Cores by the Capillary-Pressure Method; API Drilling and Production Practice, pp. 285-301.

Geffen, T.M., Owens, W.W., Parrish, D.R. and Morse, R.A. (1951): Experimental Investigation of Factors Affecting Laboratory Relative Permeability Measurements; Transactions AIME, volume 192, pp.99-110.

Gobran, B.D., Brigham, W.E. and Ramey, H.J. Jr. (1981): Absolute Permeability as a Function of Confining Pressure, Pore Pressure and Temperature; paper SPE 10156 presented at the 56th Annual Technical Conference of the Society of Petroleum Engineers, San Antonio, TX, October 5-7.

Gunter, W. (1986): Personal Communication.

Handy, L.L. and Datta, P. (1966): Fluid Distribution During Immiscible Displacement in Porous Media; Society of Petroleum Engineers Journal, volume 6(3), pp. 261-266.

Hayashitani, M., Davis, W., Novosad, J. and Batycky, J.P. (1981): Numerical Simulation of Laboratory Steamflood Experiments; Journal of Canadian Petroleum Technology, volume 20(4), pp. 91-99.

Heiba, A.A., Sahimi, M., Scriven, L.E. and Davis, H.T. (1982): Percolation Theory of Two-Phase Relative Permeability; paper SPE 11015 presented at the 57th Annual Technical Conference of the Society of Petroleum Engineers, New Orleans, LA, September 26-29.

Heiba, A.A., Davis, H.T. and Scriven, L.E. (1984): Statistical Network Theory of Three-Phase Relative Permeabilities; paper SPE/DOE 12690 presented at the Fourth Symposium on Enhanced Oil Recovery, Tulsa, OK, April 15-18.

Henning, P.J. and Polikar, M. (1986): Unpublished Results; Alberta Research Council, Edmonton, AB.

Hirasaki, G.J. (1975): Sensitivity Coefficients for History Matching Oil Displacement Processes; Society of Petroleum Engineers Journal, volume 15(1), pp. 39-49.

Isaacs, E.E. and Smolek, K. (1983): Interfacial Tension Behavior of Athabasca Bitumen/Aqueous Surfactant Systems; Canadian Journal of Chemical Engineering, volume 61(2), pp. 233-240.

Islam, M.R. and Bentsen, R.G. (1986): A Dynamic Method for Measuring Relative Permeability; Journal of Canadian Petroleum Technology, volume 25(1), pp. 39-50.

Johnson, E.F. Bossler, D.P. and Naumann, V.O. (1959): Calculations of Relative Permeability from Displacement Experiments; Transactions AIME, volume 216, pp. 370-372.

Jones, S.C. and Roszelle, W.O. (1978): Graphical Techniques for Determining Relative Permeability from Displacement Experiments; Journal of Petroleum Technology, volume 30(5), pp.807-817.

Kerig, P.D. and Watson, A.T. (1985): A New Algorithm for Estimating Relative Permeabilities from Displacement Experiments; unsolicited paper SPE 14476 submitted to the Society of Petroleum Engineers, Richardson, TX.

Koots, J.A. (1983): Oil Sands Analytical Methods Manual; Alberta Research Council, Edmonton, AB.

Korosi, A. and Fabuss, B.M. (1968): Viscosities of Binary Aqueous Solutions of NaCl, KCl, Na_2SO_4 and $MgSO_4$ at Concentrations and Temperatures of Interest in Desalination Processes; Journal of Chemical and Engineering Data, volume 13(4), pp. 548-552.

Kyte J.R. and Rapoport, L.A. (1958): Linear Waterflood Behavior and End Effects in Water-Wet Porous Media; Transactions AIME, volume 213, pp. 423-426.

Labastie, A., Guy, M., Delclaud, J.P. and Iffly, R. (1980): Effect of Flow Rate and Wettability on Water-Oil Relative Permeabilities and Capillary Pressure; paper SPE 9236 presented at the 55th Annual Technical Conference of the Society of Petroleum Engineers, Dallas, TX, September 21-24.

Land, C.S. (1968): Calculation of Imbibition Relative Permeability for Two- and Three-Phase Flow from Rock Properties; Society of Petroleum Engineers Journal, volume 8(2), pp. 149-156.

Larson, R.G., Scriven, L.E. and Davis, H.T. (1981): Percolation Theory of Two-Phase Flow in Porous Media; Chemical Engineering Science, volume 36(1), pp. 57-73.

Lefebvre du Prey, E.J. (1973): Factors Affecting Liquid-Liquid Relative Permeabilities of a Consolidated Porous Medium; Society of Petroleum Engineers Journal, volume 13(1), pp. 39-47.

Leung, L.C. (1982): Numerical Evaluation of the Effect of Simultaneous Steam and CO_2 Injection on the Recovery of Heavy Oil; paper SPE 10776 presented at the California Regional Meeting, San Francisco, CA, March 24-26.

Leverett, M.C. (1941): Capillary Behavior in Porous Solids; Transactions AIME, volume 142, pp. 152-169.

Lo, H.Y. and Mungan, N. (1973): Temperature Effect on Relative Permeabilities and Residual Saturations; Research Report RR-19, Petroleum Recovery Institute, Calgary, AB.

Maini, B.B. and Batycky, J.P. (1983): The Effect of Temperature on Heavy Oil/Water Relative Permeabilities in Horizontally and Vertically Drilled Core Plugs; paper SPE 12115 presented at the 58th Annual Technical Conference of the Society of Petroleum Engineers, San Francisco, CA, October 5-8.

Maini, B.B., Singhal, A., Okazawa, T., Chu, Y., Batycky, J.P. and Nicola, F. (1985): Measurements of Fluid and Rock Properties at Elevated Temperatures and Pressures; Report 1985-1, Petroleum Recovery Institute, Calgary, AB (November).

Maini, B.B. and Okazawa, T. (1986): Effects of Temperature on Heavy Oil-Water Relative Permeability of Sand; paper no. 86-37-78 presented at the 37th Annual Technical Meeting of the Petroleum Society of CIM, Calgary, AB, June 8-11.

Marle, C.M. (1981): Multiphase Flow in Porous Media; Gulf Publishing Company-Editions Technip, Paris.

Melrose, J.C. and Brandner, C.F. (1974): Role of Capillary Forces in Determining Microscopic Displacement Efficiency for Oil Recovery by Waterflooding; Journal of Canadian Petroleum Technology, volume 13(4), pp. 54-62.

Miles-Dixon, E., Sedgwick, G.E. and Heidrick, T.R. (1982): The X-Ray Absorption Measurement of Fluid Saturations in Oil Sand Cores; Proceedings, 1982 Symposium on Instrumentation and Control for Fossil Energy Processes, Houston, TX, June 7-9, pp. 392-399.

Miles-Dixon, E., Sedgwick, G. and Polikar, M. (1985): Unpublished Results; Alberta Research Council, Edmonton, AB.

Miller, M.A. and Ramey, H.J. Jr. (1985): Effect of Temperature on Oil/Water Relative Permeabilities of Unconsolidated and Consolidated Sands; Society of Petroleum Engineers Journal, volume 25(6), pp. 945-953.

Moore, T.F. and Slobod, R.L. (1956): The Effect of Viscosity and Capillarity on the Displacement of Oil by Water; Producers Monthly, volume 20(10), pp. 20-30 (August).

Morgan, J.T. and Gordon, D.T. (1970): Influence of Pore Geometry on Water-Oil Relative Permeability; Journal of Petroleum Technology, volume 22(10), pp. 1199-1208.

Morrow, N.R. (1970): Irreducible Wetting-Phase Saturations in Porous Media; Chemical Engineering Science, volume 25, pp. 1799-1815.

Morse, R.A., Terwilliger, P.L. and Yuster, S.T. (1947): Relative Permeability Measurements on Small Core Samples; Oil and Gas Journal, volume 46(16), pp. 109, 113, 115-116, 119-120, 122, 125.

Mungan, N. (1966): Interfacial Effects on Immiscible Liquid-Liquid Displacement in Porous Media; Society of Petroleum Engineers Journal, volume 6(3), pp. 247-253.

Mungan, N. (1972): Relative Permeability Measurements Using Reservoir Fluids; Society of Petroleum Engineers Journal, volume 12(5), pp. 398-402.

Naar, J. and Wygal, R.J. (1962): Structure and Properties of Unconsolidated Aggregates; Canadian Journal of Physics, volume 40, pp. 818-831.

Naar, J., Wygal, R.J. and Henderson, J.H. (1962): Imbibition Relative Permeability in Unconsolidated Porous Media; Society of Petroleum Engineers Journal, volume 2(1), pp. 13-17.

Naar, J., Henderson, J.H. and Wygal, R.J. (1963): Les Ecoulements Polyphases en Milieux Poreux Consolides; Revue de l'Institut Francais du Petrole, volume 18(2), pp. 196-214.

Nakornthap, K. and Evans, R.D. (1986): Temperature Dependent Relative Permeability and its Effect on Oil Displacement by Thermal Methods; SPE Reservoir Engineering, volume 1(3), pp.230-242.

Numbere, D., Brigham, W.E. and Standing, M.B. (1977): Correlations for Physical Properties of Petroleum Reservoir Brines; Stanford University Petroleum Research Institute, report no. SUPRI-TR-1, Stanford, CA (November).

Odeh, A.S. (1959): Effect of Viscosity Ratio on Relative Permeability; Transactions AIME, volume 216, pp. 346-352.

Osoba, J.S., Richardson, J.G., Kerver, J.K., Hafford, J.A. and Blair, P.M. (1951): Laboratory Measurements of Relative Permeability; Transactions AIME, volume 192, pp. 47-56.

Owens, W.W. and Archer, D.L. (1971): The Effect of Rock Wettability on Oil-Water Relative Permeability Relationships; Journal of Petroleum Technology, volume 23(7), pp. 873-878.

Perkins, F.M. Jr. and Collins, R.E. (1960): Scaling Laws of Laboratory Flow Models of Oil Reservoirs; Transactions AIME, volume 219, pp. 383-385.

Peters, E.J. (1979): Stability Theory and Viscous Fingering in Porous Media; Ph.D. Thesis, University of Alberta, Edmonton, AB.

Peters, E.J. and Flock, D.L. (1981): The Onset of Instability during Two-Phase Immiscible Displacement in Porous Media; Society of Petroleum Engineers Journal, volume 21(2), pp. 249-258.

Peters, E.J. and Khataniar, S. (1985): The Effect of Instability of Relative Permeability Curves Obtained by the Dynamic Displacement Method; unsolicited paper SPE 14713 submitted to the Society of Petroleum Engineers, Richardson, TX.

Polikar, M. (1980): Status of Relative Permeability in Athabasca Oil Sands; AOSTRA/ARC Joint Program, report no. 8081-41, Edmonton, AB.

Poston, S.W., Ysrael, S., Hossain, A.K.M.S., Montgomery, E.F. III and Ramey, H.J. Jr. (1970): The Effect of Temperature on Irreducible Water Saturation and Relative Permeability of Unconsolidated Sand; Society of Petroleum Engineers Journal, volume 10(2), pp. 171-180.

Pujol, L. and Boberg, T.C. (1972): Scaling Accuracy of Laboratory Steam Flooding Models; paper SPE 4191 presented at the

California Regional Meeting of the Society of Petroleum Engineers, Bakersfield, CA, November 8-10.

Purcell, W.R. (1949): Capillary Pressures - Their Measurement Using Mercury and the Calculation of Permeability Therefrom; Transactions AIME, volume 186, pp. 39-46.

Rapoport, L.A. and Leas, W.J. (1953): Properties of Linear Waterfloods; Transactions AIME, volume 198, pp. 139-148.

Rathmell, J.J., Braun, P.H. and Perkins, T.K. (1973): Reservoir Waterflood Residual Oil Saturation from Laboratory Tests; Journal of Petroleum Technology, volume 25(2), pp. 175-185.

Reznik, A.A., Fulton, P.F. and Colbeck, S.C., Jr. (1967): A Mathematical Model with Fractional-Wettability Characteristics; Producers Monthly, volume 31(9), pp. 22-28 (September).

Richardson, J.G., Kerver, J.K., Hafford, J.A. and Osoba, J.S. (1952): Laboratory Determination of Relative Permeability; Transactions AIME, volume 195, pp. 187-196.

Rose, W.D. (1949): Theoretical Generalizations Leading to the Evaluation of Relative Permeability; Transactions AIME, volume 186, pp. 111-125.

Rose, W.D. and Witherspoon, P.A. (1956): Trapping Oil in a Pore Doublet; Producers Monthly, volume 21(2), pp. 32-38 (Dec).

Rose, W.D. (1972): Some Problems Connected with the Use of Classical Description of Fluid/Fluid Displacement Processes; Fundamentals of Transport Phenomena in Porous Media, edited by IAHR, Elsevier Publishing Co., New York, pp. 229-240.

Sahimi, M., Heiba, A.A., Davis, H.T. and Scriven, L.E. (1986): Dispersion in Flow through Porous Media-II. Two-Phase Flow; Chemical Engineering Science, volume 41(8), pp. 2123-2136.

Salathiel, R.A. (1973): Oil Recovery by Surface Film Drainage in Mixed-Wettability Rocks; Journal of Petroleum Technology, volume 25(10), pp. 1216-1224.

Samoil, L.L. (1966): A Field Experiment in Recovery of Heavy Oil, Cold Lake, Alberta; paper presented at the 17th Annual Technical Meeting of the Petroleum Society of CIM, Edmonton, AB, May 4-6.

Sandberg, C.R., Gournay, L.S. and Sippel, R.F. (1958): The Effect of Fluid Flow Rate and Viscosity on Laboratory Determinations of Oil-Water Relative Permeabilities; Transactions AIME, volume 213, pp. 36-43.

Saraf, D.N., Batycky, J.P., Jackson, C.H. and Fisher, D.B. (1982): An Experimental Investigation of Three-Phase Flow of Water-Oil-Gas Mixtures through Water-Wet Sandstones; paper SPE 10761 presented at the California Regional Meeting of the Society of Petroleum Engineers, San Francisco, CA, March 24-26.

Sarma, H.K. and Bentsen, R.G. (1986): An Experimental Verification of a Modified Instability Theory for Immiscible Displacements in Porous Media; paper no. 86-37-76 presented at the 37th Annual Technical Meeting of the Petroleum of CIM, Calgary, AB, June 8-11.

Sayegh, S.G. and Maini, B.B. (1983): Laboratory Evaluation of the CO_2 Huff-n-Puff Process for Heavy Oil Reservoirs; paper no. 83-34-30 presented at the 34th Annual Technical Meeting of the Petroleum Society of CIM, Banff, AB, May 10-13.

Schmidt, E. (1979): Properties of Water and Steam in SI Units; 2nd edition, Springer-Verlag, Berlin.

Settari, A. and Raisbeck, J.M. (1981): Analysis and Numerical Modelling of Hydraulic Fracturing during Cyclic Steam Stimulation in Oil Sands; Journal of Petroleum Technology, volume 33(11), pp. 2201-2212.

Sigmund, P.M. and McCaffery, F.G. (1979): An Improved Unsteady-State Procedure for Determining the Relative Permeability

Characteristics of Heterogeneous Porous Media; Society of Petroleum Engineers Journal, volume 19(1), pp. 15-28.

Sinnokrot, A.A., Ramey, H.J. Jr. and Marsden, S.S. Jr. (1971): Effect of Temperature Level on Capillary Pressure Curves; Society of Petroleum Engineers Journal, volume 11(1), pp. 13-22.

Stanley, L.T. (1973): Practical Statistics for Petroleum Engineers; Petroleum Publishing Company, Tulsa, OK.

Stone, H.L. (1970): Probability Model for Estimating Three-Phase Relative Permeability; Journal of Petroleum Technology, volume 22(2), pp. 214-218.

Stone, H.L. (1973): Estimation of Three-Phase Relative Permeability and Residual Oil Data; Journal of Canadian Petroleum Technology, volume 12(4), pp. 53-61.

Stone, T. and Malcolm, J.D. (1985): Simulation of a Large Steam-CO_2 Co-Injection Experiment; Journal of Canadian Petroleum Technology, volume 24(6), pp. 51-59.

Strausz, O.P. (1977): The Chemistry of the Alberta Oil Sand Bitumen; The Oil Sands of Canada-Venezuela, D.A. Redford and A.G. Winestock, ed., CIM special volume 17, pp. 146-153.

Sufi, A.H. (1982): Temperature Effects on Oil-Water Relative Permeabilities for Unconsolidated Sands; Ph.D. Thesis, Stanford University, Stanford, CA.

Sufi, A.H., Ramey, H.J. Jr. and Brigham, W.E. (1982): Temperature Effects of Relative Permeabilities in Oil-Water Systems; paper SPE 11071 presented at the 57th Annual Technical Conference of the Society of Petroleum Engineers, New Orleans, LA, September 26-29.

Takamura, K. (1982): Microscopic Structure of Athabasca Oil Sand; Canadian Journal of Chemical Engineering, volume 60(4), pp. 538-545.

Tao, T.M. and Watson, A.T. (1984): Accuracy of JBN Estimates of Relative Permeability: Part 2-Algorithms; Society of Petroleum Engineers Journal, volume 24(2), pp. 215-223.

Torabzadeh, S.J. and Handy, L.L. (1984): The Effect of Temperature and Interfacial Tension on Water/Oil Relative Permeabilities of Consolidated Sands; paper SPE/DOE 12689 presented at the Fourth Symposium on Enhanced Oil Recovery, Tulsa, OK, April 15-18.

Wagner, O.R. and Leach, R.O. (1966): Effect of Interfacial Tension on Displacement Efficiency; Society of Petroleum Engineers Journal, volume 6(4), pp. 335-344.

Wallace, D. (1979-83): Unpublished Data; Oil Sands Sample Bank, Alberta Research Council, Edmonton, AB.

Wallace, D. (1984): Personal Communication.

Wardlaw, N.C. and Cassan, J.P. (1979): Oil Recovery Efficiency and the Rock-Pore Properties of Some Sandstone Reservoirs; Bulletin of Canadian Petroleum Geology, volume 27(2), pp. 117-138.

Waxman, M.H., Closmann, P.J. and Deeds, C.T. (1980): Peace River Tar Flow Experiments under In Situ Conditions; paper SPE 9511 presented at the 55th Annual Technical Conference of the Society of Petroleum Engineers, Dallas, TX, September 21-24.

Weinbrandt, R.M., Ramey, H.J. Jr. and Casse, F.J. (1975): The Effect of Temperature on Relative and Absolute Permeability of Sandstones; Society of Petroleum Engineers Journal, volume 15(5), pp. 376-384.

Welge, H.J. (1952): A Simplified Method for Computing Oil Recovery by Gas or Water Drive; Transactions AIME, volume 195, pp. 91-98.

Wilson, J.W. (1956): Determination of Relative Permeability under Simulated Reservoir Conditions; American Institute of Chemical Engineers Journal, volume 2(1), pp. 94-100.

Wyckoff, R.D. and Botset, H.G. (1936): The Flow of Gas-Liquid Mixtures through Unconsolidated Sands; Physics, volume 7, pp. 325-345.

Wyllie, M.R.J. and Gardner, G.H.F. (1958): The Generalized Kozeny-Carman Equation; part 1, World Oil, volume 146(4), pp. 121, 123-126, 128 (March); part 2, ibid., volume 146(5), pp. 210, 214, 216, 219-220, 225-228 (April).

Yuster, S.T. (1951): Theoretical Considerations of Multiphase Flow in Idealized Capillary Systems; Proceedings, 3rd World Petroleum Congress, The Hague, section III, pp. 437-445.

Appendix A

Packing Experiments

Table A.1 :—Preliminary Packing Experiments

Trial #	Sand Mixture	Packing Mode	Porosity (%)	Permeability to Water (d)
1	50% 60-80 mesh 50% 120-140 mesh original mixture	dry	34.4	3.65
2	50% 60-80 mesh 50% 120-140 mesh re-used mixture	wet	37.8	10.81
3	same as 2	wet	34.6	8.22
4	same as 1	dry	34.8	4.05
5	same as 1	dry	34.3	9.31
6	same as 1	wet	34.4	8.15
7	same as 1	wet	35.0	1.92
8	same as 1	wet	35.0	3.25
9	50% 60-100 mesh 50% 120-140 mesh	wet	37.6	8.05
10	50% 80-100 mesh 50% 200 mesh	wet	34.4	1.23

Table A.1 (cont.) : Preliminary Packing Experiments

Trial #	Sand Mixture	Packing Mode	Porosity (%)	Permeability to Water (d)
11	10% 60-80 mesh 25% 80-100 mesh 30% 100-200 mesh 35% 200 mesh	wet	34.7	4.86
12	60% 60-140 mesh 40% 200 mesh	wet	34.2	4.38
13	100% 200 mesh	wet	33.9	2.85
14	40% 60-140 mesh 60% 200 mesh	wet	33.9	3.75
15	50% 60-140 mesh 50% 200 mesh	wet	34.6	3.77
16	50% 80-140 mesh 50% 200 mesh	wet	34.6	4.06
17	50% 80-100 mesh 50% 200 mesh	wet	34.5	3.79
18	same as 17	dry	33.4	2.83

Appendix B

Data Measurement and Calculations

1. Pressure Drop

All permeability determinations were made from pressure drop measurements during displacement experiments. The pressure transducers used for these measurements have ranges varying from 0 - 7.5 to 0 - 690 kPa. Their stated performance specifications claim an accuracy of 0.2% of calibrated span. When calibrated against a dead weight tester, they were found to respond linearly with an accuracy within the 0.2% of the full range specification.

Figure B.1 shows the pressure drop measurement system across the core. The gravity head corrections due to upward and downward flow are derived below. The following notation is used:

$\Delta P_{u,d}$ = measured upward or downward pressure drop (pos.)

ΔP_{flow} = actual pressure drop due to flow (pos.)

ΔP_{corr} = gravity head correction (pos. or neg.)

Regardless of the direction of flow, the following relationships are valid:

$$H_a = H_b \tag{B.1}$$

$$H_d = H_a + H + H_b \tag{B.2}$$

$$P_2 = P_1 + H_a \cdot \rho_{exp} \cdot g \tag{B.3}$$

$$P_4 = P_3 + H_b \cdot \rho_{exp} \cdot g \tag{B.4}$$

$$P_5 = P_4 \tag{B.5}$$

$$P_4 = P_6 + H_d \cdot \rho_{exp} \cdot g \tag{B.6}$$

$$P_7 = P_6 + H_e \cdot \rho_{room} \cdot g \qquad (B.7)$$

$$P_8 = P_1 + H_e \cdot \rho_{room} \cdot g \qquad (B.8)$$

The pressures of interest are P_2, P_3, P_7 and P_8. Combining equations (B.4), (B.6) and (B.7), one obtains a relationship between P_3 and P_7:

$$P_7 = P_3 + \{(H_b - H_d) \cdot \rho_{exp} + H_e \cdot \rho_{room}\} \cdot g \qquad (B.9)$$

Similarly, the combination of equations (B.3) and (B.8) gives a relationship between P_2 and P_8:

$$P_8 = P_2 - (H_a \cdot \rho_{exp} + H_e \cdot \rho_{room}) \cdot g \qquad (B.10)$$

1.1 Upward Flow

For flow in the upward direction, the measured pressure drop is:

$$\Delta P_u = P_7 - P_8 \qquad (B.11)$$

Using equations (B.9) and (B.10) in conjunction with equation (B.11), the measured pressure drop can be expressed as:

$$\Delta P_u = P_3 - P_2 + (H_b - H_d + H_a) \cdot \rho_{exp} \cdot g + (H_e - H_e) \cdot \rho_{room} \cdot g$$

or, using equation (B.2):

$$\Delta P_u = P_3 - P_2 - H \cdot \rho_{exp} \cdot g \qquad (B.12)$$

The actual pressure drop is given by the expression:

$$P_3 - \Delta P_{flow,u} = P_2 + H \cdot \rho_f \cdot g \qquad (B.13)$$

Then, combining the last two equations, one obtains for the actual pressure drop:

$$\Delta P_u + H \cdot \rho_{exp} \cdot g = \Delta P_{flow,u} + H \cdot \rho_f \cdot g$$

or $$\Delta P_{flow,u} = \Delta P_u + H \cdot (\rho_{exp} - \rho_f) \cdot g \qquad (B.14)$$

The correction for the measured pressure differential is then:

$$\Delta P_{corr,u} = H \cdot (\rho_{exp} - \rho_f) \cdot g \qquad (B.15)$$

1.2 Downward Flow

The derivation in this case is similar to the previous one. The measured pressure drop now is:

$$\Delta P_d = P_8 - P_7 \qquad (B.16)$$

This becomes, in terms of P_2 and P_3 with the use of equations (B.2), (B.9) and (B.10):

$$\Delta P_d = P_2 - P_3 + H \cdot \rho_{exp} \cdot g \qquad (B.17)$$

The actual pressure drop is given by the expression:

$$P_3 + \Delta P_{flow,d} = P_2 + H \cdot \rho_f \cdot g \qquad (B.18)$$

In combining the last two equations, the actual pressure drop becomes:

$$\Delta P_d - H \cdot \rho_{exp} \cdot g = \Delta P_{flow,d} - H \cdot \rho_f \cdot g$$

or $$\Delta P_{flow,d} = \Delta P_d + H \cdot (\rho_f - \rho_{exp}) \cdot g \qquad (B.19)$$

The correction for the measured pressure differential is then:

$$\Delta P_{corr,d} = H \cdot (\rho_f - \rho_{exp}) \cdot g \qquad (B.20)$$

All displacement experiments were conducted vertically. With the gravity head correction due to upward flow as given in Equation (B.15), the actual pressure drop is given by:

$$\Delta P_{flow} = \Delta P_{meas} + \Delta P_{corr} \qquad (B.21)$$

Water was used as the fluid in the sensing lines. Therefore, no pressure drop correction was necessary during the water floods, regardless of the temperature, for absolute and effective water permeability determination. However, measurements made during the

bitumen floods required a pressure drop correction because the density of bitumen (ρ_f) is not the same as that of water (ρ_{exp}). This corrective term was found to be small when compared with the overall measured pressure drop because the density difference is relatively small. The same would also apply for experiments carried out with any other heavy oil.

2. Core Properties

2.1 Porosity

The porosity of each core was determined from the volume of its sleeve at the end of an experiment (V_{co}) and the volume of sand packed into the sleeve (V_s), and accounted for any volume changes due to the confining procedure.

$$\phi = 1 - \frac{V_s}{V_{co}} \tag{B.22}$$

2.2 Absolute Permeability

The absolute permeability of each core was determined both at room temperature and at the experimental temperature. Deionized water was used for the measurements. Darcy's equation of flow through a saturated porous medium was used to compute absolute permeability:

$$k_a\ (m^2) = \frac{q_{exp}\ (m^3/s) \cdot \mu_{w,exp}\ (Pa \cdot s) \cdot L_{co}\ (m)}{A_{co}\ (m^2) \cdot \Delta P_{flow}\ (Pa)} \tag{B.23}$$

where the volumetric flow rate of water at experimental conditions is calculated from:

$$q_{exp}\ (m^3/s) = q_{w,pump}\ (cm^3/h) \cdot \frac{\rho_{w,room}}{\rho_{w,exp}} \cdot \frac{10^{-6}}{3600} \qquad (B.24)$$

Permeability is often reported in d rather than m^2. The conversion is carried out as follows:

$$k\ (d) = 1.01325 \cdot 10^{12} \cdot k\ (m^2) \qquad (B.25)$$

3. Fluid Properties

3.1 Bitumen

The viscosity of the bitumen was determined by measuring the pressure drop across a capillary tube viscometer of known dimensions, and using Poiseuille's equation for flow through a capillary:

$$\mu_{b,exp}\ (Pa \cdot s) = \frac{\pi r_v^4\ (m^4)}{8L_v\ (m)} \cdot \frac{\Delta P_{flow}\ (Pa)}{q_{exp}\ (m^3/s)} \qquad (B.26)$$

where $(\pi r_v^4/8L_v)$ is a constant for the capillary tube. The tube used was made of titanium, which is thermally stable (very small thermal expansion coefficient), so that the constant was not affected by temperature. The viscometer was placed in a horizontal position inside the main oven. The volumetric flow rate of bitumen at experimental conditions was determined from equation (B.24).

A pycnometer was placed in the bitumen injection line, where the vertically upwards flowing fluid completely filled it. The valves at each end were closed simultaneously just before the termination of an experiment. The volume of the pycnometer was calibrated as a function of temperature, and the density of injected bitumen was calculated from the filled weight of the pycnometer:

$$\rho_{b,exp}\ (g/cm^3) = \frac{w_{b,pyc}\ (g)}{V_{pyc,exp}\ (cm^3)} \qquad (B.27)$$

3.2 Brine

Both sodium sulphate and sodium chloride aqueous brine solutions were used in the experiments. The sodium sulphate properties are given in Table 4.3 for the prevailing experimental conditions. The viscosity and density of the sodium chloride was calculated from the correlations given by Numbere et al. (1977). The equivalent salt concentration of the brine, C, was calculated in weight percent as follows:

$$C = \frac{m \cdot MW}{1000 + m \cdot MW} \cdot 100 \qquad (B.28)$$

where m is the molality of the brine as defined by Korosi and Fabuss (1968) and MW is its molecular weight.

The relative viscosity (μ_{br}/μ_w) is calculated as a function of temperature and salinity as:

$$\frac{\mu_{br}}{\mu_w} = 1 + 1.87\cdot10^{-3}C^{0.5} + 2.18\cdot10^{-4}C^{2.5} + f(T)\cdot f(C) \quad (B.29)$$

where $f(T) = T^{0.5} - 1.35\cdot10^{-2}\ T$;

and $f(C) = 2.76\cdot10^{-3}\ C - 3.44\cdot10^{-4}\ C^{1.5}$.

Similarly, the relative density (ρ_{br}/ρ_w) is calculated as a function of temperature, pressure and salinity as:

$$\frac{\rho_{br}}{\rho_w} = 1 + C[f_1(P) + C\{f_2(P)\} - T\{f_3(P)\} + T^2\{f_4(P)\}] \quad (B.30)$$

where $f_1(P) = 7.65\cdot10^{-3} - 1.09\cdot10^{-7}\ P$;

$f_2(P) = 2.16\cdot10^{-5} + 1.74\cdot10^{-9}\ P$;

$f_3(P) = 1.07\cdot10^{-5} - 3.24\cdot10^{-10}\ P$;

and $f_4(P) = 3.76\cdot10^{-8} - 1.0\cdot10^{-12}\ P$.

In the above equations, temperature is expressed in °F and pressure in psia. These correlations are accurate within 0.5% up to a temperature of 384°F (195°C), 10,000 psia (69 MPa) and a salt content of 25% by weight.

4. Steady State Experiments

4.1 Effective and Relative Permeability

Single phase flow takes place in the presence of an immobile phase at the end of a water flood when steady state conditions are reached. These conditions are referred to as the end points.

Darcy's equation was applied for determining the effective permeability to the flowing phase:

$$k_{ef} = \frac{q_{exp} \cdot \mu_{f,exp} \cdot L_{co}}{A_{co} \cdot \Delta P_{flow}} \qquad (B.31)$$

where f refers to the flowing fluid (bitumen or water). The end point relative permeability at residual saturation was calculated using the absolute permeability of the porous medium at the same experimental conditions:

$$k_{rf} = \frac{k_{ef}}{k_o} \qquad (B.32)$$

The water-bitumen mixture injection experiments were also carried out until a steady state condition was reached. At this stage, the inflow and outflow of both the bitumen and water phases were the same, with no further changes in the saturation distribution within the core. It was also assumed that the capillary pressure between the two flowing phases was negligible with respect to the pressure drop at intermediate saturations (Pujol and Boberg, 1972; Briggs, 1985). The effective and relative permeabilities to each phase were calculated from equations (B.31) and (B.32), using the actual flow rate and viscosity of that phase.

4.2 Initial and Residual Bitumen Saturations

Average initial and residual bitumen saturations in the core (with respect to a hot water flood) were calculated as follows, from the

total bitumen weights remaining in the core and wash ($w_{b,tc}$), and in the production fluids ($w_{b,pf}$):

$$S_{bi} = \left[\frac{(w_{b,tc} + w_{b,pf})}{\rho_{b,exp}} - V_{corr}\right] \cdot \frac{1}{\phi V_{co}} \qquad (B.33)$$

$$S_{br} = \frac{w_{b,tc}}{\rho_{b,exp}} \cdot \frac{1}{\phi V_{co}} \qquad (B.34)$$

where V_{corr} is the volume of the lines common to bitumen and water injection that were filled with bitumen prior to the water flood. This correction volume was measured before each experiment.

For the mixture injection experiments, the initial bitumen saturation was calculated by the same formulation as equation (B.33). However, the correction term, V_{corr}, also included the amount of bitumen present in the mixture that was injected during that portion of the experiment. The intermediate bitumen saturation was calculated similar to the residual bitumen saturation by use of equation (B.34).

5. Dynamic Displacement Experiments

The most widely used method for determining relative permeability versus saturation curves from displacement experiments is based on the technique of Welge (1952). This method was extended to individual curves by Johnson et al. (1959) and further refined by Jones and Roszelle (1978). These techniques are based on the following equations:

$$f_o = \frac{d\,(N_p)}{d\,(W_i)} \tag{B.35}$$

$$S_{w2} - S_{wi} = N_p - W_i f_o \tag{B.36}$$

$$\frac{f_o}{k_{ro}} = \frac{d\,(1/W_i I_r)}{d\,(1/W_i)} \tag{B.37}$$

$$f_o = 1 - f_w = \left[1 + \frac{k_{rw}\mu_o}{k_{ro}\mu_w}\right]^{-1} \tag{B.38}$$

where the relative injectivity, I_r, is defined by Johnson et al. (1959) as a dimensionless function of cumulative injection:

$$I_r = \frac{(q/\Delta P)}{(q/\Delta P)_{ref}} \tag{B.39}$$

and the reference condition is taken as the irreducible water (initial oil) condition. Therefore, a correction factor has to be applied in order to base relative permeabilities on the absolute permeability of the porous medium. In the case of the same constant flow rate for each flood, this multiplying factor becomes:

$$M_f = \mu_o/(\mu_w \cdot k_{roiw}) \tag{B.40}$$

The above equations apply for all situations after water breakthrough. Also, in order to calculate relative permeability, the saturation and pressure gradient history at some point in the core, say the outlet end, must be determined, and not their average values. The Jones and Roszelle (1978) approach consists of

differentiating experimental data graphically. This leads to some inaccuracies particularly if there is much scatter in the data. Therefore, the recovery and injectivity data from this study were empirically correlated (best polynomial fit) to the logarithm of the cumulative pore volumes of water injected for the determination of relative permeability relationships, as suggested by Miller and Ramey (1985):

$$N_p = a_0 + \ln(W_i)\cdot[a_1 + a_2\cdot\ln(W_i) + a_3\cdot\{\ln(W_i)\}^2] \qquad (B.41)$$

$$\ln(W_i I_r) = b_0 + \ln(W_i)\cdot[b_1 + b_2\cdot\ln(W_i)] \qquad (B.42)$$

By differentiating Equations (B.41) and (B.42) with respect to W_i, one obtains, after some manipulations, the tangent equations that satisfy Equations (B.35) and (B.37), respectively:

$$\frac{d\,(N_p)}{d\,(W_i)} = \frac{d\,(N_p)}{d\,(\ln W_i)}\cdot\frac{1}{W_i} =$$

$$= [a_1 + 2\cdot a_2\cdot\ln(W_i) + 3\cdot a_3\cdot\{\ln(W_i)\}^2]/W_i \qquad (B.43)$$

$$\frac{d\,(1/W_i I_r)}{d\,(1/W_i)} = \frac{d\,(\ln W_i I_r)}{d\,(\ln W_i)}\cdot\frac{W_i}{W_i I_r} =$$

$$= [b_1 + 2\cdot b_2\cdot\ln(W_i)]\cdot\frac{W_i}{W_i I_r} \qquad (B.44)$$

The data presented by Jones and Roszelle (1978) were tested using this fitting approach, and the comparison is shown in Figure B.2. The correlation is excellent for the oil curve. However, the calculated water curve is slightly higher.

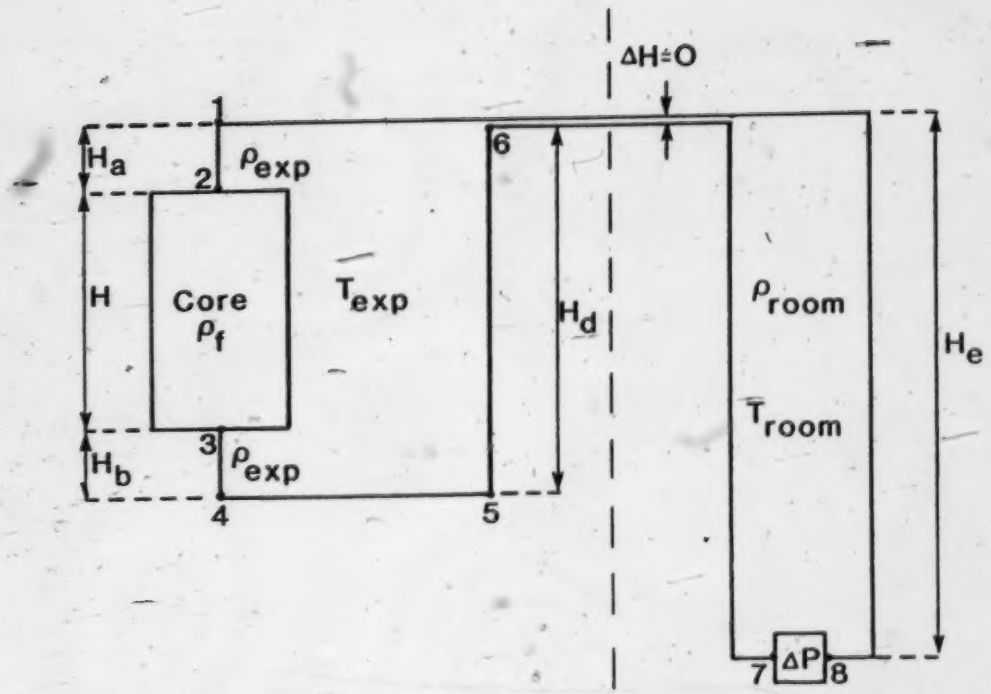

f – flowing fluid

exp – hot fluid in sensing lines at experimental conditions

room – cold fluid in sensing lines at room conditions

Figure B.1 : Pressure Drop Measurement System

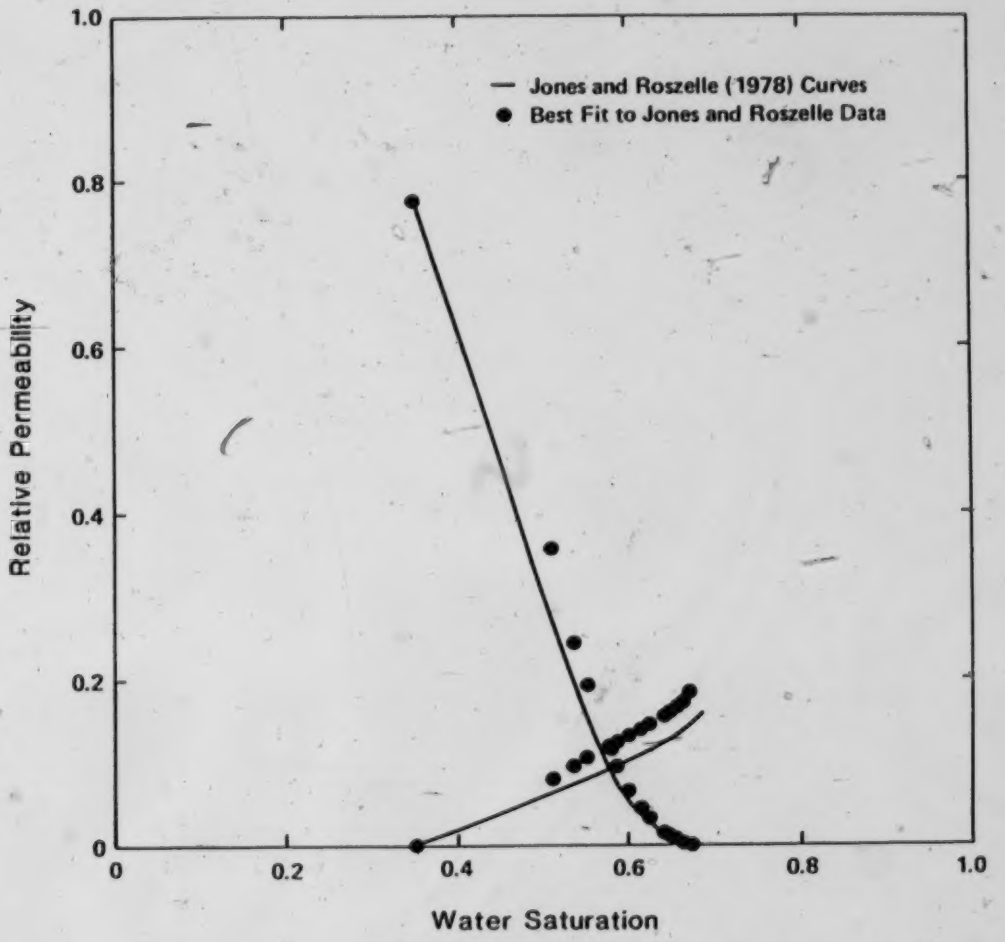

Figure B.2 : Comparison of Relative Permeability Data Obtained from Two Methods (after Jones and Roszelle, 1978)

Appendix C

Ottawa Sand Pack Properties

Table C.1 : Sieve Analysis of Ottawa Sand

Particle Size		Fractional Weight, %		
mesh	microns	70-140 sand	F-140 sand	L-140 sand*
60	250	6.5	0.2	-
70	210	6.6	-	-
80	177	9.9	0.6	-
100	149	25.8	4.7	-
120	125	20.1	9.6	-
140	105	22.2	26.3	-
170	88	7.5	23.5	40.1
200	74	1.2	12.8	21.8
230	62.5	0.2	5.8	9.9
270	53	-	14.0	23.9
325	44	-	0.8	1.4
400	37	-	0.8	1.4
>400	<37	-	0.9	1.5
	Average:	142 μm	90 μm	72 μm

* L-140 sand is the fraction of F-140 sand finer than 140 mesh.

Table C.2 : Particle Size Distribution of Outcrop Sand

Particle Size		Fractional Weight, %
mesh	microns	
18	1000	19.4
25	710	14.4
35	500	13.1
45	350	12.3
60	250	13.6
80	177	8.1
120	125	6.5
170	88	3.6
230	62.5	1.7
325	44	1.1
400	37	0.9
>400	<37	5.3
	Average :	420.0 μm

Table C.3 : Core Dimensions and Packing Properties

Core/Run No.	Sleeve Length (cm)	Sleeve Volume (cm^3)	Sand Volume (cm^3)	Pore Volume (cm^3)	Porosity ϕ (%)
END-01	22.7	273.6	177.1	96.5	35.3
END-02	22.0	266.1	173.6	92.5	34.8
END-03	22.7	274.4	176.9	97.5	35.5
END-04	21.9	264.7	170.9	93.8	35.4
END-05	22.7	270.5	174.1	96.4	35.6
END-06	21.9	263.2	169.4	93.8	35.6
END-07	21.9	263.3	169.8	93.5	35.5
END-08	22.4	264.1	172.7	91.4	34.6
END-09	22.4	261.3	170.3	91.0	34.8
END-10	22.4	253.2	166.3	86.9	34.3
END-11	22.4	260.6	171.6	89.0	34.2
END-12	22.9	266.0	178.2	87.8	33.0
END-13	22.4	253.7	163.9	89.8	35.4
END-14	22.9	267.8	179.6	88.2	32.9
END-15	22.4	263.8	174.2	89.6	34.0
END-16	22.9	269.7	181.3	88.4	32.8
END-17	22.4	253.3	166.6	86.7	34.2
END-18	22.9	266.4	179.3	87.1	32.7
END-19	22.4	263.0	178.5	84.5	32.1
END-20	22.9	263.9	175.7	88.2	33.4
END-21	22.4	257.9	169.6	88.3	34.2
END-22	22.9	265.7	177.0	88.7	33.4
END-23	22.9	257.4	168.2	89.2	34.7
END-24	22.4	257.6	165.4	92.2	35.8
END-25	22.4	247.0	161.0	86.0	34.8
END-26	22.4	271.9	182.6	89.3	32.8
END-27	22.4	257.0	167.5	89.5	34.8
END-28	22.4	267.8	175.8	92.0	34.4
END-29	22.4	263.5	176.6	86.9	33.0
END-30	22.4	264.5	180.3	84.2	31.8
END-31	22.4	261.2	177.5	83.7	32.0
MID-01	23.0	267.0	173.2	93.8	35.1
MID-02	23.0	268.2	178.5	89.7	33.4
MID-03	23.0	267.1	176.2	90.9	34.0
MID-04	23.0	267.8	175.6	92.2	34.4
MID-05	23.0	267.7	177.1	90.6	33.8
MID-06	23.0	264.5	174.6	89.9	34.0
MID-07	23.0	267.6	175.9	91.7	34.3
MID-08	23.0	267.7	176.6	91.1	34.0

Table C.3 (cont.) : Core Dimensions and Packing Properties

Core/Run No.	Sleeve Length (cm)	Sleeve Volume (cm^3)	Sand Volume (cm^3)	Pore Volume (cm^3)	Porosity ϕ (%)
MID-09	23.0	265.0	174.7	90.3	34.1
MID-10	23.0	266.1	176.8	89.3	33.6
MID-11	23.0	267.2	176.1	91.1	34.1
MID-12	23.0	266.6	175.9	90.7	34.0
DIS-01	22.8	264.4	175.0	89.4	33.8
DIS-02	22.8	266.1	177.2	88.9	33.4
DIS-03	22.8	267.0	176.9	90.1	33.7
DIS-04	22.8	265.2	175.4	89.8	33.9
DIS-05	22.8	265.3	175.8	89.5	33.7
KAY-01	22.8	264.4	174.8	89.6	33.9
KAY-02	22.8	265.6	176.4	89.2	33.6
KAY-03	22.8	264.9	174.6	90.3	34.1
KAY-04	22.8	261.7	175.6	86.1	32.9
KAY-05	22.8	264.3	176.4	87.9	33.3

Table C.4 : Absolute Permeability at Low Temperature

Core/Run No.	Temperature (°C)	Flow Rate (cm^3/h)	Pressure Drop (kPa)	Absolute Permeability (d)
END-01	20.0	80.0	2143.4	2.034
END-02	21.0	80.0	2003.0	2.069
END-03	22.6	80.0	2332.0	1.774
END-04	28.0	80.0	1907.5	1.781
END-05	18.6	80.0	2270.0	1.974
END-06	17.4	80.0	2595.2	1.672
END-07	19.6	80.0	931.9	4.548
END-08	22.0	80.0	2842.0	1.493
END-09	22.6	80.0	2708.1	1.562
END-10	22.6	80.0	2590.9	1.736
END-11	22.2	80.0	2300.4	1.918
END-12	20.6	80.0	2838.0	1.594
END-13	20.2	80.0	2789.5	1.637
END-14	22.0	80.0	2824.4	1.548
END-15	22.4	80.0	2804.4	1.501
END-16	22.2	80.0	2892.6	1.495
END-17	23.2	80.0	2141.1	2.008
END-18	23.3	80.0	2699.6	1.578
END-19	22.0	80.0	2688.0	1.585
END-20	21.8	80.0	3059.3	1.457
END-21	21.6	80.0	2653.0	1.652
END-22	23.1	80.0	3192.9	1.345
END-23	23.1	80.0	2945.3	1.505
END-24	21.8	80.0	2648.0	1.650
END-25	22.4	80.0	3038.9	1.480
END-26	25.2	240.0	77.9	145.79
END-27	20.4	80.0	3617.0	1.242
END-28	20.7	80.0	3474.5	1.235
END-29	19.6	80.0	3578.7	1.238
END-30	19.0	80.0	4632.3	0.959
END-31	20.0	80.0	4386.2	1.014
MID-01	22.5	80.0	1911.0	1.274
MID-02	22.0	80.0	2087.8	1.174
MID-03	21.2	80.0	2154.4	1.161
MID-04	20.4	80.0	2121.1	1.193
MID-05	22.7	80.0	1998.5	1.209
MID-06	23.3	80.0	1872.5	1.287
MID-07	19.9	80.0	2192.9	1.163
MID-08	20.3	80.0	2168.4	1.169

Table C.4 (cont.) : Absolute Permeability at Low Temperature

Core/Run No.	Temperature (°C)	Flow Rate (cm^3/h)	Pressure Drop (Pa)	Absolute Permeability (d)
MID-09	20.9	80.0	2054.6	1.234
MID-10	20.6	80.0	2099.2	1.209
MID-11	19.1	80.0	2234.9	1.154
MID-12	21.2	80.0	1960.9	1.278
DIS-01	22.4	80.0	3356.5	1.296
DIS-02	20.7	320.0	15128.4	1.183
DIS-03	21.2	80.0	3782.1	1.169
DIS-04	23.0	80.0	3712.9	1.152
DIS-05	23.1	80.0	3297.9	1.293
KAY-01	19.4	80.0	3661.2	1.253
KAY-02	21.6	80.0	3850.4	1.145
KAY-03	20.6	80.0	4011.5	1.122
KAY-04	23.4	80.0	3129.8	1.370
KAY-05	22.8	80.0	4065.8	1.061

Table C.5 : Absolute Permeability at High Temperature

Core/Run No.	Temperature (°C)	Flow Rate Factor	Pressure Drop (Pa)	Absolute Permeability (d)
END-01	124.7	1.062	541.6	1.869
END-02	126.0	1.063	476.9	2.028
END-03	175.0	1.117	438.1	1.682
END-04	175.2	1.117	406.9	1.744
END-05	124.6	1.062	598.1	1.713
END-06	124.8	1.061	542.5	1.802
END-07	174.4	1.116	162.5	4.409
END-08	150.0	1.088	601.1	1.424
END-09	150.0	1.088	553.0	1.564
END-10	150.4	1.088	555.6	1.654
END-11	150.6	1.088	480.4	1.857
END-12	225.2	1.194	460.7	1.379
END-13	125.0	1.061	668.5	1.584
END-14	225.5	1.195	459.8	1.372
END-15	125.2	1.062	694.0	1.466
END-16	250.4	1.248	452.3	1.291
END-17	174.6	1.117	393.0	1.981
END-18	250.6	1.248	441.0	1.339
END-19	174.4	1.116	505.8	1.483
END-20	200.6	1.154	586.0	1.192
END-21	199.0	1.151	466.0	1.477
END-22	224.8	1.194	570.0	1.118
END-23	249.9	1.247	506.9	1.208
END-24	174.6	1.116	501.0	1.527
END-25	199.0	1.151	564.4	1.273
END-26	125.2	1.062	21.0	141.05
END-27	124.0	1.062	870.5	1.212
END-28	124.8	1.063	834.8	1.206
END-29	100.4	1.042	1062.3	1.188
END-30	100.4	1.042	1386.0	0.907
END-31	100.0	1.042	1391.3	0.919
MID-01	124.7	1.062	515.3	1.150
MID-02	124.7	1.062	539.8	1.093
MID-03	125.6	1.063	540.7	1.088
MID-04	124.6	1.061	526.7	1.122
MID-05	125.0	1.060	533.7	1.102
MID-06	174.8	1.116	407.6	1.072
MID-07	125.4	1.062	547.7	1.073
MID-08	125.2	1.063	546.8	1.077

Table C.5 (cont.) : Absolute Permeability at High Temperature

Core/Run No.	Temperature (°C)	Flow Rate Factor	Pressure Drop (Pa)	Absolute Permeability (d)
MID-09	175.2	1.117	401.5	1.084
MID-10	175.2	1.117	404.1	1.073
MID-11	125.2	1.062	551.2	1.070
MID-12	125.0	1.062	430.4	1.376
DIS-01	124.4	1.061	883.9	1.197
DIS-02	124.8	1.062	3718.0	1.129
DIS-03	125.6	1.063	909.3	1.143
DIS-04	125.0	1.063	933.0	1.127
DIS-05	125.0	1.063	903.2	1.164
KAY-01	19.2	1.000	3661.2	1.253
KAY-02	20.6	1.000	3850.4	1.145
KAY-03	101.1	1.042	1260.4	1.025
KAY-04	23.4	1.000	3129.8	1.370
KAY-05	100.0	1.041	1292.8	1.012

Appendix D

Fluid Properties

Table D.1 : Viscosity and Density of Water at 7 MPa

Temperature (°C)	Viscosity (mPa.s)	Density (kg/m^3)
22*	0.992	1001.09
125	0.224	942.26
150	0.184	920.56
175	0.156	896.15
200	0.136	868.81
225	0.120	838.05
250	0.107	802.70

* Average room temperature.

Table D.2 : Viscosity and Density of 0.0704 Molal Aqueous Sodium Sulphate Solution

		Water		0.0704 Molal Sodium Sulphate Solution	
Temperature (°C)	Pressure (MPa)	Viscosity (mPa·s)	Density (kg/m^3)	Viscosity (mPa·s)	Density (kg/m^3)
25	0.1	0.8910	997.06	0.9183*	1006.03*
150	0.5	0.1823	916.76	0.1886*	926.99*
25	7.0	0.8899	1000.37	0.9171+	1009.34+
150	7.0	0.1839	920.56	0.1903+	930.83+

* Linear interpolation from Korosi and Fabuss (1968) data.

\+ Values corrected for pressure.

Table D.3 : Chemical Analysis of Athabasca Bitumen

	Laboratory Results	Typical Range (from Wallace, 1983)
Carbon	83.5 ± 0.5 wt%	82.4 - 83.9 wt%
Hydrogen	10.3 ± 0.4 wt%	10.0 - 10.8 wt%
Nitrogen	0.5 ± 0.1 wt%	0.3 - 0.7 wt%
Sulfur	4.2 ± 0.3 wt%	3.9 - 5.6 wt%
Oxygen	1.5 ± 0.2 wt%	0.6 - 1.5 wt%
H/C Molar Ratio	1.48 ± 0.6	1.43 - 1.57
Carbon Residue	12.0 wt%	10.7 - 13.7 wt%
Acid Number	2.7 ± 0.2	2.11 - 3.21
Vanadium	204 ± 20 mg/kg	151 - 211 mg/kg
Nickel	81 ± 10 mg/kg	50 - 112 mg/kg

Table D.4 : Specific Bitumen Properties

Property	Batch #1	Batch #2	Batch #3	Typical Range (from Wallace, 1983)
Asphaltene Content* (wt%)	18.0	16.9	17.5	14.0 - 18.2
Relative Density+ (15°C/15°C)	1.011	1.003	1.007	0.995 - 1.025
Gravity (°API)	8.5	9.6	9.0	10.7 - 6.5
Residual Solvent (wt%)	0.40	0.50	0.80	<1.0

* Asphaltenes are the portion of a hydrocarbon insoluble in n-pentane.

+ Relative density is defined with respect to water, at the same temperature.

Table D.5 : Measured Heavy Oil Properties at 7 MPa

Core/Run No.	Temperature (°C)	Viscosity (mPa·s)	Density (kg/m^3)
		Bitumen	
END-01	125	68.35	957.8
END-02	125	70.76	947.4
END-03	175	12.98	946.7
END-04	175	14.96	926.9
END-05	125	89.40	980.6
END-06	125	84.24	950.3
END-07	175	17.40	927.1
END-08	150	31.34	939.4
END-09	150	30.44	940.9
END-10	150	31.13	940.0
END-11	150	28.34	940.3
END-12	225	4.89	887.0
END-13	125	74.34	951.7
END-14	225	4.82	889.7
END-15	125	74.12	952.9
END-16	250	3.24	875.9
END-17	175	15.04	926.9
END-18	250	3.12	879.5
END-19	175	14.50	925.4
END-20	200	8.10	913.6
END-21	200	8.36	899.4
END-22	225	5.32	894.0
END-23	250	3.53	881.8
END-24	175	14.04	920.3
END-25	200	8.28	914.9
END-26	125	73.23	953.1
END-27	125	69.97	953.7
END-28	125	69.19	953.0
END-29	100	217.31	968.6
END-30	100	237.33	968.3
END-31	100	212.45	967.4
MID-01	125	66.26	950.6
MID-02	125	66.54	951.6
MID-03	125	65.77	948.6
MID-04	125	63.19	948.8
MID-05	125	63.99	948.8
MID-06	175	13.79	918.4
MID-07	125	66.38	946.0
MID-08	125	64.82	947.0

Table D.5 (cont.) : Measured Heavy Oil Properties at 7 MPa

Core/Run No.	Temperature (°C)	Viscosity (mPa·s)	Density (kg/m^3)
MID-09	175	13.86	918.4
MID-10	175	13.82	918.8
MID-11	125	65.62	947.0
MID-12	125	80.40	949.4
DIS-01	125	65.56	946.8
DIS-02	125	65.39	947.4
DIS-03	125	65.76	947.8
DIS-04	125	65.97	947.4
DIS-05	125	67.17	947.2
	Kaydol		
KAY-01	20	205.54	884.0
KAY-02	20	180.03	884.1
KAY-03	100	6.56	839.3
KAY-04	20	189.66	910.6
KAY-05	100	5.34	869.5

Appendix E

End Point Results

Table E.1 : Data for End Point Calculations

Core/Run No.	Pressure Drop bitumen flood (kPa)	Pressure Drop water flood (Pa)	Bitumen Weight core (g)	Bitumen Weight production (g)
END-01	231.44	7310.0	50.60	39.90
END-02	179.28	9103.0	54.90	34.30
END-03	49.34	3139.0	39.60	45.60
END-04	52.43	3035.0	38.90	45.60
END-05	264.30	9660.0	54.82	40.41
END-06	271.74	7944.0	52.22	38.94
END-07	24.30	2958.0	42.95	39.89
END-08	128.63	5088.0	41.60	38.87
END-09	116.38	4785.0	41.52	40.17
END-10	113.58	3639.0	35.78	44.97
END-11	92.66	3697.0	36.76	46.64
END-12	53.96*	3444.0	42.41	35.63
END-13	289.89	7471.0	41.77	38.56
END-14	75.11*	13935.0	45.07	34.37
END-15	335.65	8273.0	43.34	39.43
END-16	19.91	19210.0	45.12	36.11
END-17	51.98	3034.0	31.96	44.79
END-18	18.96	36560.0	38.91	40.86
END-19	64.23	4009.0	34.03	40.95
END-20	48.56	2746.0	40.91	38.20
END-21	41.39	1692.0	44.17	32.92
END-22	38.71	2377.0	33.87	40.59
END-23	21.21	17710.0	42.57	39.25
END-24	62.13	3949.0	39.39	43.53
END-25	38.98	1692.0	35.44	38.35
END-26	10.24	239.8	36.90	37.00
END-27	355.58	10864.0	42.12	40.53
END-28	351.88	11016.0	44.00	41.91
END-29	1034.49	20743.0	34.26+	36.94
END-30	1475.05	27271.0	33.21+	35.61
END-31	1470.91	24049.0	44.89	37.02

* pressure drop did not stabilize during these experiments

\+ portion of sample lost during analysis; actual weight greater than that reported

Table E.2 : End Point Relative Permeabilities and Saturations

Core/Run No.	Relative Permeability to Bitumen	Relative Permeability to Water	Bitumen Saturation Initial	Bitumen Saturation Final
END-01	0.712	0.074	0.931	0.547
END-02	0.848	0.052	0.977	0.626
END-03	0.741	0.140	0.876	0.429
END-04	0.746	0.134	0.931	0.447
END-05	0.899	0.062	0.960	0.580
END-06	0.750	0.069	0.982	0.586
END-07	0.746	0.055	0.915	0.495
END-08	0.797	0.118	0.896	0.485
END-09	0.787	0.115	0.912	0.485
END-10	0.803	0.153	0.945	0.438
END-11	0.776	0.130	0.954	0.439
END-12	*	0.134	0.950	0.545
END-13	0.765	0.089	0.898	0.489
END-14	*	0.033	0.960	0.574
END-15	0.684	0.083	0.927	0.508
END-16	0.695	0.024	0.997	0.583
END-17	0.728	0.130	0.911	0.398
END-18	0.686	0.012	0.989	0.508
END-19	0.730	0.126	0.914	0.435
END-20	0.723	0.214	0.930	0.508
END-21	0.692	0.274	0.928	0.556
END-22	0.654	0.240	0.887	0.427
END-23	0.796	0.029	0.989	0.541
END-24	0.726	0.127	0.924	0.464
END-25	0.882	0.333	0.894	0.450
END-26	0.673	0.088	0.826	0.434
END-27	0.758	0.080	0.926	0.493
END-28	0.731	0.076	0.939	0.502
END-29	0.790	0.051	*	*
END-30	0.789	0.051	*	*
END-31	0.708	0.058	0.966	0.554

* not available due to experimental difficulties
(see Table E.1 for explanations)

Table E.3 : Fluid Properties in End Point Experiments

Core/Run No.	M_r	$\sigma_{b/w}$ (mN/m)	N_c	$Lv\mu_w$ ($cm^2 \cdot cp/min$)
END-01	31.7	11.61	$1.07 \cdot 10^{-6}$	0.599
END-02	19.7	11.50	$1.08 \cdot 10^{-6}$	0.568
END-03	15.7	9.20	$0.98 \cdot 10^{-6}$	0.436
END-04	17.2	9.19	$0.98 \cdot 10^{-6}$	0.420
END-05	27.4	11.60	$1.07 \cdot 10^{-6}$	0.605
END-06	34.2	11.63	$1.07 \cdot 10^{-6}$	0.581
END-07	8.2	9.24	$0.99 \cdot 10^{-6}$	0.425
END-08	25.3	10.40	$1.05 \cdot 10^{-6}$	0.507
END-09	24.3	10.37	$1.05 \cdot 10^{-6}$	0.510
END-10	31.2	10.38	$1.14 \cdot 10^{-6}$	0.544
END-11	25.0	10.38	$1.11 \cdot 10^{-6}$	0.529
END-12	*	6.77	$1.22 \cdot 10^{-6}$	0.376
END-13	38.8	11.58	$1.13 \cdot 10^{-6}$	0.625
END-14	*	6.80	$1.22 \cdot 10^{-6}$	0.374
END-15	40.6	11.55	$1.14 \cdot 10^{-6}$	0.599
END-16	1.0	5.57	$1.38 \cdot 10^{-6}$	0.345
END-17	17.1	9.23	$1.09 \cdot 10^{-6}$	0.461
END-18	0.5	5.57	$1.40 \cdot 10^{-6}$	0.350
END-19	16.0	9.24	$1.11 \cdot 10^{-6}$	0.445
END-20	17.6	8.02	$1.13 \cdot 10^{-6}$	0.415
END-21	24.4	8.01	$1.10 \cdot 10^{-6}$	0.406
END-22	16.2	6.80	$1.21 \cdot 10^{-6}$	0.377
END-23	1.2	5.60	$1.36 \cdot 10^{-6}$	0.362
END-24	15.7	9.21	$1.02 \cdot 10^{-6}$	0.453
END-25	22.9	8.04	$1.13 \cdot 10^{-6}$	0.425
END-26+	42.6	11.59	$3.43 \cdot 10^{-6}$	1.754
END-27	32.7	11.65	$1.15 \cdot 10^{-6}$	0.625
END-28	31.9	11.61	$1.11 \cdot 10^{-6}$	0.596
END-29	49.9	12.77	$1.32 \cdot 10^{-6}$	0.746
END-30	54.1	12.78	$1.36 \cdot 10^{-6}$	0.745
END-31	61.1	12.81	$1.37 \cdot 10^{-6}$	0.758

* k_{rbiw} not available (see Table E.2)

\+ nominal flow rate three times higher than other experiments

Table E.4 : Initial Oil Sand Core Parameters

Experiment #	Run Temperature (°C)	Initial Oil & Connate Water Saturations	End Point Relative Permeability
MID-01	125.0	0.874/0.126	0.764
MID-02	125.0	0.800/0.200	0.760
MID-03	125.0	0.911/0.089	0.810
MID-04	125.0	0.893/0.107	0.759
MID-05	125.0	0.914/0.086	0.771
MID-06	175.0	0.736/0.264	0.808
MID-07	125.0	0.925/0.075	0.772
MID-08	125.0	0.906/0.094	0.749
MID-09	175.0	0.883/0.117	0.817
MID-10	175.0	0.800/0.200	0.826
MID-11	125.0	0.831/0.169	0.776
MID-12	125.0	1.071*	0.827
DIS-01	125.0	0.860/0.140	0.726
DIS-02	125.0	0.859/0.141	0.640
DIS-03	125.0	0.770/0.230	0.666
DIS-04	125.0	0.879/0.121	0.684
DIS-05	125.0	0.886/0.114	0.651
KAY-01	20.0	0.900/0.100	0.669
KAY-02	20.0	0.966/0.034	0.714
KAY-03	100.0	0.953/0.047	0.601
KAY-04	20.0	0.953/0.047	0.626
KAY-05	100.0	0.942/0.058	0.535

* value greater than 1.0 due to analytical error

Appendix F

Unsteady State Experiments

Table F.1 : Measured Parameters for Unsteady State Experiments - Bitumen , 125°C -

Expt. No.	Flow Rate (cm^3/h)	Water Injected (PV)	Pressure Drop (water flood) (kPa)	Recovery (%)
DIS-4	80.0	1.17	30.252	33.0
DIS-5	80.0	1.33	29.991	33.7
DIS-4	80.0	2.33	23.597	39.1
DIS-5	80.0	2.50	24.292	39.6
DIS-1	80.0	3.93	12.883	41.2
DIS-2	320.0	4.21	53.227	41.8
DIS-4	80.0	4.76	20.778	45.6
DIS-5	80.0	4.87	22.083	45.3
DIS-3	80.0	9.45	7.224	46.5
DIS-1	80.0	9.65	9.486	50.2
DIS-2	320.0	9.88	45.653	51.7
DIS-3	80.0	18.86	5.675	53.3
DIS-1	80.0	19.32	8.455	56.5
DIS-2	320.0	19.44	50.777	58.8
DIS-3	80.0	29.88	4.199	57.7
DIS-3	80.0	48.66	3.155	61.1

Table F.2 : Data for JBN Calculations
- Bitumen , 125°C -

Water Injected (PV)	Oil Produced (PV)	Recovery (%)	Relative Injectivity I_r	$W_i I_r$
1.17	0.28	33.0	13.266	15.521
1.33	0.29	33.7	13.858	18.431
2.33	0.33	39.1	17.008	39.628
2.50	0.34	39.6	17.108	42.771
3.93	0.35	41.2	27.814	109.310
4.21	0.36	41.8	31.839	134.042
4.76	0.39	45.6	19.315	91.939
4.87	0.39	45.3	18.820	91.654
9.45	0.40	46.5	55.161	521.270
9.65	0.43	50.2	37.776	364.540
9.88	0.44	51.7	37.122	366.760
18.86	0.45	53.3	70.213	1324.221
19.32	0.48	56.5	42.382	818.827
19.44	0.50	58.8	33.375	648.813
29.88	0.49	57.7	94.899	2835.569
48.66	0.52	61.1	126.287	6145.114

Table F.3 : Relative Permeability and Fractional Flow Curves - Bitumen , 125 °C - (from JBN calculations)

Water Saturation	Relative Permeability to Water	Relative Permeability to Bitumen	Ratio(w/b)	Fractional Flow
0.149	0.000	0.673	0.0000	0.000
0.374	0.033	0.491	0.0672	0.951
0.379	0.034	0.465	0.0731	0.955
0.407	0.041	0.358	0.1145	0.971
0.411	0.042	0.345	0.1217	0.973
0.439	0.050	0.273	0.1832	0.982
0.444	0.051	0.263	0.1939	0.983
0.453	0.054	0.246	0.2195	0.985
0.454	0.055	0.243	0.2263	0.985
0.504	0.076	0.167	0.4551	0.993
0.505	0.077	0.165	0.4667	0.993
0.507	0.078	0.163	0.4785	0.993
0.558	0.113	0.110	1.0273	0.997
0.560	0.115	0.108	1.0648	0.997
0.594	0.152	0.080	1.9000	0.998
0.629	0.216	0.053	4.0755	0.999

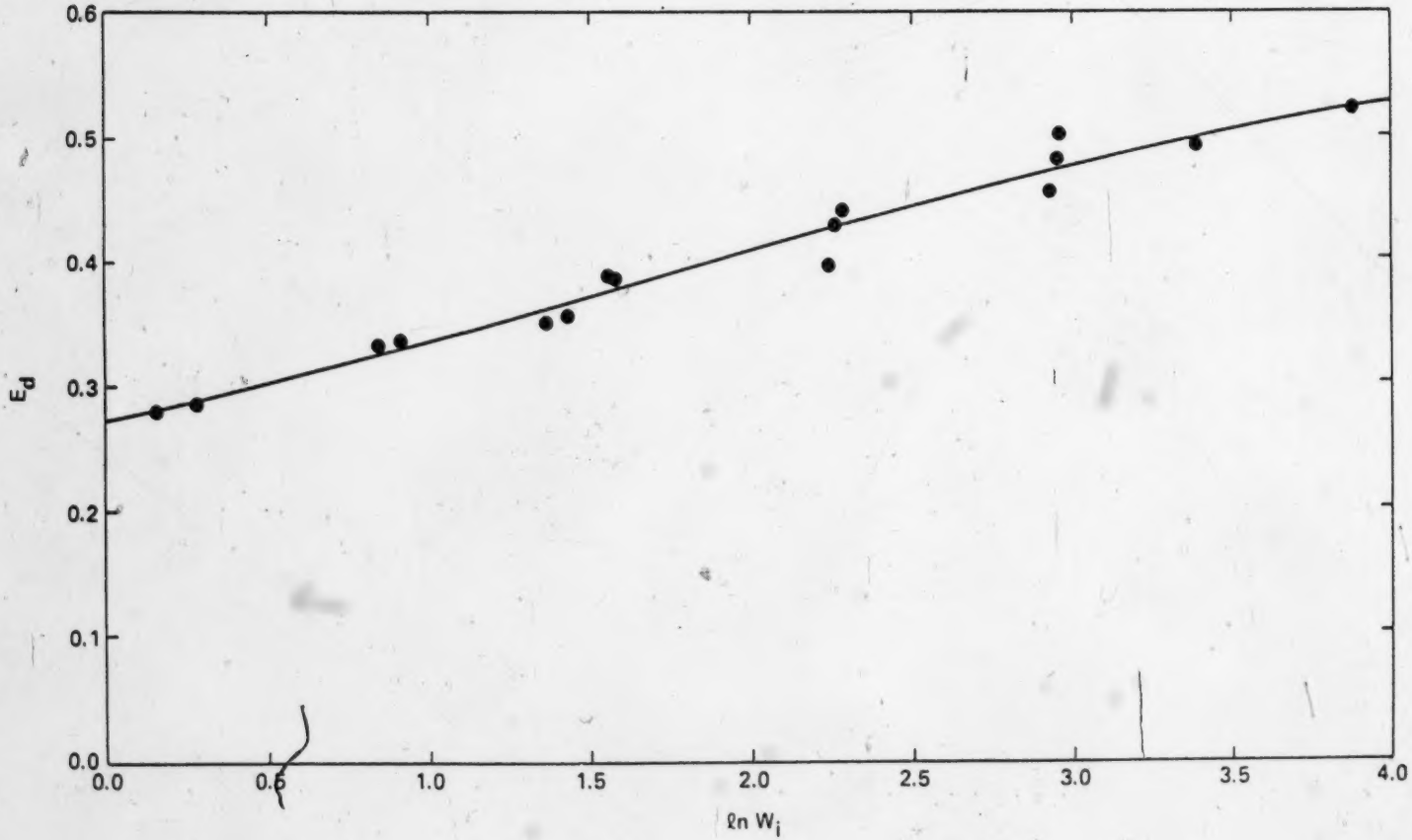

Figure F.1 : Post-Breakthrough Recovery Function for Bitumen Experiments

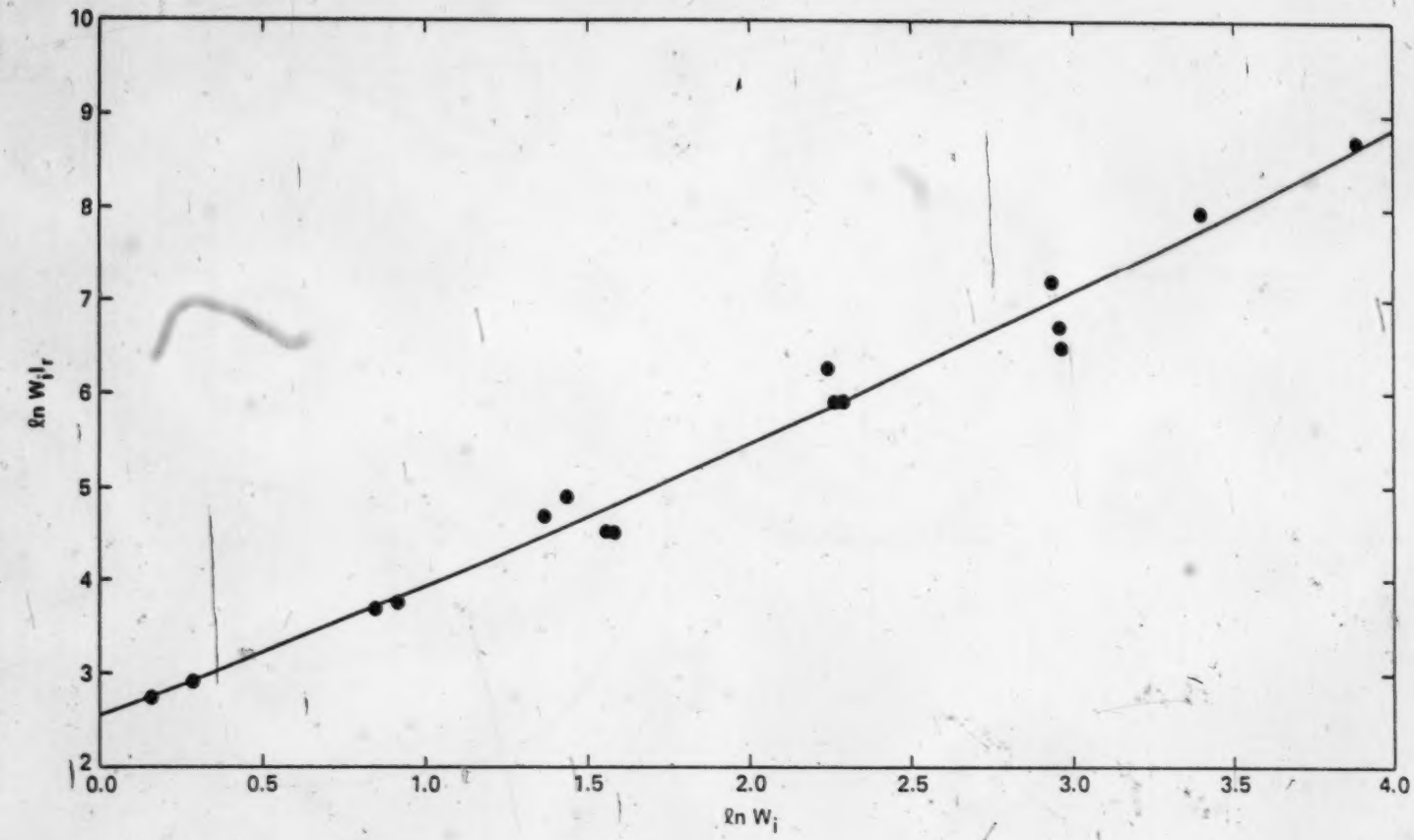

Figure F.2 : Relative Injectivity Function for Bitumen Experiments

Appendix G

Kaydol Experiments

Table G.1 : Refractive Index Calibration for Kaydol-Mineral Spirit Mixtures

Weight of Kaydol in Mixture, w_K (%)	Refractive Index, n_D (micron)
0.0	1.4363
10.0	1.4410
20.0	1.4443
30.0	1.4484
40.0	1.4523
50.0	1.4563
60.0	1.4607
70.0	1.4644
80.0	1.4685
90.0	1.4730
100.0	1.4771

Linear regression analysis : $n_D = 4.045 \cdot 10^{-4} w_K + 1.4363$

$(r^2 = 0.9996)$

Table 6.2 : Measured Data for JBN Calculations
- Kaydol #1 , 20°C -

Water Injected (PV)	Oil Produced (PV)	Pressure Drop (kPa)	Relative Injectivity I_r	$W_i I_r$
0.000	0.000	652.605	1.679	0.000
0.022	0.022	462.047	2.371	0.053
0.082	0.078	308.823	3.548	0.291
0.201+	0.134	190.213	5.760	1.158
0.275	0.156	158.617	6.907	1.903
0.409	0.179	128.608	8.519	3.488
0.514	0.190	109.002	10.051	5.163
0.663*	0.201	94.022	11.653	7.721
0.782	0.212	86.670	12.641	9.882
0.975	0.223	73.316	14.944	14.574
1.214	0.235	66.789	16.404	19.907
1.437	0.246	60.912	17.987	25.845
1.839	0.257	53.085	20.639	37.953
2.241	0.268	48.008	22.821	51.141
2.643	0.279	43.957	24.924	65.874
3.000	0.290	41.581	26.348	79.054

\+ true breakthrough

* inferred breakthrough

Table G.3 : Relative Permeability and Fractional Flow Curves - Kaydol #1 , 20°C - (from JBN calculations)

Water Saturation	Relative Permeability to Water	Relative Permeability to Kaydol	Relative Permeability Ratio(w/b)	Fractional Flow
0.100	0.000	0.669	0.0000	0.000
0.231	0.028	0.702	0.0399	0.653
0.249	0.034	0.594	0.0571	0.919
0.260	0.038	0.543	0.0700	0.933
0.272	0.044	0.492	0.0894	0.947
0.282	0.051	0.459	0.1043	0.957
0.290	0.057	0.442	0.1290	0.962
0.299	0.066	0.429	0.1538	0.968
0.306	0.073	0.426	0.1714	0.972
0.312	0.081	0.426	0.1901	0.974
0.317	0.086	0.428	0.2009	0.976

Table G.4 : Measured Data for JBN Calculations
- Kaydol #2 , 20°C -

Water Injected (PV)	Oil Produced (PV)	Pressure Drop (kPa)	Relative Injectivity I_r	$W_i I_r$
0.000	0.000	752.668	1.300	0.000
0.023	0.022	552.708	1.771	0.040
0.067	0.078	393.046	2.490	0.168
0.112	0.135	270.587	3.617	0.406
0.142	0.157	230.800	4.241	0.603
0.213+	0.179	188.601	5.190	1.125
0.307	0.202	145.663	6.719	2.060
0.381	0.224	124.406	7.868	3.000
0.471	0.235	107.301	9.122	4.296
0.710*	0.258	85.645	11.428	8.117
0.830	0.269	78.067	12.538	10.404
0.979	0.280	69.515	14.080	13.789
1.144	0.291	63.888	15.320	17.523
1.398	0.303	55.711	17.569	24.560
1.592	0.314	51.109	19.151	30.493
1.757	0.325	48.083	20.356	35.760
2.145	0.336	43.357	22.575	48.433
2.415	0.348	42.356	23.108	55.795
2.848	0.359	39.005	25.093	71.468
3.057	0.364	36.980	26.468	80.922

\+ true breakthrough

* inferred breakthrough

Table G.5 : Relative Permeability and Fractional Flow Curves - Kaydol #2 , 20°C - (from JBN calculations)

Water Saturation	Relative Permeability to Water	Relative Permeability to Kaydol	Relative Permeability Ratio(w/b)	Fractional Flow
0.034	0.000	0.714	0.0000	0.000
0.229	0.033	0.586	0.0563	0.911
0.236	0.038	0.598	0.0635	0.920
0.245	0.044	0.602	0.0731	0.929
0.253	0.050	0.599	0.0835	0.938
0.266	0.058	0.585	0.0991	0.947
0.274	0.064	0.571	0.1121	0.953
0.281	0.069	0.558	0.1237	0.957
0.295	0.079	0.526	0.1502	0.965
0.304	0.085	0.504	0.1687	0.968
0.317	0.094	0.471	0.1996	0.973
0.323	0.099	0.455	0.2176	0.975

Table 6.6 : Measured Data for JBN Calculations
- Kaydol #3 , 100°C -

Water Injected (PV)	Oil Produced (PV)	Pressure Drop (kPa)	Relative Injectivity I_r	$W_i I_r$
0.000	0.000	41.206	1.184	0.000
0.003	0.000	38.880	1.255	0.004
0.034	0.033	36.079	1.352	0.046
0.080	0.066	33.701	1.448	0.116
0.095	0.099	34.104	1.430	0.136
0.126	0.133	32.314	1.510	0.190
0.188	0.188	28.495	1.712	0.321
0.249	0.244	24.610	1.982	0.494
0.295	0.299	19.916	2.449	0.723
0.357	0.354	16.023	3.045	1.086
0.418+	0.387	13.883	3.514	1.470
0.588*	0.421	12.361	3.947	2.319
0.772	0.443	11.265	4.331	3.344
1.003	0.465	10.451	4.668	4.681
1.326	0.487	9.799	4.979	6.601
1.587	0.498	9.155	5.329	8.458
1.849	0.509	8.894	5.485	10.140
2.126	0.520	8.633	5.651	12.011
2.218	0.523	8.589	5.680	12.596
2.802	0.531	8.085	6.034	16.909
3.233	0.542	7.911	6.167	19.937

\+ true breakthrough

* inferred breakthrough

Table G.7 : Relative Permeability and Fractional Flow Curves - Kaydol #3 , 100°C - (from JBN calculations)

Water Saturation	Relative Permeability to Water	Relative Permeability to Kaydol	Relative Permeability Ratio(w/b)	Fractional Flow
0.047	0.000	0.601	0.0000	0.000
0.383	0.110	0.426	0.2582	0.857
0.407	0.127	0.355	0.3577	0.893
0.432	0.143	0.289	0.4948	0.920
0.459	0.162	0.225	0.7200	0.944
0.476	0.173	0.187	0.9251	0.956
0.491	0.183	0.158	1.1582	0.964
0.504	0.192	0.133	1.4436	0.971
0.508	0.195	0.126	1.5476	0.973
0.531	0.210	0.090	2.3333	0.982
0.544	0.219	0.071	3.0845	0.986

Table 6.8 : Measured Data for JBN Calculations
- Kaydol #4 , 20°C -

Water Injected (PV)	Oil Produced (PV)	Pressure Drop (kPa)	Relative Injectivity I_r	W_iI_r
0.000	0.000	960.033	0.983	0.000
0.015	0.017	882.982	1.069	0.017
0.031	0.032	807.224	1.170	0.036
0.046	0.061	701.603	1.346	0.062
0.062	0.075	612.012	1.543	0.095
0.077	0.097	530.307	1.780	0.138
0.093	0.119	448.343	2.106	0.196
0.108	0.134	389.133	2.426	0.263
0.124	0.148	344.143	2.744	0.340
0.139	0.163	311.565	3.030	0.422
0.155	0.177	279.245	3.381	0.523
0.217+	0.206	229.084	4.122	0.893
0.248	0.221	208.141	4.536	1.123
0.294	0.235	183.449	5.147	1.514
0.325	0.244	171.771	5.497	1.787
0.356	0.250	160.017	5.900	2.101
0.387	0.255	153.590	6.147	2.379
0.418	0.261	146.888	6.428	2.686
0.433	0.267	142.737	6.615	2.867
0.464	0.273	130.483	7.236	3.360
0.480	0.279	127.807	7.388	3.545
0.526	0.284	120.030	7.866	4.140
0.557	0.290	112.603	8.385	4.672
0.635	0.302	102.725	9.191	5.833
0.697	0.308	94.697	9.971	6.945
0.743*	0.313	89.021	10.606	7.880
0.805	0.319	82.969	11.380	9.160
0.882	0.325	79.093	11.938	10.533
0.913	0.331	76.317	12.372	11.299
0.975	0.337	73.141	12.909	12.589
1.084	0.342	68.289	13.826	14.981
1.130	0.348	65.863	14.335	16.199
1.254	0.354	61.812	15.275	19.152
1.331	0.360	58.536	16.130	21.473
1.455	0.366	55.235	17.094	24.873
1.548	0.372	52.860	17.862	27.650
1.687	0.377	49.259	19.168	32.342
1.827	0.383	46.808	20.171	36.845
1.950	0.389	44.807	21.072	41.100
2.152	0.397	41.631	22.680	48.799

Table G.8 (cont.) : Measured Data for JBN Calculations
- Kaydol #4 , 20°C -

Water Injected (PV)	Oil Produced (PV)	Pressure Drop (kPa)	Relative Injectivity I_r	$W_i I_r$
2.245	0.401	40.656	23.224	52.127
2.384	0.406	38.955	24.237	57.779
2.585	0.412	37.205	25.378	65.605
2.817	0.418	34.904	27.051	76.210
2.926	0.424	34.139	27.657	80.916
3.173	0.430	32.457	29.090	92.313
3.390	0.435	31.039	30.419	103.123
3.684	0.441	29.277	32.249	118.813
4.009	0.447	27.342	34.532	138.450
4.211	0.453	26.876	35.130	147.917
4.536	0.459	25.680	36.767	166.760
4.721	0.464	25.067	37.667	177.837
5.108	0.470	23.844	39.597	202.278
5.433	0.476	23.027	41.004	222.791
5.789	0.482	22.118	42.689	247.147
6.161	0.488	21.474	43.969	270.892
6.563	0.493	20.852	45.280	297.197
6.935	0.499	20.256	46.613	323.260
7.477	0.505	19.590	48.196	360.354
7.864	0.511	19.255	49.035	385.598
8.483	0.517	18.868	50.041	424.496
8.885	0.522	18.638	50.660	450.135
9.721	0.528	18.551	50.897	494.792
10.279	0.534	18.181	51.932	533.797
18.978**	0.583	33.445**	28.231	535.782
19.783	0.587	32.492	29.059	574.881
21.068	0.592	38.905	24.269	511.298
22.756	0.598	43.582	21.665	492.989
24.273	0.604	47.108	20.043	486.495
26.177	0.610	52.034	18.145	474.984
27.709	0.615	51.334	18.393	509.650
29.319	0.621	52.034	18.145	532.004
40.991	0.642	103.800	9.096	372.860
41.951	0.644	106.326	8.880	372.525

\+ true breakthrough

* inferred breakthrough

** Because of an unexpected pressure behaviour, the data from this point onward have not been included in the relative permeability calculations.

Table G.9 : Relative Permeability and Fractional Flow Curves - Kaydol #4 , 20°C - (from JBN calculations)

Water Saturation	Relative Permeability to Water	Relative Permeability to Kaydol	Relative Permeability Ratio(w/b)	Fractional Flow
0.047	0.000	0.626	0.0000	0.000
0.284	0.027	0.586	0.0461	0.897
0.290	0.029	0.582	0.0499	0.905
0.297	0.032	0.577	0.0555	0.913
0.300	0.033	0.575	0.0574	0.916
0.305	0.035	0.571	0.0613	0.921
0.312	0.039	0.565	0.0690	0.928
0.316	0.040	0.562	0.0712	0.931
0.323	0.044	0.556	0.0791	0.938
0.328	0.047	0.552	0.0851	0.941
0.334	0.051	0.545	0.0936	0.946
0.339	0.053	0.541	0.0980	0.949
0.345	0.057	0.534	0.1067	0.953
0.351	0.061	0.528	0.1155	0.956
0.356	0.065	0.523	0.1243	0.959
0.363	0.070	0.515	0.1359	0.962
0.366	0.072	0.512	0.1406	0.964
0.371	0.076	0.506	0.1502	0.966
0.377	0.080	0.499	0.1603	0.968
0.383	0.086	0.492	0.1748	0.971
0.392	0.094	0.481	0.1954	0.974
0.397	0.098	0.475	0.2063	0.975
0.404	0.104	0.467	0.2227	0.977
0.409	0.109	0.460	0.2370	0.978
0.410	0.111	0.458	0.2424	0.979
0.414	0.114	0.454	0.2511	0.979
0.420	0.120	0.446	0.2691	0.981
0.423	0.124	0.442	0.2805	0.981
0.429	0.130	0.434	0.2995	0.983
0.434	0.136	0.428	0.3178	0.984
0.439	0.141	0.421	0.3349	0.985
0.443	0.147	0.415	0.3542	0.985
0.448	0.153	0.408	0.3750	0.986
0.453	0.158	0.402	0.3930	0.987
0.459	0.165	0.394	0.4188	0.988
0.463	0.170	0.389	0.4370	0.988
0.469	0.178	0.380	0.4684	0.989
0.473	0.183	0.375	0.4880	0.989
0.480	0.193	0.366	0.5273	0.990
0.485	0.199	0.359	0.5543	0.991

Table G.10 : Measured Data for JBN Calculations
- Kaydol #5 , 100°C -

Water Injected (PV)	Oil Produced (PV)	Pressure Drop (kPa)	Relative Injectivity I_r	$W_i I_r$
0.000	0.000	40.761	1.119	0.000
0.098	0.100	32.684	1.396	0.134
0.114	0.114	31.679	1.440	0.164
0.130	0.128	30.295	1.506	0.195
0.145	0.149	28.982	1.574	0.229
0.161	0.171	27.333	1.669	0.269
0.177	0.185	26.498	1.722	0.305
0.193	0.199	25.084	1.819	0.351
0.209	0.213	24.136	1.890	0.394
0.224	0.228	22.844	1.997	0.448
0.240	0.242	22.082	2.066	0.496
0.256	0.256	20.982	2.175	0.557
0.272	0.277	19.512	2.338	0.635
0.288	0.299	17.863	2.554	0.734
0.303	0.313	16.402	2.782	0.844
0.319	0.327	14.631	3.119	0.995
0.335	0.341	12.696	3.594	1.204
0.351	0.356	12.365	3.690	1.294
0.382	0.384	11.517	3.962	1.515
0.430+	0.398	10.847	4.207	1.808
0.446	0.404	10.573	4.316	1.923
0.461	0.410	10.173	4.485	2.069
0.477	0.415	9.973	4.575	2.183
0.525	0.421	9.559	4.773	2.504
0.540	0.427	9.398	4.855	2.623
0.572	0.432	9.124	5.007	2.860
0.619	0.438	8.876	5.140	3.184
0.667	0.444	8.568	5.326	3.551
0.698	0.450	8.420	5.419	3.784
0.762	0.455	8.041	5.674	4.321
0.809*	0.461	7.919	5.762	4.661
0.888	0.467	7.776	5.868	5.210
0.951	0.472	7.693	5.931	5.641
1.014	0.478	7.458	6.118	6.205
1.078	0.484	7.144	6.387	6.882
1.172	0.489	6.850	6.661	7.809
1.267	0.495	6.773	6.737	8.536
1.646**	0.518	9.916**	4.601	7.576
1.789	0.523	9.768	4.671	8.354

Table G.10 (cont.) : Measured Data for JBN Calculations
- Kaydol #5 , 100°C -

Water Injected (PV)	Oil Produced (PV)	Pressure Drop (kPa)	Relative Injectivity I_r	$W_i I_r$
1.915	0.529	9.525	4.791	9.174
2.168	0.541	9.203	4.958	10.748
2.737	0.558	9.107	5.010	13.711
3.068	0.563	8.581	5.318	16.316
3.290	0.569	8.411	5.425	17.845
3.495	0.575	8.263	5.522	19.299
3.811	0.582	8.111	5.626	21.439
4.127	0.586	7.954	5.736	23.674
4.364	0.592	7.937	5.749	25.088
4.680	0.597	7.846	5.816	27.218
5.217	0.603	7.650	5.965	31.119
5.644	0.609	7.558	6.037	34.070
6.165	0.615	7.398	6.168	38.027
18.347	0.643	6.415	7.113	130.501
25.694	0.649	6.240	7.313	187.888
42.758	0.653	5.977	7.634	326.412

\+ true breakthrough

* inferred breakthrough

** Because of an anomaly in the pressure drop behaviour, data from this point onward have been considered for relative permeability calculations.

Table G.11 : Relative Permeability and Fractional Flow Curves - Kaydol #5 , 100°C - (from JBN calculations)

Water Saturation	Relative Permeability to Water	Relative Permeability to Kaydol	Relative Permeability Ratio(w/b)	Fractional Flow
0.058	0.000	0.535	0.0000	0.000
0.478	0.181	0.209	0.8660	0.942
0.489	0.187	0.191	0.9791	0.949
0.498	0.192	0.178	1.0787	0.953
0.513	0.201	0.155	1.2968	0.961
0.540	0.217	0.119	1.8235	0.972
0.553	0.226	0.104	2.1731	0.976
0.560	0.230	0.095	2.4211	0.979
0.566	0.235	0.088	2.6705	0.980
0.575	0.241	0.079	3.0506	0.983
0.583	0.246	0.072	3.4167	0.985
0.588	0.250	0.067	3.7313	0.986
0.595	0.255	0.061	4.1803	0.988
0.604	0.263	0.053	4.9623	0.990
0.611	0.268	0.048	5.5833	0.991
0.619	0.274	0.042	6.5238	0.992
0.687	0.343	0.006	57.1667	0.999
0.700	0.361	0.002	180.5000	1.000
0.714	0.385	0.000	infinity	1.000

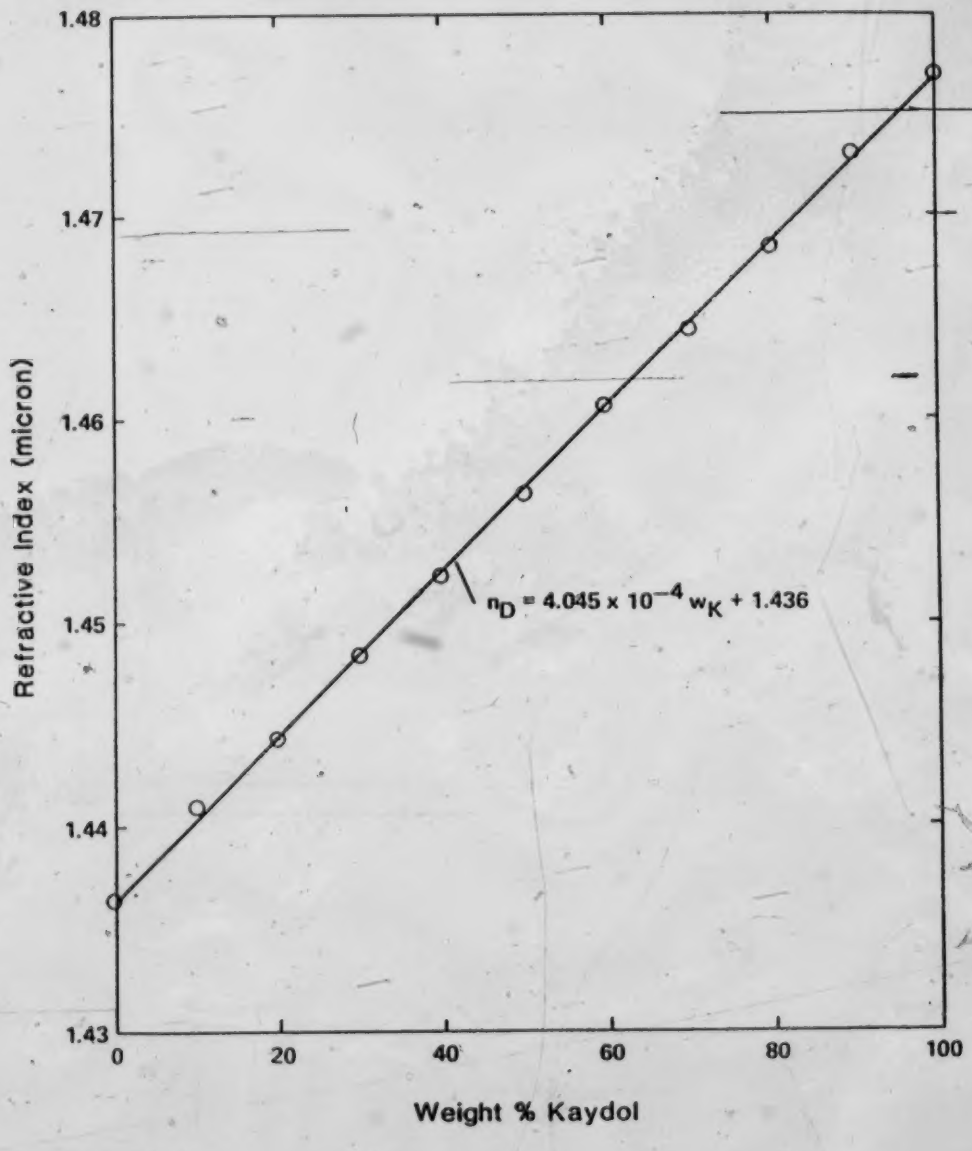

Figure G.1 : Refractive Index Calibration for Kaydol-Mineral Spirit Mixtures

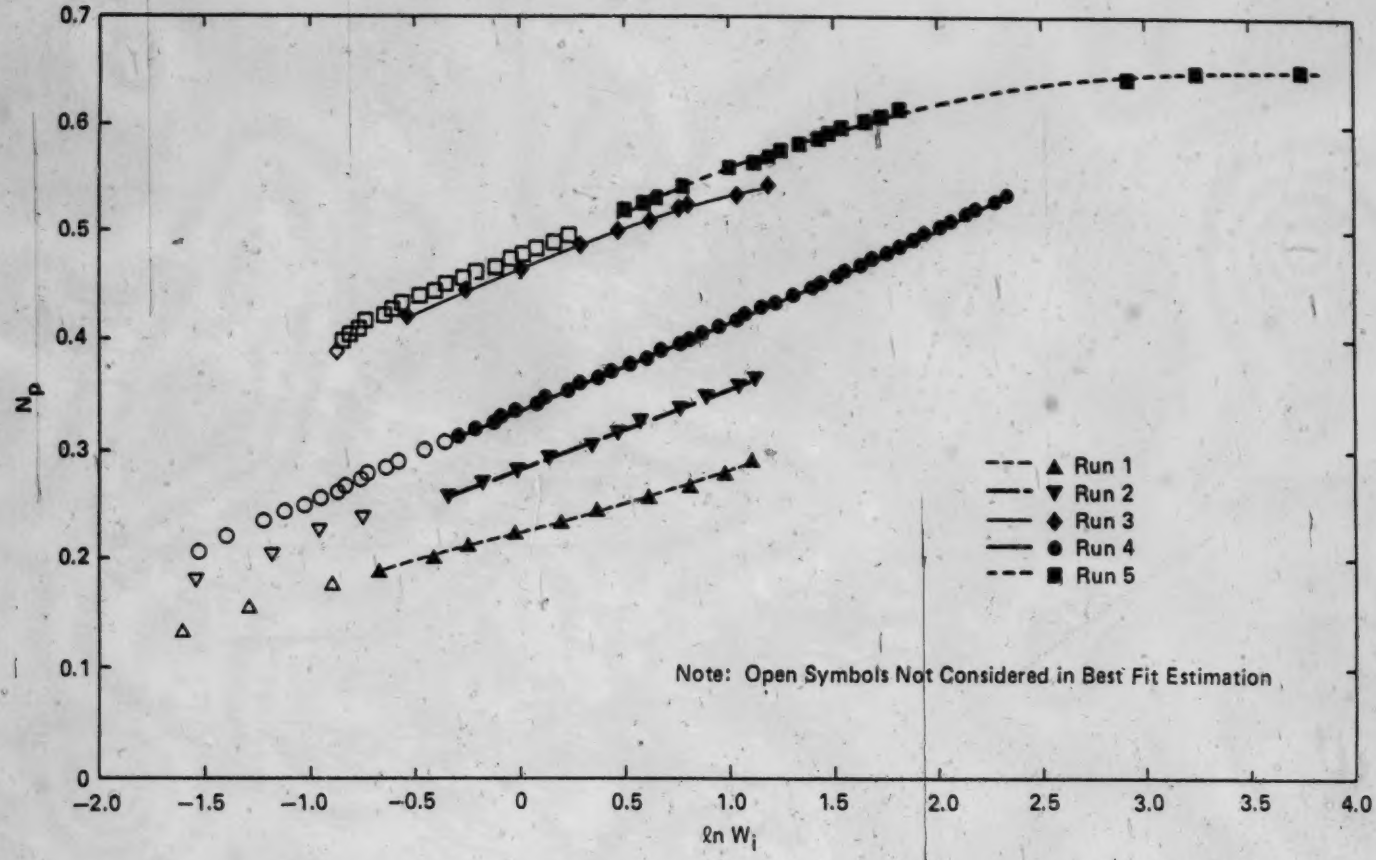

Figure 6.2 : Post-Breakthrough Recovery Functions for Kaydol Experiments

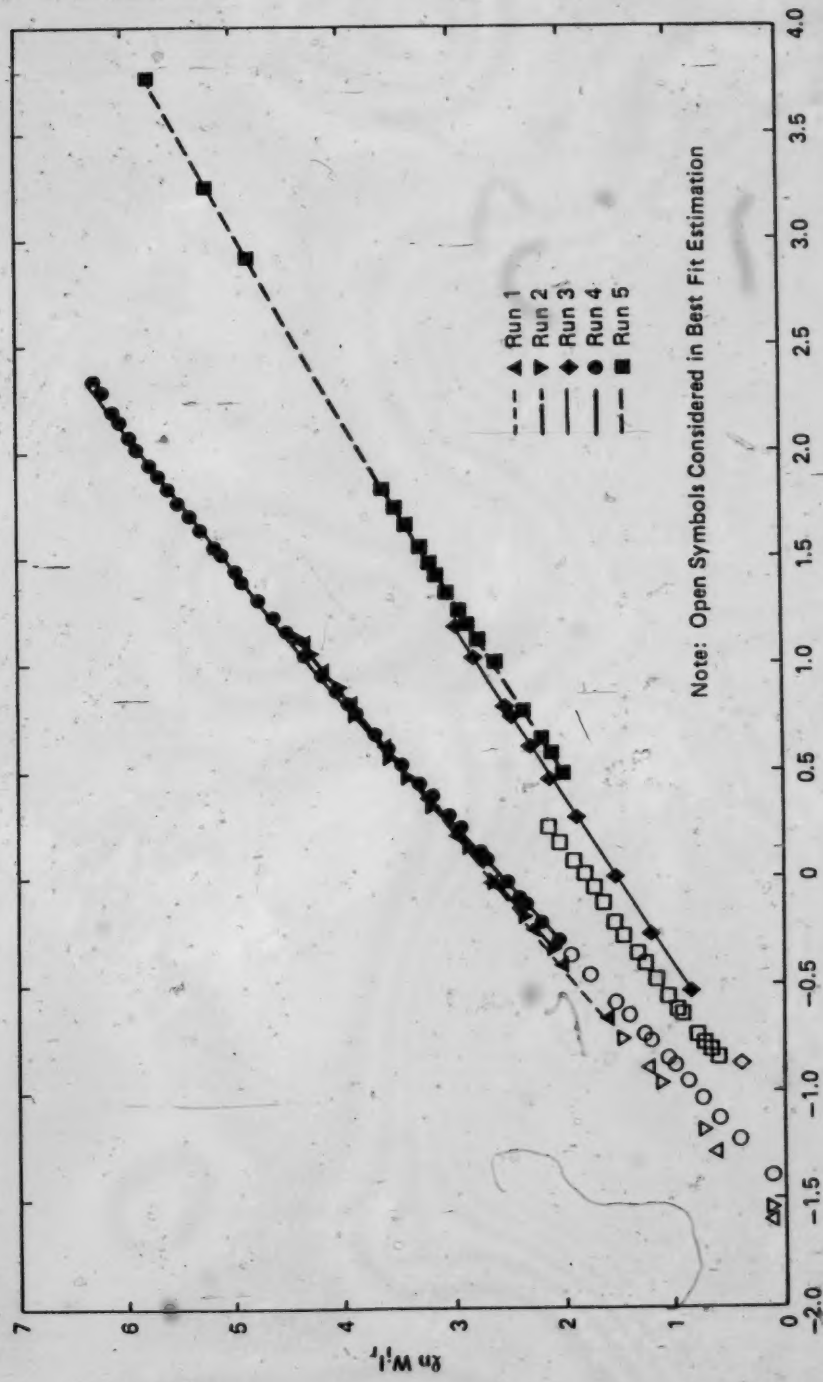

Figure 6.3 : Relative Injectivity Functions for Kaydol Experiments

Appendix H

Statistical Analysis

The analysis presented herein is intended to give an overview of some basic statistical definitions and calculation procedures used in this document. It is assumed that the data fall into an approximately normal distribution or that the histogram of the observations fits into a bell-shaped curve. Statistical inference is used to correlate the data by making statements about an entire population based on a random sample of observations from that population.

The average or mean, $\bar{x}$, of a sample of n observations is:

$$\bar{x} = \frac{\sum_{i=1}^{n} x_i}{n} \qquad (H.1)$$

The sample standard deviation, s, is given by:

$$s = \left[\frac{\sum_{i=1}^{n} (x_i - \bar{x})^2}{n - 1} \right]^{0.5} \qquad (H.2)$$

In order to estimate the mean, m, of a population, and to find how close $\bar{x}$ is likely to be to m, the concept of a confidence interval is used. A 95% confidence interval is calculated from the sample, which will cover the unknown population mean 95% of the time. The value 95% is defined as the confidence level of the interval. When the standard deviation of an entire population is unknown, the usual two-sided t confidence interval for the population mean is:

$$\bar{x} - t^*(s/\sqrt{n}) \leq m \leq \bar{x} + t^*(s/\sqrt{n}) \qquad (H.3)$$

where t* is the value found in a table of Student's t-distribution with $(n-1)$ degrees of freedom for the desired confidence level. The factor $(s/\sqrt{n})$ is also called the estimated standard deviation of the sampling distribution of $\bar{x}$. Furthermore, a t-test can be used as a tool to test hypotheses for individual population means, and for comparing two means.

When one wants to compare data from more than two different populations, one may use an analysis of variance. A one-way analysis of variance is a statistical procedure that determines if the variation between groups or populations is significantly different from the variation within a group or population, provided that there is a random sample from each population. Individual confidence intervals for each population mean are calculated in a similar manner to equation (H.3) by:

$$\bar{x}_j - t^*(s_p/\sqrt{n_j}) \leq m_j \leq \bar{x}_j + t^*(s_p/\sqrt{n_j}) \qquad \text{(H.4)}$$

where s_p is the pooled estimate of the common standard deviation to all populations and is expressed as:

$$s_p = (MS_{error})^{0.5} \qquad \text{(H.5)}$$

Also, t* is the value from a t-table corresponding to the desired confidence level and the degrees of freedom associated with the mean square error, MS_{error}, which is defined as:

$$MS_{error} = \frac{SS_{error}}{DF_{error}} = \frac{\sum_{j=1}^{R} \sum_{i=1}^{n} (x_{ij} - \bar{x}_j)^2}{\sum_{j=1}^{R} N_j - R} \qquad (H.6)$$

where $\sum_{j=1}^{R} N_j$ is the total number of observations for all populations. The above equation applies to the variation within any population. Similarly, for the variation between R populations:

$$MS_{factor} = \frac{SS_{factor}}{DF_{factor}} = \frac{\sum_{j=1}^{R} \bar{N}_j (\bar{x}_j - x_{overall})}{R - 1} \qquad (H.7)$$

A useful statistical test, called the F-test, is performed to check if the variation between populations (MS_{factor}) is greater than the variation due to random error within a population (MS_{error}). The F-ratio is calculated as:

$$F = \frac{MS_{factor}}{MS_{error}} \qquad (H.8)$$

Then, the critical F-ratio, F*, is determined from an F-table distribution with the knowledge of the confidence level, the degrees of freedom for the numerator and the denominator of the F-ratio:

$$F^* = F(CL;\ DF_{factor};\ DF_{error}) \qquad (H.9)$$

If F is larger than F*, one concludes that there is a significant statistical difference between these populations.

Statistical calculations have been performed using SPSS[x], a computing system specifically developed for this function. This program is available on the University of Alberta's MTS system. The tabulated t and F distribution percentiles to determine the appropriate t* and F*, respectively, can be found in Stanley (1973). The following example will try to illustrate some of the statistical concepts that have been presented above.

For the end point experiments, the absolute permeability of each core was initially determined at room temperature. An analysis of variance showed that the room temperature absolute permeabilities of the cores were not statistically different. For the statistical analysis, the cores were grouped according to the final experimental temperature level (variable V2, Table H.1). The results shown in Table H.2 (computer output). . The 95% confidence intervals for the average permeability of each temperature level in Table H.2 indicate no difference as shown by their overlap for all but one average permeability (level 2). The calculated F-value (F=2.72) is larger than the critical F*-value (F*=2.26). However, a multiple group comparison test (Scheffé) indicates that no two groups are significantly different at the 0.05 level of probability. These results have formed the basis for the determination of the effect of temperature on absolute permeability that is presented in Figure 4.1 (Section 4.1.3).

Table H.1 : Data for Variance Analysis

Core/Run No.	Permeability (d) V1	Experimental Temperature (°C)	Temp. Level V2
END-01	2.034	124.7	3
END-02	2.069	126.0	3
END-03	1.774	175.0	5
END-04	1.781	175.2	5
END-05	1.974	124.6	3
END-06	1.672	124.8	3
END-07	*	174.4	5
END-08	1.493	150.0	4
END-09	1.562	150.0	4
END-10	1.736	150.4	4
END-11	1.918	150.6	4
END-12	1.594	225.2	7
END-13	1.637	125.0	3
END-14	1.548	225.5	7
END-15	1.501	125.2	3
END-16	1.495	250.4	8
END-17	2.008	174.6	5
END-18	1.578	250.6	8
END-19	1.585	174.4	5
END-20	1.457	200.6	6
END-21	1.652	199.0	6
END-22	1.345	224.8	7
END-23	1.505	249.9	8
END-24	1.650	174.6	5
END-25	1.480	199.0	6
END-26	*	125.2	3
END-27	1.242	124.0	3
END-28	1.235	124.8	3
END-29	1.238	100.4	2
END-30	0.959	100.4	2
END-31	1.014	100.0	2
MID-01	1.274	124.7	3
MID-02	1.174	124.7	3
MID-03	1.161	125.6	3
MID-04	1.193	124.6	3
MID-05	1.209	125.0	3
MID-06	1.287	174.8	5
MID-07	1.163	125.4	3
MID-08	1.169	125.2	3
MID-09	1.234	175.2	5
MID-10	1.209	175.2	5
MID-11	1.154	125.2	3
MID-12	1.278	125.0	3

Table H.1 (cont.) : Data for Variance Analysis

Core/Run No.	Permeability (d) V1	Experimental Temperature (°C)	Temp. Level V2
DIS-01	1.296	124.4	3
DIS-02	1.183	124.8	3
DIS-03	1.169	125.6	3
DIS-04	1.152	125.0	3
DIS-05	1.293	125.0	3
KAY-01	1.253	19.2	1
KAY-02	1.145	20.6	1
KAY-03	1.122	101.1	2
KAY-04	1.370	23.4	1
KAY-05	1.061	100.0	2

* larger sand fraction

- O N E W A Y -

VARIABLE V2 'temperature level' BY VARIABLE V1 'absolute permeability'

1. ANALYSIS OF VARIANCE

SOURCE	D.F.	SUM OF SQUARES	MEAN SQUARES	F RATIO	F PROB.
BETWEEN GROUPS	7	1.2308	.1758	2.7205	.0199
WITHIN GROUPS	43	2.7792	.0646		
TOTAL	50	4.0100			

GROUP	COUNT	MEAN	STANDARD DEVIATION	STANDARD ERROR	MINIMUM	MAXIMUM	95 PCT CONF INT FOR MEAN
Grp 1	3	1.2560	.1125	.0650	1.1450	1.3700	.9765 TO 1.5355
Grp 2	5	1.0788	.1073	.0480	.9590	1.2380	.9455 TO 1.2121
Grp 3	22	1.3742	.3031	.0646	1.1520	2.0690	1.2398 TO 1.5086
Grp 4	4	1.6772	.1903	.0952	1.4930	1.9180	1.3744 TO 1.9801
Grp 5	8	1.5660	.2947	.1042	1.2090	2.0080	1.3197 TO 1.8123
Grp 6	3	1.5297	.1066	.0615	1.4570	1.6520	1.2649 TO 1.7944
Grp 7	3	1.4957	.1325	.0765	1.3450	1.5940	1.1665 TO 1.8248
Grp 8	3	1.5260	.0453	.0262	1.4950	1.5780	1.4134 TO 1.6386
TOTAL	51	1.4174	.2832	.0397	.9590	2.0690	1.3377 TO 1.4970
FIXED EFFECTS MODEL			.2542	.0356			1.3456 TO 1.4891
RANDOM EFFECTS MODEL				.0781			1.2328 TO 1.6020

RANDOM EFFECTS MODEL - ESTIMATE OF BETWEEN COMPONENT VARIANCE 0.0201

Tests for Homogeneity of Variances

Cochrans C = Max. Variance/Sum(Variances) = .3402, P = .078 (Approx.)
Bartlett-Box F = 1.974 , P = .057
Maximum Variance / Minimum Variance 44.753

2. MULTIPLE RANGE TEST : SCHEFFE PROCEDURE

RANGES FOR THE 0.050 LEVEL - 5.59 5.59 5.59 5.59 5.59 5.59 5.59

THE RANGES ABOVE ARE TABLE RANGES.
THE VALUE ACTUALLY COMPARED WITH MEAN(J)-MEAN(I) IS.. 0.1798 * RANGE * DSQRT(1/N(I) + 1/N(J))

NO TWO GROUPS ARE SIGNIFICANTLY DIFFERENT AT THE 0.050 LEVEL

Table H.2 : Variance Analysis Results

CURRICULUM VITAE

Marcel Polikar

PERSONAL DATA

Date of Birth	12 September 1952
Place of Birth	Paris, France
Marital Status	Married, one child
Languages Spoken	English and French fluently

POST-SECONDARY EDUCATION

1977	M.Sc. Chemical Engineering, University of Saskatchewan, Saskatoon, Saskatchewan.
1974	Diploma, Chemical Engineering, Swiss Federal Institute of Technology (EPF), Lausanne, Switzerland

HONOURS AND AWARDS

1976	University of Saskatchewan Summer Scholarship

EMPLOYMENT HISTORY

1978 to Date	Research Engineer, Alberta Research Council, Oil Sands Research Department, Edmonton, Alberta.
1978	Research Associate, University of Alberta, Department of Chemical Engineering, Edmonton, Alberta
1977 - 1978	Research Assistant, University of Saskatchewan, Department of Chemical Engineering, Saskatoon, Saskatchewan
1974 - 1977	Teaching high school and undergraduate university level

PROFESSIONAL ASSOCIATIONS

- Association of Professional Engineers, Geologists and Geophysicists of Alberta (P.Eng.)
- Petroleum Society of CIM
- Society of Petroleum Engineers of AIME
- Society of Core Analysts
- Canadian Society for Chemical Engineering

CURRICULUM VITAE (cont.)

PUBLICATIONS

Effect of Temperature on Bitumen-Water End Point Relative Permeabilities and Saturations, M. Polikar, F. Ferracuti, V. DeCastro, V.R. Puttagunta and S.M. Farouq Ali, Jour. Can. Pet. Tech. 25, 5, 44-50 (1986)

Relative Permeability Curves for Bitumen and Water in Oil Sand Systems, M. Polikar, V.R. Puttagunta, S.M. Farouq Ali and V. DeCastro, Paper No. 86-37-03, Proc. 37th Annual Technical Meeting of the Petroleum Society of Can. Inst. Mines, Calgary (June 8-11, 1986).

Temperature Effects on Bitumen-Water Relative Permeabilities, M. Polikar, F. Ferracuti, V. DeCastro, V.R. Puttagunta and S.M. Farouq Ali, Paper No. 85-36-14, Proc. 36th Annual Technical Meeting of the Petroleum Society of Can. Inst. Mines, Edmonton, Alberta (June 2-5, 1985).

Preparation of Bitumen from Oil Sand by Centrifugation, D. Wallace, M. Polikar and F. Ferracuti, Fuel 63, 6, 862-864 (1984).

Experimental and Numerical Study of Drag on an Isolated Permeable Sphere, J.H. Masliyah, K. Nandakumar and M. Polikar, Paper No. 33-6, Proc. 30th Canadian Chemical Engineering Conference, Edmonton, Alberta (October 19-22, 1980).

Terminal Velocity of Porous Spheres, J.H. Masliyah and M. Polikar, Can. J. Chem. Eng. 58, 3, 299-302 (1980).

Inhibition of Corrosion of Steel Pipe in Aqueous Solution Using Chromates, M. Polikar, Master of Science Thesis, University of Saskatchewan (June 1977).

Distillation of a Surface Tension Negative System - Influence of Surfactant Addition, A.B. Ponter, M. Polikar, P. Trauffler and S. Vijayan, Tenside 13, 4, 201-203 (1976).

Etude Expérimentale concernant l'Influence d'un Agent Tensio-Actif sur la Mouillabilité du Système Eau-Acide Formique dans des Conditions de Distillation, M. Polikar, Diploma Thesis, Ecole Polytechnique Fédérale de Lausanne (July 1974).